NAVIGATION WITH LIMITED PRIOR INFORMATION
USING TIME DIFFERENCE OF ARRIVAL MEASUREMENTS
FROM SIGNALS OF OPPORTUNITY

THESIS

Christopher M. Rondeau, Captain, USAF

AFIT/GE/ENG/10-32

DEPARTMENT OF THE AIR FORCE
AIR UNIVERSITY

AIR FORCE INSTITUTE OF TECHNOLOGY

Wright-Patterson Air Force Base, Ohio

AFIT/GE/ENG/10-32

NAVIGATION WITH
LIMITED PRIOR INFORMATION USING
TIME DIFFERENCE OF ARRIVAL MEASUREMENTS
FROM SIGNALS OF OPPORTUNITY

THESIS

Presented to the Faculty

Department of Electrical and Computer Engineering

Graduate School of Engineering and Management

Air Force Institute of Technology

Air University

Air Education and Training Command

In Partial Fulfillment of the Requirements for the

Degree of Master of Science in Electrical Engineering

Christopher M. Rondeau, B.S.E.E.

Captain, USAF

December 2010

AFIT/GE/ENG/10-32

NAVIGATION WITH
LIMITED PRIOR INFORMATION USING
TIME DIFFERENCE OF ARRIVAL MEASUREMENTS
FROM SIGNALS OF OPPORTUNITY

Christopher M. Rondeau, B.S.E.E.

Captain, USAF

Approved:

/signed/   18 Nov 2010
_____   _____
Dr. Richard K. Martin (Chairman)   date

/signed/   18 Nov 2010
_____   _____
Dr. Matthew C. Fickus (Member)   date

/signed/   18 Nov 2010
_____   _____
Maj Kenneth Fisher, PhD (Member)   date

/signed/   18 Nov 2010
_____   _____
Dr. Michael A. Temple (Member)   date

AFIT/GE/ENG/10-32

Abstract

The Global Positioning System (GPS) provides world-wide availability to high-accuracy navigation and positioning information. However, the threats to GPS are increasing, and many limitations of GPS are being encountered. Simultaneously, systems previously considered as viable backups or supplements to GPS are being shut down. This creates the need for system alternatives.

Navigation using signals of opportunity (SoOP) exploits any signal that is available in a given area, regardless of whether or not the original intent of the signal was for navigation. Common techniques to compute a position estimate using SoOP include received signal strength, angle of arrival, time of arrival, and time difference of arrival (TDOA). To estimate the position of a SoOP receiver, existing TDOA algorithms require one reference receiver and multiple transmitters, all with precisely known positions.

This thesis considers modifications to an existing algorithm to produce a comparable position estimate without requiring precise a priori knowledge of the transmitters or reference receiver(s). Using Amplitude Modulation (AM) SoOP, the effect of erroneous a priori data on the existing algorithm are investigated. A proof-of-concept for three new estimation algorithms is presented in this research. Two of the estimators successfully demonstrate comparable performance to the existing algorithm. This is demonstrated in six different transmitter environments using four different receiver configurations.

Acknowledgements

Table of Contents

List of Figures

List of Tables

List of Abbreviations

NAVIGATION WITH
LIMITED PRIOR INFORMATION USING
TIME DIFFERENCE OF ARRIVAL MEASUREMENTS
FROM SIGNALS OF OPPORTUNITY

I. Introduction

This chapter provides the necessary basis and motivation for researching navigation using time difference of arrival (TDOA) measurements from signals of opportunity (SoOP). The chapter begins with a background discussion, followed by a description of the research goals and assumptions made in order to limit the scope of this research. A review of related research and a justification are briefly presented, and the chapter is concluded with an organizational outline for the remaining chapters.

1.1   Background

Precision navigation and positioning is no longer a luxury, but rather a requirement for modern systems. United States Air Force doctrine declares navigation and positioning "vital to Air Force operations" [6]. The more precise and reliable navigation and positioning data become, the more such a system enables its users. The Global Positioning System (GPS) is capable of delivering world-wide, sub-meter accuracy and has therefore been the driving factor behind the increased demand for such accuracy. However, there are conditions where GPS is unreliable or unavailable, such as urban environments, inside buildings, and within areas of intentional or unintentional jamming. Therefore, the need has greatly increased for a viable navigation and positioning technique other than GPS with precision on a similar order.

GPS is among many systems that utilize an approach called *radiolocation*. Radiolocation is most commonly defined as a navigation and positioning technique used to locate a transmitter by measuring parameters of a received signal that subsequently

is used to derive a position estimate [4]. There is some ambiguity on the specific meaning of the terms radiolocation, radionavigation, and radiodetermination. For this thesis, the term radiolocation will be considered generally to mean "the determination of the position, velocity and/or other characteristics of any object [transmitter or receiver]...by means of the propagation properties of radio waves," as defined by United States Federal Standard 1037C [31]. The general concept of radiolocation was first documented in 1891 [43]. In the 1920s and into the World War II era, the Long Range Aid to Navigation (LORAN) was introduced [32]. LORAN was among the first major systems to employ radiolocation, and since then, the technique has been extended to the NAVSTAR-GPS satellite navigation system (later the name was shortened to "GPS") [32]. As the world-wide availability and precision of GPS increased, many other applications found use for the GPS signals, such as commerce, telecommunications, and agriculture [33]. As a result, the value of GPS as a potential target for hostile forces or individuals has greatly increased.

GPS user equipment is vulnerable to both intentional and unintentional interference, resulting in possible denial of service over large geographical areas. Many fielded systems have not been tested in extreme outages, and the synergistic effects of such an outage are largely unknown [14, 40]. GPS jamming equipment is relatively simple, and given the characteristics of the GPS signal, a low-power jammer can result in an intentional GPS denial of service [20]. GPS outages may also result from unintentional friendly sources. For example, on 22 January 2007, an operator error denied GPS from approximately 1200 - 1600 PST, affecting medical paging, cell phone towers, and United States Coast Guard operations around San Diego, California [3]. Naturally occurring conditions pose a dynamic threat to GPS as well. The impact of charged-particle radiation from a solar storm, for example, is unknown and untested, and the next solar maximum is forecast for 2012 [22].

As the threats to GPS and the corresponding synergistic impacts grow, legacy systems are being reduced or eliminated. The reasoning is both technological and political. In recent years, LORAN was commonly viewed as a "backup" system to

GPS. While international communities explored LORAN-C (a variant of LORAN), as a risk mitigation for GPS vulnerabilities, the United States has begun the incremental shut down of LORAN, viewing it as redundant and costly compared to the increasing capabilities of GPS [2]. As non-GPS navigation systems continue to be targeted for shut down and no replacement or new systems are scheduled for operation, the frequency spectrum remains full of signals which can be received and used for navigation — regardless if that is the intent of the signal.

SoOP are signals transmitted for non-navigation purposes that are freely available in most environments and may be exploited for navigation. SoOP are convenient for navigation, because they are often more numerous and include, but are not limited to [17, 44]:

- Amplitude modulation (AM) and frequency modulation (FM) radio stations

- Analog/digital television

- Wireless local area network (WLAN) signals such as WiFi and WiMax

- Digital Audio Broadcasts (DAB) and Digital Video Broadcasts (DVB)

- Cellular and mobile phone network base stations

- Radar sites

- Radio Frequency (RF) beacons/transponders

- Partially available GPS

- Communications satellite signals

- Celestial and other signals from nature.

Navigation via SoOP makes use of the available frequency spectrum in a given environment (and the supporting infrastructure). One such method of navigation via SoOP is using TDOA measurements. Current algorithms require at least a pair of receivers to receive the same SoOP. The position of one receiver must be known a priori. From multiple TDOA measurements between the receivers, a series of ranges

from the receiver to the transmitter are estimated and from that a position estimate is computed. This research will concentrate on using TDOA measurement techniques on received SoOP, specifically those from AM transmissions.

1.2 Research Goals

Precise a priori information regarding the position of transmitters and at least one reference receiver in an environment where GPS is unavailable may not be accessible. Therefore, the primary goal of this research is to prove the concept that a revised TDOA algorithm using SoOP is sufficient for navigation with transmitter and reference receiver position information either unreliable or unavailable. This is demonstrated by the simulation of such a system using broadcast AM signals. The secondary goal of this research is to examine the effect of erroneous prior information on the existing estimation algorithm.

1.3 Assumptions

For this research, the following assumptions were made about the SoOP and the receiver capability:

1. SoOP have an established infrastructure in and around a potential Area of Responsibility (AOR).

2. SoOP transmitters broadcast AM signals in the band of 530 to 1700 kHz.

3. SoOP broadcast precisely on the expected broadcast carrier frequency.

4. SoOP transmitters do not interfere with each other.

5. There is no multipath present.

6. All receivers have a real-time, noiseless sync for TDOA estimation.

7. All receivers and transmitters are static.

To successfully navigate in a GPS-denied environment using SoOP, assumptions were made for both the signals and the corresponding impact on constructing a re-

ceiver. The SoOP must be readily accessible and supported with a pre-established infrastructure. It is assumed that a receiver can be built to receive the SoOP. For this research, the signals of interest are in the commercial AM band as defined by the Federal Communications Commission (FCC) in the United States [9]. The remaining assumptions were made to limit the scope of this thesis to a proof-of-concept regarding the a priori information about the transmitters and receivers.

1.4 Related Research

This section discusses radiolocation systems that can exploit SoOP and outlines recent research that has been presented by the community. These systems are presented in terms of two categories: non-TDOA and TDOA-based. The section begins with non-TDOA-based systems followed by TDOA-based systems including examples of fielded TDOA systems. The section concludes with a summary of recent research regarding radiolocation via SoOP utilizing TDOA measurements.

1.4.1 Non-TDOA-based Navigation Systems.
Generally, four techniques comprise non-TDOA-based navigation systems: Received Signal Strength (RSS), Angle of Arrival (AOA), Time of Arrival (TOA), and Frequency Difference of Arrival (FDOA).

1.4.1.1 Received Signal Strength.
Radiolocation using RSS measurements is a common method for obtaining a navigation solution. RSS uses a known mathematical model describing the path loss with distance. The collected measurements are combined with the model of the channel to compute the navigation solution. While the approach is simple to implement, it relies on assumptions about the local physical topography and is susceptible to multipath fading and shadowing [4, 28].

1.4.1.2 Angle of Arrival.
AOA has been a prevalent technique for computing navigation solutions in coastal regions, though the technique is not limited to this environment. To compute a navigation solution, special antennae arrays,

called interferometers, receive signals from a transmitter. From the received signals, the azimuth (i.e., AOA) is computed by calculating a line of bearing (LOB) from the transmitter. The position estimate is calculated at the intersection of two lines (assuming they intersect) or using triangulation when more transmitters are in the network. The position estimate is computed with higher accuracy when using two or more sources as shown in Figure 1. This technique is passive, and no time synchronization between receivers is required. However, the hardware to implement AOA can be large and complex [25]. Furthermore, AOA is dependent on line of sight to the transmitter, and there is a strong correlation between the accuracy of the solution and the distance between the receivers and transmitters [4, 7, 28].
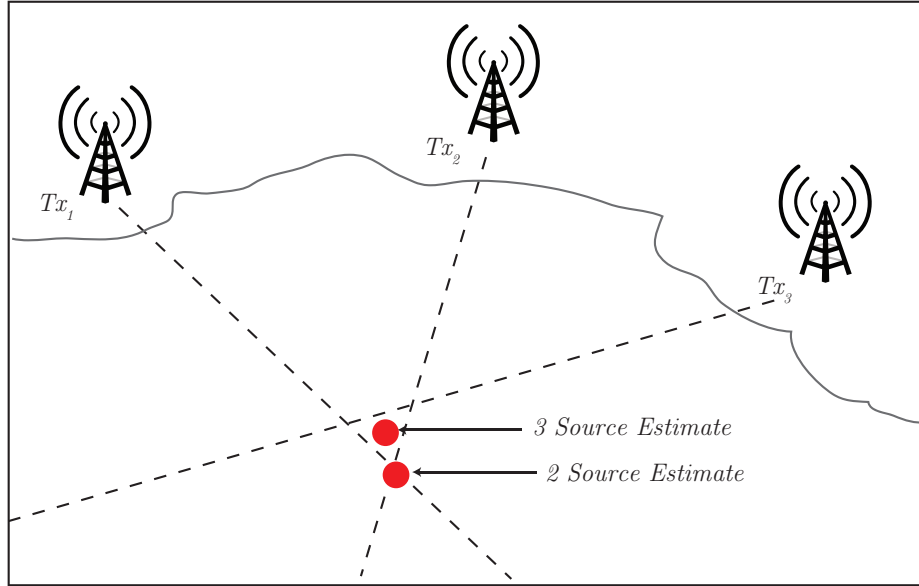
Figure 1:   Radiolocation via AOA

1.4.1.3 Time of Arrival.   TOA exploits the propagation time between the transmitter and the receiver to compute a navigation solution. The one-way propagation time between the transmitter and each receiver is computed. This time measurement is converted into a range distance between a transmitter and receiver assuming the signal travels at the speed of light. Geometrically, the receiver must lie on a circle centered at the transmitter. By using at least three receivers as shown in

Figure 2, the position of the receiver is given by the intersection of the three circles [4]. GPS is an example of a system that implements TOA. This type of system is highly dependent on clock synchronization between the receiver and transmitter [7, 28, 42].
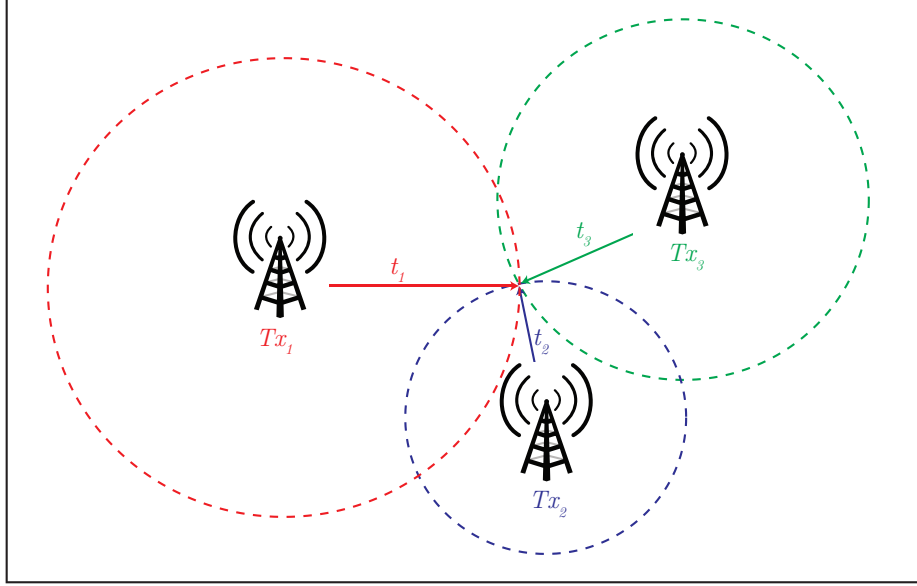
Figure 2:   Radiolocation via TOA

1.4.1.4   Frequency Difference of Arrival.   If there is movement between the receiver and transmitter, a frequency shift relative to the expected transmitted frequency will exist. This difference can be exploited to compute a position estimate. The receivers must have the ability to measure frequency with more accuracy than the smallest possible shift in order for the system to detect movement. FDOA can be difficult to implement and is often costly [30, 38].

1.4.2   TDOA-based Navigation Systems.   TDOA-based systems focus on measuring the difference in arrival times of two transmitted signals by a single receiver, or by differencing the arrival time of a single signal at two or more receivers [42]. For this research, the former system is referred to as *source localization*, and the latter system, which was implemented in this research, is referred to as *navigation*. TDOA positioning may also be referred to as "hyperbolic" or "multi-lateration" positioning. To illustrate this technique, a two receiver scenario is described. One receiver has an

unknown position and is referred to as the "mobile receiver," while the position of the other is known a priori and is referred to as the "reference receiver." These two receivers share a data link from which the difference in arrival times of a signal are computed. Since only the difference in arrival times is computed, clock synchronization is not required (unlike TOA). From the TDOA measurement, a range estimate between the mobile receiver and the transmitter is computed. Using signals from at least three different transmitters allows for a two-dimensional position estimate to be computed as shown in Figure 3. Two examples of fielded systems that employ TDOA that will be discussed here are LORAN and NAVSYS Corporations GPS Jammer and Interference Location System.
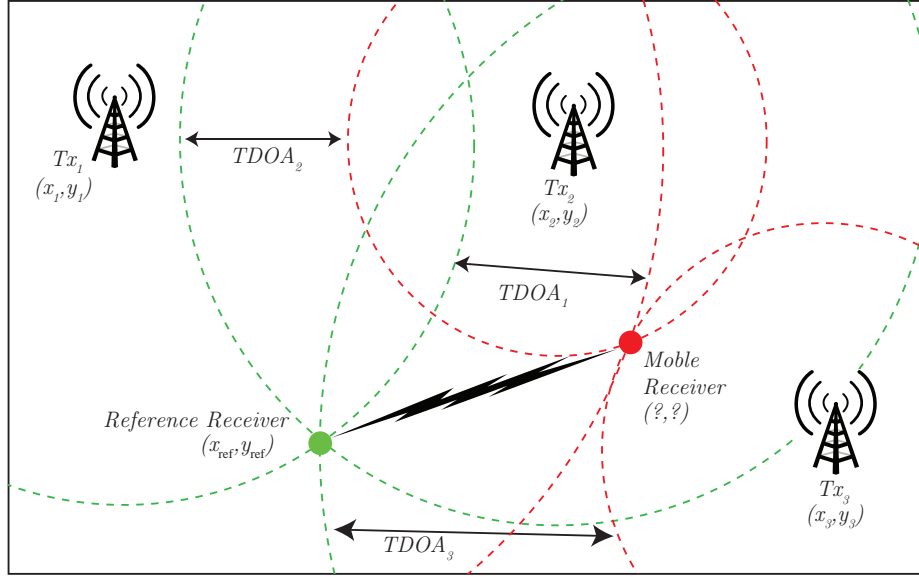
Figure 3:   Radiolocation via TDOA Using Three Transmitters and Two Receivers

1.4.2.1 LORAN.   LORAN operates in the Low Frequency band at 90 to 110 kHz and was developed for aircraft and maritime navigation near coastal areas. The system consists of multiple transmitters that are synchronized in time. An aircraft or ship measures the TDOA of the signals from different transmitters. Each TDOA measurement defines a hyperbolic line of position (LOP). The LOP intersection produces a navigation solution [29, 42].

8

1.4.2.2   GPS Jammer and Interference Location System.   NAVSYS corporation designed a system to mitigate GPS jamming and interference. The system uses multiple terrestrial receivers at known locations to determine the location of a single transmission source (i.e., the GPS jamming device). This allows for the GPS interference to be mitigated or avoided. [7, 28, 42].

1.4.3   Previous TDOA SoOP Radiolocation.   There has been recent research that utilized TDOA as the technique to navigate using various SoOP (or combinations of signals). The simulations presented in this thesis focused specifically on the TDOA algorithm as executed using AM signals. However, the principles from prior research that employed a TDOA technique using any SoOP are considered relevant and are discussed here.

Hall designed, built, and evaluated an AM SoOP radiolocation system [16]. He determined relative positions between the reference and mobile receiver (referred to as baselines) from observations of the carrier phases of various signals from broadcast AM stations near Boston, Massachusetts. His system determined the horizontal components of the baseline to approximately ten-meter uncertainties for baseline lengths up to about 35 kilometers. Hall's system did all computations post data capture, and therefore, did not navigate real-time. He also designed and implemented a method that enabled the ambiguity of the carrier-phase to be resolved instantaneously without position initialization or signal-tracking continuity. Hall also documented impediments to AM SoOP radiolocation. Specifically, he showed how AM transmitter uncertainty causes uncertainty in the receiver position. His sub-meter geodetic surveys of 29 Boston area transmitters showed some position errors exceeding 100 meters. However, when the inherent risks of the AM signals and errors of a priori data can be accounted for, AM remains a viable signal for radiolocation. He further showed the strengths of AM as a SoOP for radiolocation by demonstrating its robustness to environmental conditions, such as wooded areas, that GPS was much more susceptible

to. Hall's findings provided validation that AM signals are a suitable SoOP to use in the proof-of-concept simulations conducted in this research.

Fisher introduced the concept of navigation potential (NP) and detailed the process to determine the NP of a signal as compared to GPS [10]. This concept allows the usefulness of a signal for navigation to be quantified. He also provided a theoretical performance limit of the navigation parameters of received signals. Furthermore, by modeling multipath errors, he demonstrated a more realistic predictor of a given system performance as compared to a metric based on the transmitted signal in measurement noise alone.

Eggert explored the NP of the National Television Systems Committee (NTSC) broadcast signals using a TDOA algorithm in both high and low multipath environments. He developed three data reduction algorithms to estimate the TDOA. One algorithm modified the classical cross-correlation approach, and the other two differenced the TOA of the signal at each receiver. The linear fit peak estimator allowed for more precise determination of the acutal cross-correlation peak in the TDOA estimation. His results also showed multipath to be the dominant source of errors, which he mitigated using a locally fabricated antenna. His collected NTSC broadcast signals showed TDOA errors ranging from 1 to 200 meters with typical errors between 10 to 40 meters. His subsequent simulations using eight television stations near Dayton, Ohio produced typical range errors of approximately 40 meters. Accuracy was reduced to 100 meters in high multipath environments. Finally, he demonstrated that TDOA measurement accuracy of 5 to 10 meters was required to provide position estimates with 10 meter accuracy to mirror readily available single frequency GPS receivers [7]. The NTSC signals are of a much higher bandwidth than the AM signals explored in this research, but Eggert's results provide a useful baseline for the validity of the simulation data presented here.

Kim analyzed the NP of AM and FM radio signals for the purposes of navigation in large urban areas where GPS is typically degraded or unavailable. He explored two

correlation algorithms to measure the TDOA at the receiver. He further detailed the correlation characteristics of both AM and FM signals depending on the type of message signal being modulated (song or voice). His system model was validated by using a reference signal with known characteristics (a 31-Gold coded waveform) and then analyzing AM and FM signals from various sources. His simulations used eight different combinations of his two correlation methods, modulation types, and message signals. His work showed two of the combinations using FM were the most promising for navigation purposes. The AM signals he examined yielded limited potential using either of his two correlation methods [23]. For the purposes of this research, the correlation methods and characteristics of the AM signals Kim analyzed that produced the limited NP are noted as inherents risks of using AM SoOP. Specifically, there was no significant difference in the correlation characteristics of AM voice or AM song when compared to each other.

McEllroy showed promising results for using AM signals for navigation. He evaluated four methods for estimating the cross-correlation peak within a sampled portion of the cross-correlation data for use in TDOA estimation. His system implemented a peak estimator based on Eggert's linear fit peak estimator. The simulations he created attempted to model real-world AM signal characteristics, including the transmitter source, receivers, propogation effects, inter-receiver frequency errors, noise, and multipath. He tested a hardware system using the simulated techniques and found that selecting a proper analog front-end is crucial to the successful operation of the navigation system. Furthermore, he also documented several real-world error sources including potential errors in the position of the AM transmitters from the FCC, power line noise, and instability of local oscillators between receivers. In his simulations at signal-to-noise ratio (SNR) levels of 60 dB, with no multipath, no frequency errors, and no integer ambiguity (i.e., ideal conditions), he was able to demonstrate sub-meter accuracy. As SNR decreased, the variation in position estimates increased [28]. Like Eggert and Hall, McEllroy further confirms multipath as the most significant source of errors for AM TDOA navigation.

Velotta examined using Orthogonal Frequency Division Multiplexing (OFDM) signals for navigation. His approach exploited feature detection using characteristics of OFDM signals instead of a correlation technique [42]. Similar signal features like those of OFDM signals are not present in AM signals and served as the justification to pursue a simple cross-correlation technique for this research.

Montminy explored the geolocation of a hostile transmitter using TDOA measurements of low-power RF signals. She employed a weighted least squares solution to estimate the transmitter's location, and by analyzing the variance of the estimate, was able to determine whether or not the received signal was line-of-sight (LOS) [30]. This technique is useful for multipath mitigation and works within the estimation algorithm. This research did not model multipath; however, given that it is a significant source of potential error, the technique is noted for future work in this area.

1.5 Justification

Wireless communications continue to improve and an increasing number of SoOP are avaliable for exploitation. As the GPS limitations and threats continue to be an issue for users, the desire to supplement or replace GPS in certain applications is ever present. While higher bandwidth signals are more likely to provide higher precision, the supporting equipment comes at a cost of user convenience — equipment size or computation time, for example. AM SoOP could potentially be integrated into fielded navigation systems. The existing worldwide infrastructure of broadcast AM signals makes these transmissions ideal for widespread implementation. Furthermore, the techniques demonstrated with AM signals can also be applied to higher bandwidth signals for additional precision. This research seeks to prove the concept that these advantages can be exploited while also limiting the amount of a priori data currently required to make such a system useful.

1.6   Organization

Chapter II discusses the necessary background information for broadcast AM signals and the TDOA algorithms. Chapter III explains the methodology used for data collection in the simulation environment and the TDOA, correlation and position estimation algorithms including the derivation of new algorithms presented in this research. Chapter IV details the results from the simulations described in Chapter III. Chapter V gives an overall summary and conclusions of the thesis followed by potential future work and follow-on areas of study.

II. Technical Background

This chapter provides the technical background for the topics involved in this research. First, an overview of the characteristics of broadcast AM signals is provided. Next, current TDOA positioning techniques are derived followed by a discussion of signal evaluation and correlation theory. Last, the error statistics used in this research are discussed, specifically the Cramér-Rao Lower Bound (CRLB) for the range and position estimation techniques, the generalized variance, and the mean square error (MSE).

2.1 Broadcast AM Characteristics

Since AM signals are the SoOP used in this research, a discussion of the signal characteristics is useful. For broadcast AM, the message signal is modulated and transmitted. A basic amplitude modulated signal is of the form

$$s(t) = A_c \, m(t) \, cos(2\pi f_c t), \tag{1}$$

where

$s(t)$ is the amplitude modulated signal that is transmitted,

A_c is the amplitude of the carrier frequency,

$m(t)$ is the message signal that is being modulated,

f_c is the carrier frequency.

In the United States, the AM band spans 530 kHz to 1700 kHz with corresponding wavelengths from 566 meters to 175 meters [9]. The carrier frequencies in the band are spaced 10 kHz apart, and the carrier frequencies are required to be maintained within ±2 Hz. Unlike other bands, there is no guard band, meaning there is no additional bandwidth reserved between the channels for interference protection. For the broadcast signals, the message content is either voice or music in the 50 Hz to 16 kHz range. The broadcasts can only be transmitted one channel at a time; therefore, stereo effects cannot be achieved [10]. AM broadcast signals travel primarily

as groundwaves (especially in daytime hours) which propagate with phase velocities that depend on the electrical properties of the ground. When AM signals travel as groundwaves, they are susceptible to overhead and underground conductors such as power lines. Conversely at nighttime, when the D-layer of the ionosphere recombines, AM signals reflect off the ionosphere which enables skywave propagation. This phenomenon could potentially lead to interference of distant stations at night [16]. As a result of these transmission characteristics, the FCC categorizes each channel which, in turn, dictates the allowable parameters of each station's transmission.

Broadcast AM stations are divided into three categories (or channels): Clear, Regional, and Local channels [5]. Clear channels service a wide area and are free of interference on the same and adjacent channels. Regional channels service populated areas and surrounding rural areas. Local channels service a city or town and the surrounding area. Local channels reduce transmitter power at night so as not to interfere with other distant stations [10]. For navigation purposes, this results in fewer potential navigation signals.

Having presented some basic characteristics of the signals, and the associated risks with using them for navigation, the broadcast AM band is attractive for SoOP navigation for several reasons:

1. Signals from many AM stations are generally available world-wide and certainly in most parts of the United States.

2. Compared to GPS, transmitters are nearby, ground-based and stationary.

3. The long wavelengths, relative to GPS wavelengths, of the carrier frequencies enable the potential for indoor and underwater navigation.

4. The band has a broad frequency range at lower frequencies (relative to other bands) and low bandwidths that simplify the receiver design.

5. Signals are typically received with a higher SNR than GPS.

As discussed, GPS signals may be unreliable or denied, especially in many environments that military applications might encounter. The characteristics of AM signals may actually allow for better performance compared to other SoOP. For example, shorter wavelengths of FM and television broadcast signals do not penetrate buildings as well as AM signals [16]. To further illustrate this point, the skin depth of AM signals in freshwater is approximately 10 meters. This enables the ability to navigate with an antenna slightly below the surface of the water as opposed to slightly above the surface [16]. Therefore, taking the risks and benefits of broadcast AM into account, the AM signals become an attractive SoOP for navigation. Furthermore, the limitations and simple signal characteristics of AM make it an ideal choice for proof-of-concept demonstrations of the TDOA algorithms.

2.2 TDOA Positioning

TDOA positioning is an extension of the multi-lateration technique, that is, using distances from known locations to compute a position estimate [29]. The technique described here consists of multiple transmission sources at known locations and two receivers as previously discussed — a reference receiver at a known location and a mobile receiver at an unknown location. The goal is to determine the relative position between the reference and the mobile receivers and to estimate a range from the mobile receiver to the transmitter. This range estimate defines a hyperbola consisting of possible locations of the mobile receiver. The shape may be a circle or sphere, rather than a hyperbola, depending on the system. For the purposes of explanation, the shape will be discussed as a hyperbola, unless otherwise noted. Given enough measurements (in an ideal case), the intersection of the hyperbolae will be the final position estimate.

In the case where hyperbolae intersect, a straightforward approach uses geometric interpretation to calculate the intersection. However, when time measurement errors are present (for example, in the form of a clock bias between the receivers), the hyperbolae may not intersect. The theory for position estimation has been thor-

oughly developed yielding several methods to solve the hyperbolic equations in these non-ideal conditions [4]. One technique computes an exact solution to the hyperbolic TDOA equations, however, the constraint may exist such that the number of measurements must be exactly equal to the number of unknown position coordinates [8, 18]. Another option is to use Taylor-series expansion to linearize the equations and solve for position iteratively [11, 39]. Other techniques are based on least squares minimization of the location error to solve for a position estimate [1, 13, 19, 36, 37].

To illustrate the TDOA algorithm, the following sections develop the range estimation and position estimation concepts and techniques. For range estimation, the case of synchronized receivers is presented first, followed by discussion of the unsynchronized case. The position estimate is subsequently derived using the output from the range estimates for both cases (the synchronized case being represented by a clock bias of zero).

2.2.1 Range Estimation. The two-receiver TDOA system requires that the transmitters and the reference receiver be at known locations. This case (for a single transmitter) is shown in Figure 4. Both the mobile and reference receivers time tag a received signal, and the TDOA is computed through a real-time data link. The time difference is converted into a distance by multiplying by the speed of the signal, typically assumed to be the speed of light. Since the range between the reference receiver and the transmitter is known, and the range between the two receivers is estimated via TDOA, the computation of a range estimate between the transmitter and the mobile receiver is made possible. If there are at least three transmitters available, multi-lateration techniques can be used to estimate the mobile receiver's position. If the receivers are synchronized with perfect TDOA estimates, the range estimates define circles that will intersect exactly as was shown in Figure 3. The synchronized and unsynchronized cases are overlayed and shown for three transmitters in Figure 5.
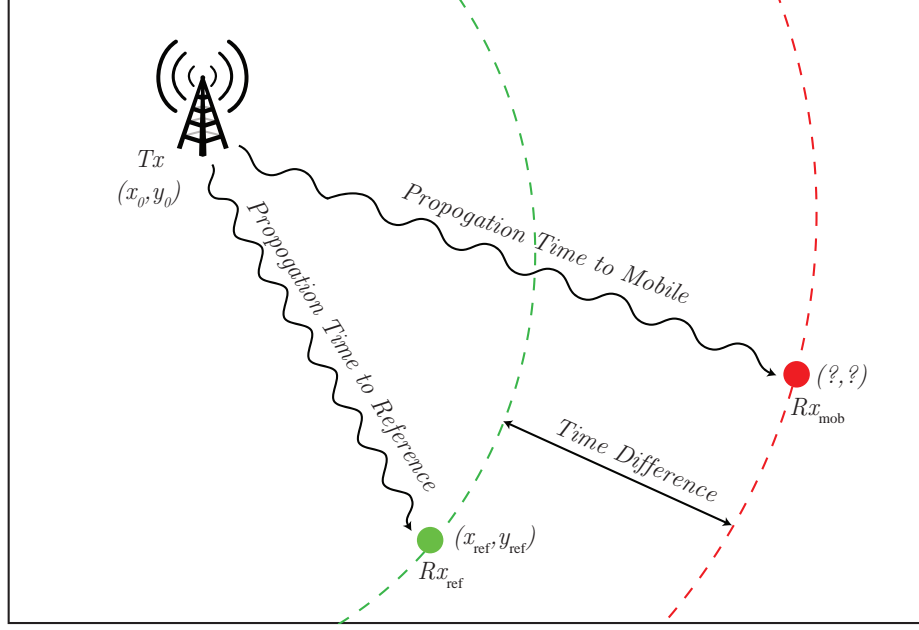
Figure 4:   Range Estimation From TDOA

Removing the assumption that the receivers are synchronized allows for a more generalized development of the range estimate. In the case where no clock bias exists or the receivers are synchronized, the error terms are considered to be zero. The following mathematical development is taken from Eggert [7] and McEllroy [28]. The local received time of the signal from the kth transmitter at each receiver is defined by some universal true time:

$$\hat{t}_{\text{ref}}^{(k)} = t_{\text{ref}}^{(k)} + \epsilon_{\text{ref}} \tag{2}$$

$$\hat{t}_{\text{mob}}^{(k)} = t_{\text{mob}}^{(k)} + \epsilon_{\text{mob}} \tag{3}$$

where

$\hat{t}_{\text{ref}}^{(k)}$ is the reception time at Rx_{ref} of the kth SoOP with respect to its clock,

$\hat{t}_{\text{mob}}^{(k)}$ is the reception time at Rx_{mob} of the kth SoOP with respect to its clock,

$t_{\text{ref}}^{(k)}$ and $t_{\text{mob}}^{(k)}$ are the true reception times of the kth SoOP at each receiver,

ϵ_{ref} and ϵ_{mob} are the reference and mobile receiver clock biases, respectively.

18
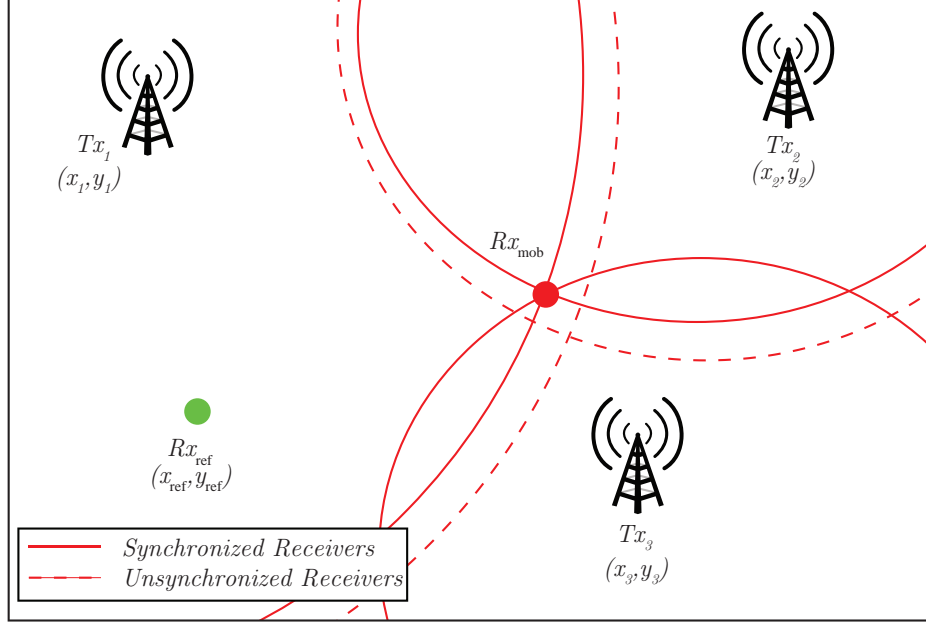
Figure 5:   Estimations From Synchronized and Unsynchronized Receivers

The terms in (2) and (3) are combined, and the true times and biases are grouped. For notational convenience, the superscript is omitted and the TDOA measurement from the kth transmitter is rewritten as

$$
\begin{aligned}
\hat{d} &= \hat{t}_{\mathrm{mob}} - \hat{t}_{\mathrm{ref}} \\
&= (t_{\mathrm{mob}} + \epsilon_{\mathrm{mob}}) - (t_{\mathrm{ref}} + \epsilon_{\mathrm{ref}}) \\
&= \frac{r_{\mathrm{mob}} - r_{\mathrm{ref}}}{c} + \underbrace{(\epsilon_{\mathrm{mob}} - \epsilon_{\mathrm{ref}})}_{\delta t}
\end{aligned}
\tag{4}
$$

where

$\hat{d}$ is the measured TDOA,

r_{mob} and r_{ref} are the actual ranges between the transmitter and receivers,

δt the clock bias difference (system clock bias) in seconds,

c is the speed of light.

Therefore, in an ideal channel (no noise, no multipath, etc.), the entire magnitude of the TDOA error is the system clock bias. This is significant because most applications may not be able to guarantee clock synchronization, or it may not be known if the clocks are synchronized. Therefore, the system clock bias becomes an unknown parameter that must be estimated. Adding another unknown to the system of equations requires the addition of one more transmitter to the minimum number required to compute a solution. For example, to estimate the three-dimensional position of a receiver with system clock bias, a minimum of four transmitters is required.

Separating the TDOA measurement from (4) into terms of known and unknown parameters, the expression becomes

$$
\begin{aligned}
\hat{d} &= \frac{r_{\text{mob}} - r_{\text{ref}}}{c} + \delta t \\
c\hat{d} &= r_{\text{mob}} - r_{\text{ref}} + \underbrace{c\delta t}_{b} \\
c\hat{d} + r_{\text{ref}} &= r_{\text{mob}} + b
\end{aligned}
\tag{5}
$$

where

$(c\hat{d} + r_{\text{ref}})$ is a pseudorange measurement from the transmitter to the Rx_{mob},

r_{mob} is the actual (unknown) range from transmitter to the Rx_{mob},

b is the (unknown) system clock bias with units of meters.

The ranges from (5) are illustrated in Figure 6.

2.2.2 Position Estimation Algorithm.   Continuing with the development from Eggert [7] and McEllroy [28], the unknown parameters from the right-hand side of (5) can be determined. The following development closely follows the GPS positioning calculations by combining (5) and multi-lateration techniques to solve for the unknown parameters. The range from the kth transmitter to the mobile receiver is described in terms of Euclidean distance:
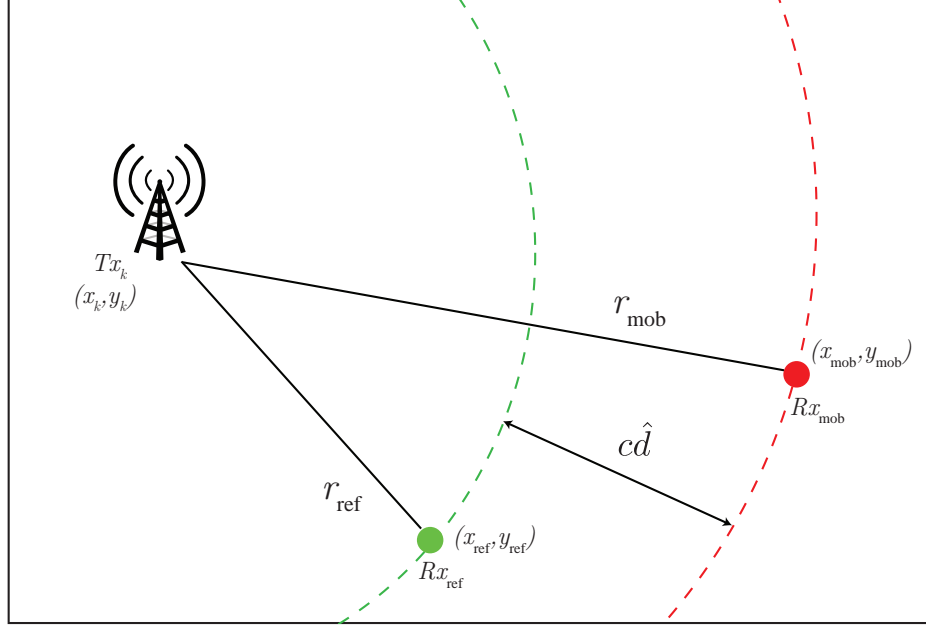
Figure 6:   Visualization of Range Estimation Parameters

$$r_{\text{mob}}^{(k)} = \sqrt{\left(x^{(k)} - x_{\text{mob}}\right)^2 + \left(y^{(k)} - y_{\text{mob}}\right)^2 + \left(z^{(k)} - z_{\text{mob}}\right)^2} \tag{6}$$

where

$r_{\text{mob}}^{(k)}$ is the true range from the kth transmitter to the mobile receiver,

$< x^{(k)}, y^{(k)}, z^{(k)} >$ is the known position of the kth transmitter,

$< x_{\text{mob}}, y_{\text{mob}}, z_{\text{mob}} >$ is the unknown position of the mobile receiver.

Adding the bias to (6) yields a pseudorange (as described in (5)) which represents the measured pseudorange from the TDOA measurement and is given by

$$\rho_{\text{mob}}^{(k)} = r_{\text{mob}}^{(k)} + b \tag{7}$$

where

ρ_{mob}^{k} is the pseudorange from the kth transmitter to the mobile receiver,

r_{mob}^{k} is the true range given in (6).

These equations contain four unknowns, specifically the three coordinates of the mobile receiver $< x_{\text{mob}}, y_{\text{mob}}, z_{\text{mob}} >$ and the system clock bias b. Provided that a minimum of four transmitter sources are able to be measured, the simplest approach is to use the *Newton-Raphson method*. This is an iterative process based on gradient descent which has been specifically derived for the source localization problem by Chan and Ho [19] and for the navigation problem for the two-receiver TDOA system discussed thus far by Eggert [7] and McEllroy [28]. An initial guess for the position mobile receiver $< x_0, y_0, z_0 >$ and of the system clock bias b_0 are used to linearize the equations and then, assuming convergence, iterate until the solution produces an error below a predetermined threshold. Based on the coordinates of the initial guess, a pseudorange from the kth transmitter to the mobile receiver is

$$\rho_0^{(k)} = \sqrt{\left(x^{(k)} - x_0\right)^2 + \left(y^{(k)} - y_0\right)^2 + \left(z^{(k)} - z_0\right)^2} + b_0. \tag{8}$$

Therefore, the difference between the measured psuedorange (using the expression in (7)) and the range estimate using the initial guess (using the expression in (8)) is

$$\Delta\rho^{(k)} = \rho_{\text{mob}}^{(k)} - \rho_0^{(k)}. \tag{9}$$

Rewriting (9) in vector form for a total number of K transmitters gives the observation vector:

$$\boldsymbol{h} = \begin{bmatrix} \Delta\rho^{(1)} \\ \Delta\rho^{(2)} \\ \vdots \\ \Delta\rho^{(K)} \end{bmatrix} \tag{10}$$

Let $\mathbf{x}^{(k)} =< x^{(k)}, y^{(k)}, z^{(k)} >$ be the vector containing the known coordinates of the kth transmitter and $\mathbf{x}_0 =< x_0, y_0, z_0 >$ be the vector containing the coordinates for

22

the initial guess. Using a least squares solution, the corrections to the initial estimate is written as:

$$\begin{bmatrix} \Delta\hat{\mathbf{x}} \\ \Delta\hat{b} \end{bmatrix} = (\mathbf{G}^T\mathbf{G})^{-1}\mathbf{G}^T\boldsymbol{h} \qquad (11)$$

where

$$\mathbf{G} = \begin{bmatrix} (-\boldsymbol{a}^{(1)})^T & 1 \\ (-\boldsymbol{a}^{(2)})^T & 1 \\ \vdots \\ (-\boldsymbol{a}^{(K)})^T & 1 \end{bmatrix} \qquad (12)$$

$$\mathbf{a}^{(k)} = \frac{\mathbf{x}^{(k)} - \mathbf{x}_0}{||\mathbf{x}^{(k)} - \mathbf{x}_0||} \qquad (13)$$

As (11) is solved iteratively, it produces corrections to the initial estimate. The guess is then refined by adding the correction to the guess and repeating the process:

$$\hat{\mathbf{x}} = \mathbf{x}_0 + \Delta\hat{\mathbf{x}} \qquad (14)$$

$$\hat{b} = b_0 + \Delta b \qquad (15)$$

Assuming convergence, the iterations continue until the desired threshold for the magnitude of the output of (11) is met. Once the threshold is met, the values computed in (14) and (15) become the final estimate for the mobile receiver position and the system clock bias, respectively.

2.3 Signal Evaluation

Section 2.2.1 reviewed the TDOA algorithm using the difference of the time of arrival at two receivers. If the receivers are stationary, correlation analysis is performed. If the receivers are in motion, the complex ambiguity function can be

used to extract the time difference. This thesis does not examine the case where the receivers are in motion, however, the reader is referred to Hall [16] and Montminy [30] for further information. Given that the receivers remain stationary for this research, the following section describes how the TDOA can be determined by correlation of the two received signals. First, the general theory of correlation is discussed. Second, the process for determination of the TDOA is derived for an ideal, noiseless case. Third, the ideal process is modified to account for the presence of additive white Gaussian noise (AWGN).

2.3.1 *Correlation Theory.* There are two basic forms of correlation: cross-correlation and auto-correlation. Generally, correlation describes a measure of "similarity" between two signals [26]. The difference between the two forms of correlation involves the inputs to the function. Cross-correlation measures similarity between two different signals, whereas auto-correlation measures similarity between two regions of the same signal. The generalized cross-correlation function of two real signals x and y is

$$R_{xy}(\tau) = E[x(t)y(t-\tau)] \tag{16}$$

where E is the expected value operator. Due to the fact that the signals are observed for a finite observation time, $R_{xy}(\tau)$ can only be estimated. An estimate of the delay is provided by the argument τ that maximizes (16). Assuming ergodicity, (16) can be rewritten as

$$\hat{R}_{xy}(\tau) = \frac{1}{T-\tau} \int_{\tau}^{T} x(t)y(t-\tau)dt \tag{17}$$

where T is the observation time [24, 30]. This expression is for continuous-time cross-correlation. For discrete-time cross-correlation, (17) is written as

24

$$\hat{R}_{xy}(m) = \frac{1}{N} \sum_{n=0}^{N-1} x[n]y[n-m] \qquad (18)$$

2.3.2 Ideal TDOA Measurements Using Correlation. In terms of the two-receiver TDOA case discussed previously, the similarity measured by the cross-correlation is a function of the relative time difference between the signals [26]. The two signals input to the correlation algorithm are modeled as the same signal from a given transmitter where one signal is time delayed relative to the other, as illustrated in Figure 7.
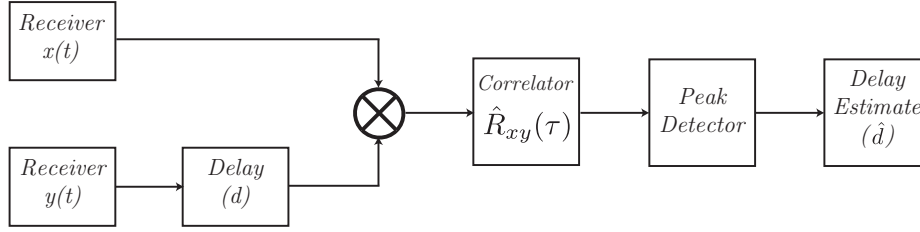
Figure 7:   TDOA Measurement From Correlation

For the general case, let two signals $x(t)$ and $y(t)$ be sampled with a sample interval of Δt. The discrete-time cross-correlation of the two signals $\hat{R}_{xy}$ is given by (18). The correlator processes the sampled signals for a range of time shifts until the cross-correlation peak occurs. The time shift corresponding to the peak is the delay estimate $\hat{d}$. Written in terms of a maximum likelihood (ML) estimator $\hat{d}$ becomes

$$\hat{d} = \arg\max_{m} \left[\hat{R}_{xy}(m) \right] = (\bar{n} - m)\Delta t \qquad (19)$$

where $\bar{n}$ denotes the middle of the time shift index. The difference between m and $\bar{n}$ is the delay estimate in units of samples which is then converted into seconds by multiplying by Δt. This is converted into a TDOA pseudorange measurement by multiplying by the speed of light as described in Section 2.2.1, specifically in (5).

Figure 8 further illustrates this concept of using correlation to detect such a time delay (i.e., measure a TDOA). The plotted output is the cross-correlation of two random signals, both with a length of 6000 samples. The two signals are the same,

except one is shifted in time by 200 samples. Note that the cross-correlation peak occurs 200 samples off the center of the sample index. Therefore, when subtracted from the center of the sample index, the delay estimate is product of the measured 200 samples and the appropriate Δt .
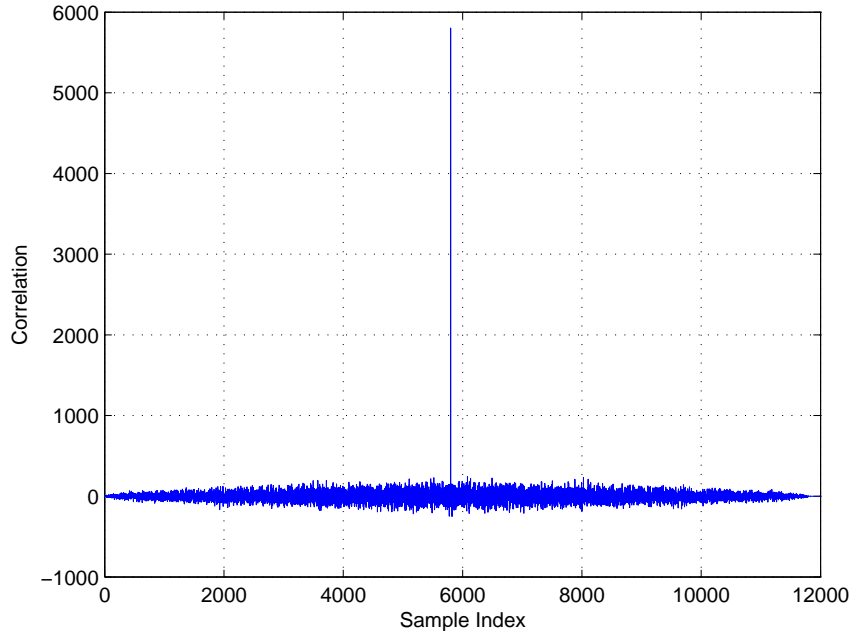
Figure 8:   Cross-Correlation of Sample Signals

2.3.3   Non-ideal TDOA Measurements Using Correlation.   The examples presented thus far have been for an ideal, noiseless channel. In a real-world channel model, noise, multipath, and other interference sources degrade and ultimately distort the signals and affect the delay estimate. Error analysis has shown filtering prior to the correlation improves the accuracy of the delay estimate [15, 24]. The ultimate effect of the filtering accentuates the signal characteristics at which the SNR is the highest and simultaneously suppress the noise from the channel [24]. In the frequency domain, filtering is the same as multiplying the power spectral density by some weighting function. The selection of the weighting function requires some a priori knowledge about the signal and noise characteristics, which may not be available

in a SoOP environment. However, in some SNR conditions it has been shown that the ML estimator (as described in Section 2.3.2) is equivalent to filtering [24]. Advanced techniques like the linear fit peak estimators presented by Eggert and McEllroy enhance performance of the correlator in poor SNR environments [7, 28].

This thesis focuses on a proof-of-concept; therefore, simplifying assumptions are made. To maximize computational efficiency, the general correlator was used without a fit peak estimator. It is also assumed that sufficient a priori information about the channel was not available. Therefore, optimal filtering could not be guaranteed, and as such, filtering was not implemented.

To model the channel for this research, there were many different aspects to account for. Modeling the channel as an AWGN channel provided an adequate model for most of the characteristics [21, 35]. In order to limit the scope of this research to a proof-of-concept, multipath was not accounted for in the channel model. Multipath mitigation is a vital technique to ensure accurate TDOA estimation in channels where multipath occurs. The reader is referred to Eggert [7] and McEllroy [28] for discussion on multipath mitigation techniques.

2.4   Error Statistics

To evaluate the accuracy and effectiveness of the estimators in this research, two quantities are derived: the covariance and the MSE. Inherent in the discussion of the covariance measurement is the CRLB. As discussed in this chapter, the range estimator output provides the input to the position estimator. Hence it is beneficial to examine the theoretical bound for both estimators in terms of the CRLB as well as the statistics gathered from simulations. This section first examines the derivation for the CRLB of the range and position estimates, followed by a discussion of the generalized variance, and concludes with an explanation of the MSE.

2.4.1   CRLB Derivation.   The CRLB assumes an unbiased estimator (in this case either range or position) and is the theoretical lower bound for the variance [19].

This section explicitly derives the CRLB for the baseline, two-receiver case presented in the preceeding sections. This serves as background for the derivation of the CRLB for variations of the estimator presented in Chapter III.

    2.4.1.1 CRLB on Range Estimation.   Section 2.2.1 describes the theoretical delay from which a range estimate is computed in (7). Section 2.3.2 expands on this concept and describes the measured delay in terms of a ML estimator. The following result for the CRLB of the TDOA range estimate is rigorously derived by Hahn and Tretter [15] and again discussed by Chan and Ho [19]. Whereas both of these works define the TDOA vector in terms of a source localization problem, the TDOA measurements presented here are in terms of the navigation problem. Recall the definition for the TDOA measurement from the kth transmitter as defined in (4). Let the vector of all TDOA measurements be defined as

$$\hat{\boldsymbol{d}} = [\hat{d}_1 \ \hat{d}_2 \ ... \ \hat{d}_K]^T \tag{20}$$

Each measurement in $\hat{\boldsymbol{d}}$ is dependent on both the signal and the noise which are assumed to be mutually independent, zero mean, stationary Gaussian random processes. The estimated TDOAs are distributed

$$\hat{\boldsymbol{d}} \backsim \mathcal{N}(\boldsymbol{d}, \boldsymbol{Q}) \tag{21}$$

where $\boldsymbol{d}$ is the vector similar to $\hat{\boldsymbol{d}}$ containing the actual TDOA measurements and $\boldsymbol{Q}$ is

$$\boldsymbol{Q} \;=\; \left\{ \frac{2T}{2\pi} \int_0^{\Omega} \omega^2 \frac{S(\omega)^2}{1 + S(\omega)\mathrm{tr}\boldsymbol{N}(\omega)^{-1}} \right.$$
$$\left. \times \left[\mathrm{tr}\left(\boldsymbol{N}(\omega)^{-1} \right) \boldsymbol{N}_p(\omega)^{-1} - \boldsymbol{N}_p(\omega)^{-1}\mathbf{1}\mathbf{1}^T\boldsymbol{N}_p(\omega)^{-1} \right] d\omega \right\}^{-1}. \tag{22}$$

Here,

T is the observation time,

0 to Ω is the frequency band processed,

$S(\omega)$ is the signal power spectrum,

$\boldsymbol{N}(\omega)$ is the noise power spectral matrix,

$\boldsymbol{N}_p(\omega)$ is the lower right $K - 1$ by $K - 1$ partition of $\boldsymbol{N}(\omega)$,

$\mathbf{1}$ is a vector of unity which has the same size as $\boldsymbol{N}_p(\omega)$.

Assumptions about the characteristics allow (22) to be simplified. Let the signal and noise spectra be defined as

$$S(\omega) = \varepsilon \ , \ 0 \le \omega \le \Omega \tag{23}$$

$$N(\omega) = \frac{N_0}{2} \ , \ 0 \le \omega \le \Omega \tag{24}$$

Under this assumption, everything except the ω^2 term in (22) is constant over the frequency band. The noise is further assumed to be spatially incoherent, which allows for the simplification of $\boldsymbol{Q}$ as described by Chan and Ho [19]:

$$\boldsymbol{Q} = \frac{1}{2} g^{-1} \begin{bmatrix} K-1 & -1 & -1 & \ldots & -1 \\ -1 & K-1 & -1 & \ldots & -1 \\ \vdots & \vdots & \vdots & \vdots & \vdots \\ -1 & -1 & -1 & \ldots & K-1 \end{bmatrix}^{-1} \tag{25}$$

$$g = \frac{T}{2\pi} \int_0^\Omega \omega^2 \frac{S(\omega)^2/N(\omega)^2}{1 + KS(\omega)/N(\omega)} d\omega \tag{26}$$

This expression for $\boldsymbol{Q}$ of the range estimate in (25) and (26) incorporates the assumptions made for the characteristics of the signal and noise that are consistent with the model used for this research.

29

2.4.1.2 CRLB on Position Estimation. The CRLB derivation of the position estimate has been rigorously developed for the source localization problem [11, 15, 19, 39]. The derivation of the CRLB of the position estimate for the navigation problem discussed in this research is presented in Section 3.4.2. The general CRLB for the case of a vector parameter and Gaussian observations is presented here using the derivation presented by Kay [21]. Let the vector of Gaussian observations be distributed

$$x \backsim \mathcal{N}(\boldsymbol{\mu}(\boldsymbol{\theta}), \boldsymbol{C}(\boldsymbol{\theta})) \tag{27}$$

where both the mean and covariance may depend on $\boldsymbol{\theta}$. The CRLB is

$$\mathrm{COV}(\boldsymbol{\theta}) \geq \boldsymbol{B} \tag{28}$$

$$\boldsymbol{B}_{ij} = \left[\left(\frac{\partial \boldsymbol{\mu}}{\partial \theta_i} \right)^T \boldsymbol{C}^{-1} \left(\frac{\partial \boldsymbol{\mu}}{\partial \theta_j} \right) + \frac{1}{2} \mathrm{tr} \left(\boldsymbol{C}^{-1} \frac{\partial \boldsymbol{C}}{\partial \theta_i} \boldsymbol{C}^{-1} \frac{\partial \boldsymbol{C}}{\partial \theta_j} \right) \right]^{-1} \tag{29}$$

For the specific case where the covariance is not a function of the parameter to be estimated $\boldsymbol{\theta}$, the distribution becomes

$$x \backsim \mathcal{N}(\boldsymbol{\mu}(\boldsymbol{\theta}), \sigma^2 \boldsymbol{I}) \tag{30}$$

which simplifies the expression for the CRLB to

$$\boldsymbol{B}_{ij} = \frac{1}{\sigma^2} \left[\left(\frac{\partial \boldsymbol{\mu}}{\partial \theta_i} \right)^T \left(\frac{\partial \boldsymbol{\mu}}{\partial \theta_j} \right) \right]^{-1} \tag{31}$$

2.4.2 Generalized Variance. In this research, both the CRLB and simulated data provide a covariance matrix describing characteristics of the estimator. In the case of the position estimate, and, assuming the error distribution is Gaussian, these matrices can be overlaid with the biased position estimate (or true position for an

unbiased estimator) to provide intuition of the relative accuracies of the final position estimate. From the covariance matrix, the circular error probable (CEP) can be approximated or error ellipses can be defined. Both of these measures offer intuition about geometric accuracy of the estimator. A similar measure of the covariance that reduces the matrix to some scalar value is computed by taking the determinant of a portion of the covariance matrix. Let the covariance matrix of the parameter $\boldsymbol{\theta}$ be

$$\text{COV}(\boldsymbol{\theta}) = \boldsymbol{C} \tag{32}$$

To illustrate the potential need to partition $\boldsymbol{C}$, consider the case described in Section 2.2.2. Using that estimator, $\boldsymbol{C}$ is a 3×3 matrix where the elements of the third row and third column are functions of the system clock bias. In terms of the position estimate, the relevant position data is contained in the upper left 2×2 partition:

$$\boldsymbol{C}_p = \begin{bmatrix} C_{1,1} & C_{1,2} \\ C_{2,1} & C_{2,2} \end{bmatrix} \tag{33}$$

The determinant of $\boldsymbol{C}_p$ results in a scalar in units of meters raised to the fourth power (m^4). Therefore, the fourth root of the determinant produces a scalar in units of meters and will herein be referred to as the "generalized variance":

$$\sigma_g = |\boldsymbol{C}_p|^{1/4} \tag{34}$$

The generalized variance is used in this research to plot the CRLB of an estimator and to compare covariance data from simulation outputs.

2.4.3 MSE Calculation. The true usefulness of the error statistics ultimately lies in how well the mathematical assumptions correspond to the actual navigational measurements. Thus far, the error statistics have relied on the assumption that the

measurement error has zero-mean and the variance is known on the basis of a priori information and has known covariances with other measurements. In the case where the bias value is known to be present but the value is unknown, the total MSE can be described by the variance due to the random error plus the square of the error bias [11, 21].

To define the MSE, let the bias of a general estimator $\hat{\theta}$ of the parameter θ be

$$\text{Bias}(\hat{\theta}) = \text{E}\left[\hat{\theta} - \theta\right]. \tag{35}$$

The MSE for $\hat{\theta}$ is

$$
\begin{aligned}
\text{MSE}(\hat{\theta}) &= \text{E}\left[(\hat{\theta} - \theta)^2\right] \\[2ex]
&= \text{E}\left[\left\{(\hat{\theta} - \text{E}[\hat{\theta}]) + (\text{E}[\hat{\theta}] - \theta)\right\}^2\right] \\[2ex]
&= \text{E}\left[(\hat{\theta} - \text{E}[\hat{\theta}])^2\right] + (\text{E}[\hat{\theta}] - \theta)^2 \\[2ex]
&= \text{VAR}(\hat{\theta}) + \text{Bias}(\hat{\theta})^2. \tag{36}
\end{aligned}
$$

2.5 Summary

This chapter provided the background necessary for further discussion of the exploitation of AM SoOP for navigation using TDOA measurements. First, the characteristics of broadcast AM signals were discussed. Next, the TDOA positioning algorithm was derived followed by a discussion of TDOA estimation. Finally, the different measures of error statistics were discussed, including the CRLB, the generalized variance, and MSE. This chapter provided a review of existing work which served as a technical baseline for the new material that is presented in the following chapters.

III. Methodology

This chapter describes the methodology used for performing the proof-of-concept simulations for AM SoOP navigation using TDOA measurements. Chapter II provided the background, and this chapter synthesizes those concepts into the overall methodology. First, an overview of the simulation environment is provided, and each functional component in the system model is explained. This forms the basis for the baseline simulation using the TDOA algorithm from Chapter II. Second, the model is expanded into cases where error is inserted into the a priori data, as well as cases where assumptions about the a priori data are removed and the estimation algorithms for such cases are derived. Third, the order of simulation and description of the simulation environment are provided. Fourth, the error statistics are further derived from Chapter II.

3.1 System Model Overview

In order to successfully engage in the proof-of-concept simulations, the baseline simulation environment must first be established for comparison to the new estimation algorithms. The system model arranged generic AM transmitters in real-world configurations, and simulated signals were transmitted from each station. Receivers collected and sampled the signals received through an AWGN channel. Pseudoranges were computed from the TDOA algorithm discussed in Chapter II, and a two-dimensional position estimate was produced along with the estimated system clock bias. The system model used for the simulation environment in this research is shown in Figure 9.

The blocks for the modulator and demodulator and the simulation of multipath and path loss are shaded to indicate where those functions could be added; however, for this simulation environment, they were not included. The *baseline* simulation will herein refer to the implementation of the baseline TDOA estimation algorithm discussed in Chapter II in the final block of the system block diagram. Specifically, the baseline simulation incorporated the true known positions for the transmitters and
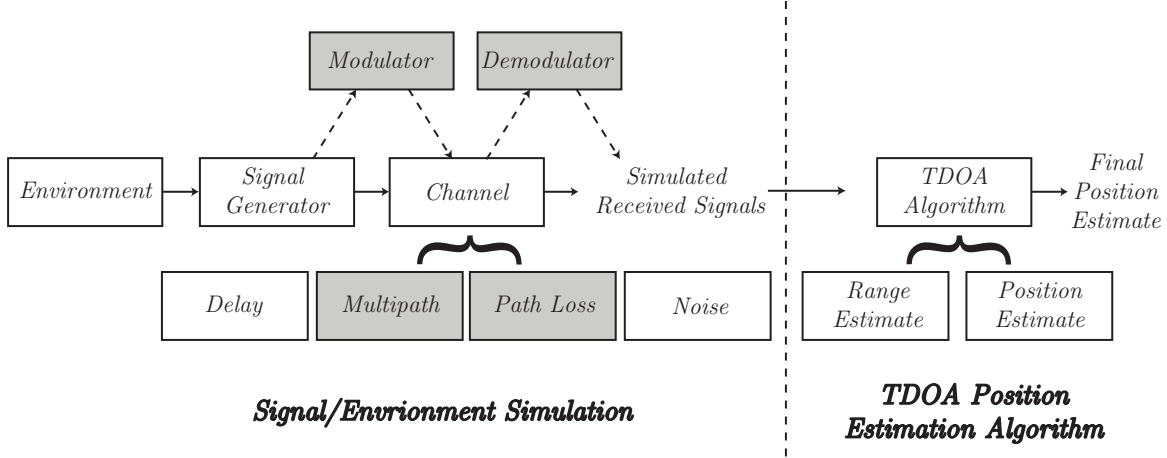
Figure 9:   System Block Diagram (Inactive Blocks Shaded)

the reference receiver in the calculation of the final position estimate. The baseline simulation was used to validate the simulation environment and used to compare the performance of the new estimation algorithms presented in this research. The following sections discuss each block in the system block diagram. All simulations were executed using Matlab® .

3.1.1   Environment.   There are two components to the Environment block: the locations of the transmitters and the locations of the receivers. The construction of the transmitter configurations is discussed followed by a description of the receiver configurations.

3.1.1.1   Transmitter Configurations.   To generate realistic AM transmission environments, FCC data was used to place the transmitters [9]. The FCC database contained two-dimensional information for each transmitter and provided the relative distance and angle from any one of the transmitters. This conveniently allowed for the transmitters to be placed using a generic coordinate system in the simulation environment. The reference transmitter (from which all distances and angles were computed in the FCC database) was centered at $(0,0)$, and the remaining transmitters were placed using the range and angle data. A total of six transmitter configurations were generated. One configuration was arbitrarily generated (not using

34

any FCC data). The remaining five configurations were chosen from locations across the United States based on uniqueness relative to the other configurations and the ability to compare to previous work (if applicable). The six configurations are shown in Figure 10.

Previous research included real-world signal collections in Boston, MA [16] and Cincinnati, OH [7, 28]. As such, AM configurations from both cities were used. Phoenix, AZ, Seattle, WA, and Los Angeles, CA all presented unique transmitter configurations compared to the other configurations. In previous sections, the inaccuracies of the transmitter position data is noted. In the simulation environment, this is not a concern as the true transmitter positions are defined in the environment. Furthermore, the interest is primarily in generating representative transmitter configurations so that the proof-of-concept simulations closely model real-world conditions.

3.1.1.2 Receiver Configurations. The relative position of either the reference or mobile receiver to the transmitters affects the accuracy of the TDOA measurement and overall system output. Therefore, it was prudent to ensure that a sufficient number of variations were examined. The local coordinates of the transmitters remained constant and the coordinates of the reference and mobile receivers were changed based on the simulation type. For all receiver configurations, the reference receiver(s) was placed in the same location, and the mobile receiver position was varied. Figure 11 displays the four possible receiver configurations for a two-receiver TDOA computation. Note that the reference receivers labeled Rx_{Ref2} and Rx_{Ref3} are only used in the multiple reference receiver estimator case presented in Section 3.2.3.

Selecting a transmitter configuration and receiver configuration pair allowed for the computation of the LOS propagation time from each transmitter to each receiver. This simulated time was needed to ultimately simulate the TDOA. For a given transmitter and receiver pair, the LOS propagation time is

$$t_{prop} = \frac{\sqrt{(x_{Rx} - x_{Tx})^2 + (y_{Rx} - y_{Tx})^2 + (z_{Rx} - z_{Tx})^2}}{c}, \tag{37}$$
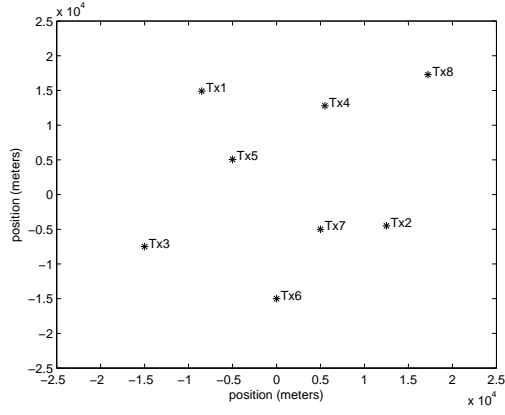
(a) Arbitrary
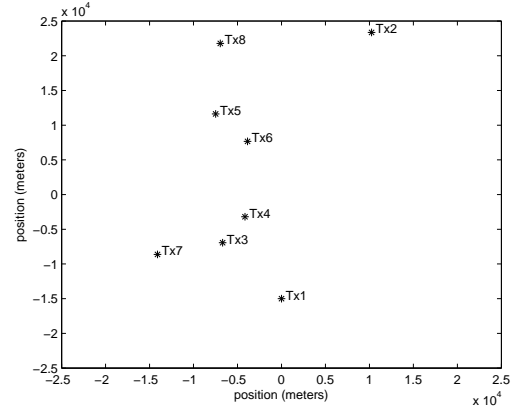
(b) Cincinnati
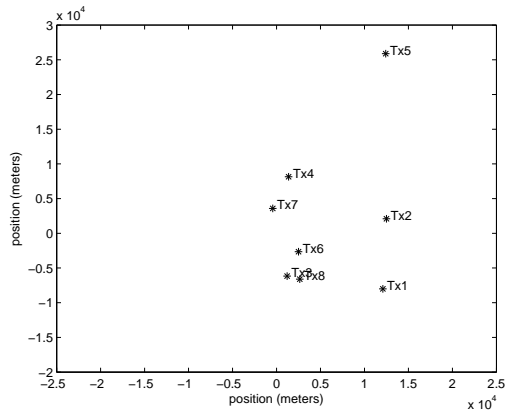
(c) Phoenix
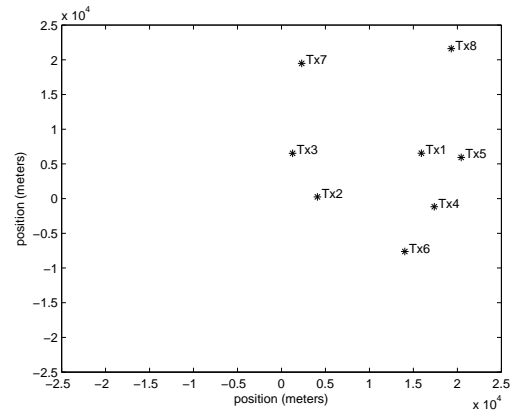
(d) Seattle
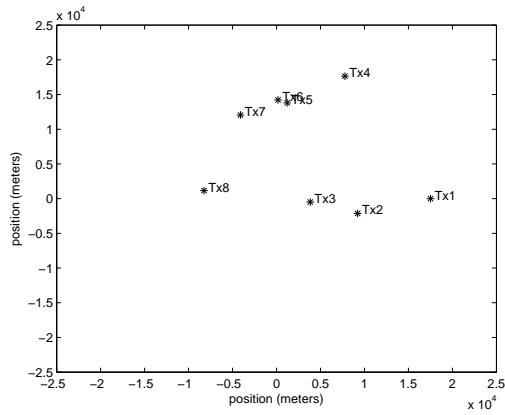
(e) Boston
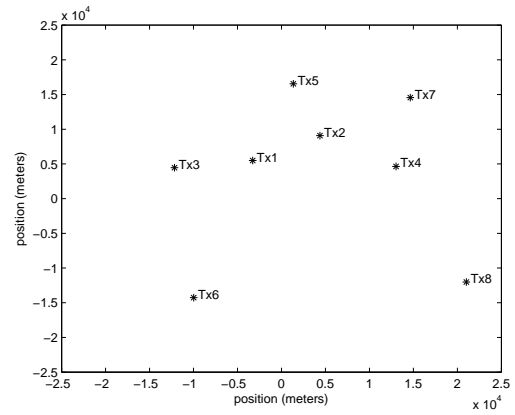
(f) Los Angeles

Figure 10:   Transmitter Configurations

36
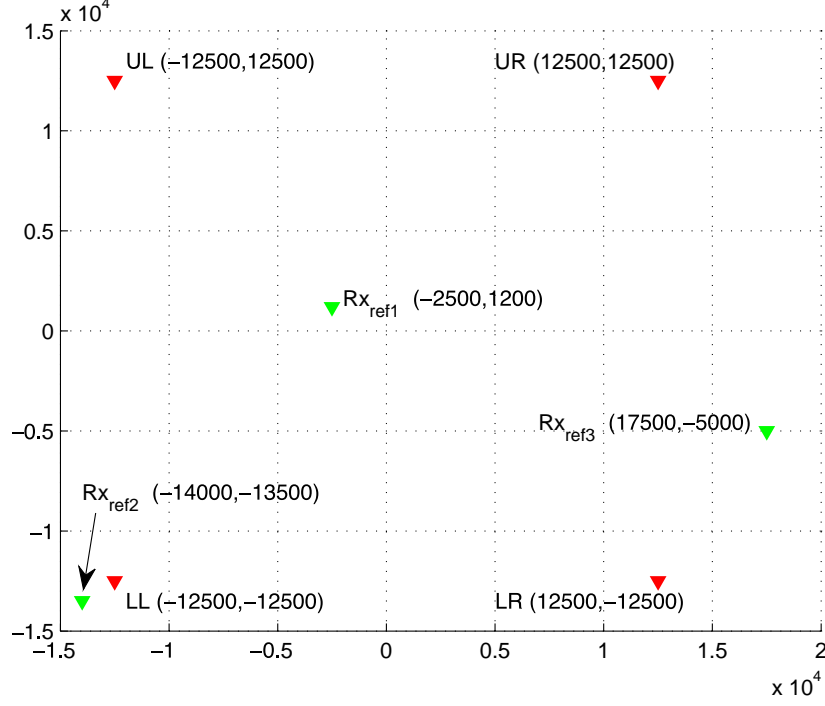
Figure 11:   Receiver Configurations

where

(x_{Rx}, y_{Rx}, z_{Rx}) are the coordinates of the receiver,

(x_{Tx}, y_{Tx}, z_{Tx}) are the coordinates of the transmitter,

c is the speed of light.

3.1.2   AM Signal Generator.   To create the AM signals, message signals of two types were selected: voice and music. These were selected to be representative of the general content of broadcast AM stations. All samples were from various sources in Waveform Audio File Format (WAV) and were sampled at 44.1 kHz. The signals are briefly characterized in Table 1.

A basic broadcast AM signal was modeled after (1). The inputs to $m(t)$ were previously discussed, and the values for the remaining parameters are readily available from the FCC and individual broadcast AM stations.

Table 1: Message Signal Descriptions

Transmitter #	Type	Description
1	Voice	Talk Radio (Male Voices)
2	Voice	Talk Radio (One Male Voice)
3	Voice	Talk Radio (One Male Voice)
4	Voice	Recorded Speech (One Male Voice)
5	Both	Talk Radio (Male Voices & Music)
6	Music	Male Lead Singer
7	Voice	Talk Radio (One Male Voice)
8	Voice	Talk Radio (One Male Voice)

For computational efficiency, the signals were simulated at baseband, that is, not actually modulated and demodulated. Since this research deals only in a simulation environment, the advantages to operating at bandpass, such as smaller antenna size, are not able to be exploited [41]. Furthermore, examples have been used to illustrate how the number of simulation steps and corresponding simulation time are both significantly reduced by simulating at baseband. The main disadvantage to simulation at baseband is that only the spectral bandwidth around the carrier frequency is represented. Non-linear behavior outside of the baseband frequencies is lost, for example, carrier frequency harmonics [12]. However, for this proof-of-concept, the simulation environment is only required to be representative so that the basic structure and results are meaningful in application. Such phenomena that are excluded by simulating at baseband would unnecessarily complicate the results and make analysis of the results unreliable. Therefore, computational efficiency outweighed the disadvantages and the simulations were conducted at baseband.

In a real-world system, both receivers would sample a section of the AM signal. For this simulation, each receiver sampled the first 10000 samples of the simulated AM signals.

3.1.3 Channel. In this system model, the channel is the sole source of errors introduced to the transmitted signals. As seen in Figure 9, there are four components to the channel block: delay, multipath, path loss, and noise.

3.1.3.1 Delay.   From the configurations described in Section 3.1.1.1 the average magnitude of distance between transmitters was 10^0 to 10^1 km. The propagation time is computed in (37). The average magnitude of the propagation time for the average distances of the transmitters and receivers in the simulation was 10 to 100 μsec. In order to adequately simulate the delay of the signals, they were upsampled using linear interpolation so that the correlation algorithm could detect a reasonably small delay. Therefore, the signal data were sampled at 10 MHz. This was based on the determination that the Nyquist sampling rate was 40 kHz based on the knowledge that the maximum possible frequency in the voice or music message signal was approximately 16 kHz.

Given that the simulation environment was sampled at 10 MHz, the sample period T_s was 0.1 μsec, sufficiently below any delay given the transmitter and receiver configurations. This corresponds to a distance of approximately 29.98 meters, which was the lower limit on the fidelity of the simulation environment. For distances smaller than 29.98 meters, the simulation would be unable to quantize the delay and the TDOA algorithm unable to detect it (since it would not detect any delay present).

To account for the propagation delay, the communication signals discussed in Section 3.1.2 were input in the channel function along with the corresponding propagation time as calculated in (37). Using the sampling frequency $f_s = 10$ MHz and the corresponding sample period, the quantized delay was

$$d_{quant} = \frac{t_{prop}}{T_s} \tag{38}$$

where the delay was rounded to the nearest integer value. The delayed signal was shifted such that the value at the index of the shift was moved to the initial position. The signal was zero-padded at the end of the function to preserve equal signal lengths. This concept is illustrated in Figure 12 where the delayed signal is actually time-advanced, resulting in a 5 sample relative delay between the two signals.

Original Signal $\boxed{A}\boxed{B}\boxed{C}\boxed{D}\boxed{E}\boxed{F}\boxed{G}\cdots\boxed{Q}\boxed{R}\boxed{S}\boxed{T}\boxed{U}\boxed{W}$

5-sample Delay

zero-padding

Delayed Signal $\boxed{F}\boxed{G}\boxed{H}\boxed{I}\boxed{J}\boxed{K}\boxed{L}\cdots\boxed{V}\boxed{W}\boxed{0}\boxed{0}\boxed{0}\boxed{0}$

Sample Index: 1 2 3 4 5 6 7 $\cdots$
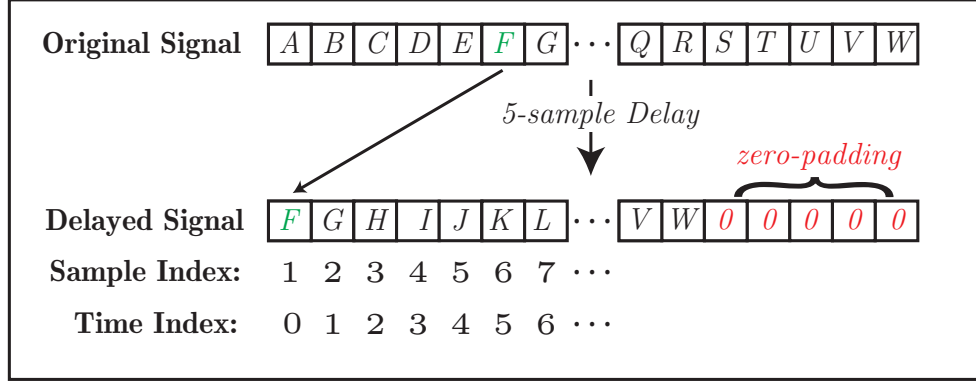
Time Index: 0 1 2 3 4 5 6 $\cdots$

Figure 12:   Zero-padding to Simulate Signal Delay

The following example depicts the output of the whole process and how the quantized delay appears in the simulation environment. The original signal is a sine wave; this is analogus to the signals generated as a result of the discussion in Section 3.1.2. In this example, the $d_{quant} = 5$ samples or equivalently a time delay of 0.5 μsec. This delay is shown in Figure 13.

Overall, the effect of applying the delay to the simulated signals allowed for the TDOA algorithm to estimate a delay and output a position estimate. However, a real-world channel does not simply delay a signal. There are other aspects of the channel that must also be accounted for.

3.1.3.2   Multipath.   As described in Section 1.3, multipath was not considered in this proof-of-concept simulation. However, since multipath is a real-world source of significant error, the position to insert such a channel characteristic was included.

3.1.3.3   Path Loss.   Similar to simulating multipath as part of the channel, the path loss could affect the accuracy of the received signal and the position estimate. For simplicity of the proof-of-concept, path loss was not explicitly accounted for as part of the channel. The block is left as an indication of where path loss would be accounted for. In this simulation, the path loss was generally accounted for as

40
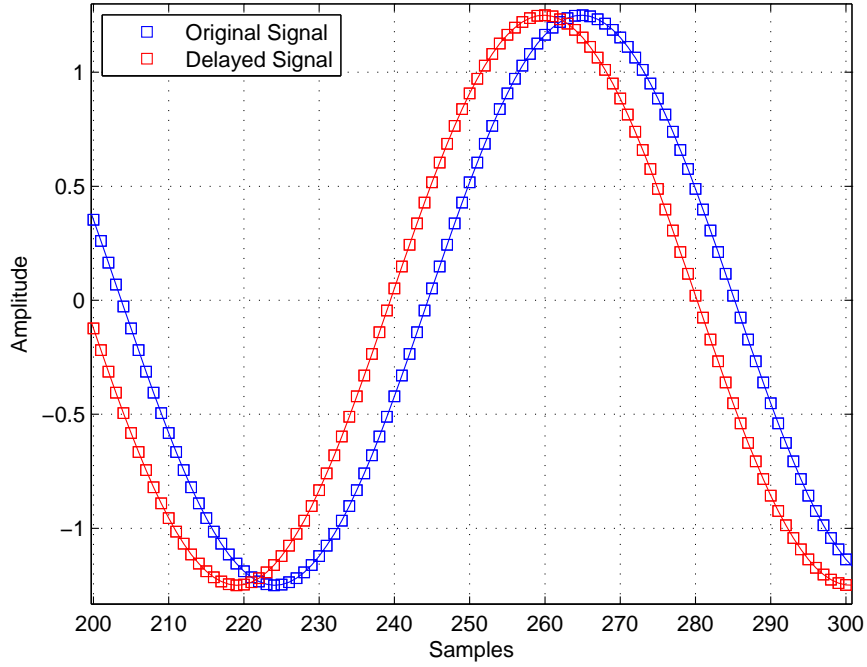
Figure 13:   Sample of 0.5 μsec Delay

part of the overall SNR, hence the signal degradation over the channel was fully consolidated in the simulation of the channel noise.

3.1.3.4   Noise.   The final step in the channel was to add noise to the signal. As discussed in Section 2.3.3, AWGN is a sufficient representative of real-world noise. The Matlab® awgn function was utilized for this purpose. The parameters of the awgn function allowed for the overall channel SNR to be regulated by the amount of noise (relative to the existing signal power). The awgn function calculated the signal power and adjusted the noise power to output the desired SNR in dB. SNR is the ratio of the average signal power to the average noise power and is of the form shown in (39), obtained from [7] and [28].

$$SNR_{dB} = 10 \log_{10} \left(\frac{P_{signal}}{P_{noise}} \right) \tag{39}$$

3.1.4   TDOA Algorithm.   The final step in the system was to input the received signal into the TDOA algorithm. This algorithm consisted of the computation of a range estimate from the mobile receiver (Section 2.3) to the transmitter and subsequently the computation of the ML estimate for the mobile position of the receiver and the system clock bias (Section 2.2).

3.1.4.1   Range Estimation.   Recall from Section 2.2.2 that a range estimate from the transmitter to the mobile receiver must exist to begin the iterations using the baseline estimation algorithm. The TDOA measurement is required to compute the range estimate for the transmitter to the mobile receiver given by (5). As detailed in Section 2.3, cross-correlation is the among the techniques that are considered low-complexity and computationally efficient.

The real-time data link required no actual implementation in the simulation environment — it inherently existed. The inputs to the correlation algorithm were two signals from the same transmitter that had the appropriate channel effects added to simulate the received signal at each receiver. The mean was computed and subtracted from each received signal then the two signals were cross-correlated using the `Matlab`® `xcorr` function. The index of the peak value was identified and subtracted from the middle of the index according to (19), and the result was the quantized TDOA. The quantized TDOA was multiplied by the sample period T_s to convert it into units of time. From this measurement, the pseudorange from the transmitter to the mobile receiver was computed according to (5). This process is shown in Figure 14.
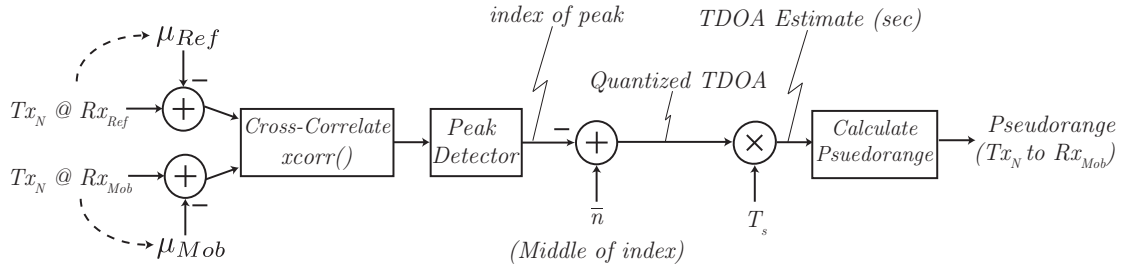

Figure 14:   TDOA Measurement via Cross-Correlation

42

3.1.4.2 Position Estimation. The TDOA pseudoranges were computed for all of the transmitters to the mobile receiver. This was accomplished by repeating the process described in Section 3.1.4.1 for all received signals. These signals were grouped into a vector and given as an input to the baseline estimation algorithm as described in Section 2.2.2 and specifically as part of the input to (11).

The other part to the baseline estimation algorithm was the initial guess. For the baseline simulation, all coordinates were in a relative frame. The initial estimate was (0,0) based on the fact that the system assumes that the mobile receiver could be anywhere in the frame and had an equal probability of being in any quadrant. Different configurations test the effect of distance between the initial guess and the true position of the mobile receiver. The initial guess for the system clock bias (herein referred to as "clock bias") was 0 sec.

The baseline estimation algorithm is an iterative process. The number of iterations directly depends on the threshold set on the output of (14) and (15). The magnitude of these thresholds can be tailored based on previous knowledge of the environment, desired accuracy if one direction is not a critical as others, computation time, and other considerations. For this simulation, the threshold was set based on the best possible outcome due to the sampling frequency f_s. For the distance coordinates, the correction threshold is set to 10^{-6} meters — that is, the algorithm iterates until the estimated position error for each coordinate drops below the threshold. For the clock bias, the threshold was set at 10^{-9} meters. This threshold corresponds to a clock bias of approximately 3.3×10^{-18} seconds which is a sufficiently low correction to the clock bias given that some systems may have a clock bias of up to 10^{-5} seconds. If the threshold conditions are not met in under 100 iterations, the estimate at the 100th iteration is considered the final estimate and the iteration process is aborted.

3.2 Variations on Baseline Estimator

The algorithm development in Chapter II and the simulation environment discussed in this chapter thus far have been based on the two-receiver baseline model

where the positions of the transmitters and the reference receiver were known a priori. This section discusses how the simulation environment was modified to simulate the removal of those assumptions as well as present the derivation for three additional position estimation algorithms referred to herein as "estimators."

3.2.1 Imprecise Prior Information. To examine the effect of imprecise a priori information, two cases are presented. The first case is imprecise a priori transmitter position information. The second case is imprecise a priori reference receiver position information.

3.2.1.1 Imprecise Transmitter Positions. To analyze the effect of imprecise transmitter positions, the simulation environment was produced in the same way as discussed in Section 3.1, and the true coordinates of the transmitters were used to generate the AM signals and the corresponding delays. The true coordinates were also used in the range and position estimation algorithms. Therefore, erroneous transmitter position data was generated to replace the truth data as inputs to both algorithms. Given that the errors from the FCC may be up to or exceed 100 meters, and most site surveys can be accomplished with an accuracy of approximately $\pm$ 10 meters [16], the error for each transmitter coordinate is distributed (in units of meters)

$$\epsilon_{Tx_x}^{(k)} \backsim \mathcal{U}[-15, 15] \tag{40}$$

The built-in $\texttt{Matlab}^{\circledR}$ function $\texttt{rand}$ was used to generate the errors which were then combined for for the vector $\boldsymbol{\epsilon}_{Tx}$ — the vector of error parameters for each coordinate of each transmitter. Figure 15 shows the error parameter generation and the modification to the system block diagram from Figure 9.

The result is that the truth data was used only to generate the signals. The erroneous transmitter positions were then used in the range estimate described in Section 2.2.1 and the position estimate in Section 2.2.2.
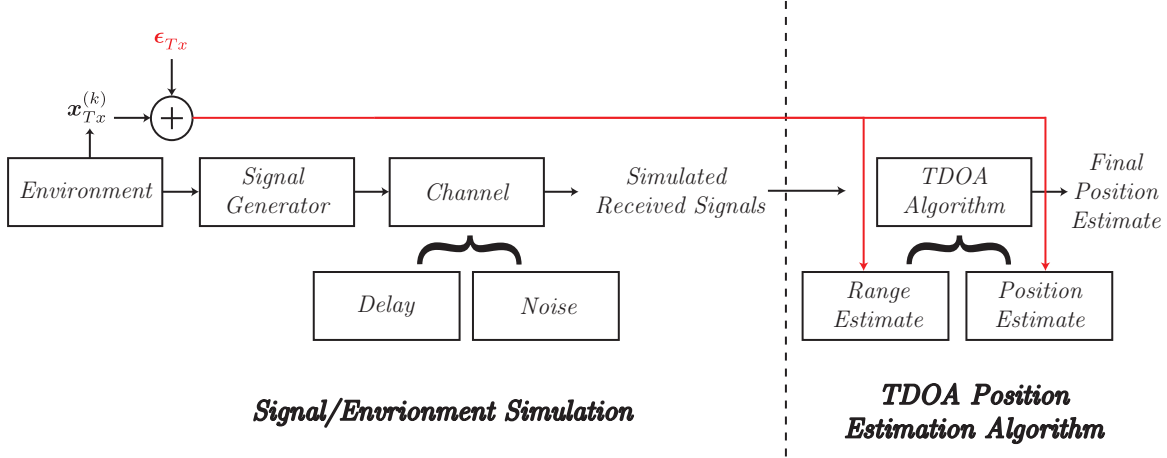
Figure 15:   Simulated Error in Transmitter Position

3.2.1.2   Imprecise Reference Receiver Position.   The exact position of the transmitter was one component of the a priori knowledge that enabled both estimators to produce a final estimate. The other component required for the estimator was the exact position of the reference receiver. Specifically, the position of the reference receiver was explicitly used in the TDOA calculation of the range estimate described in Section 2.2.1. The error parameter is distributed (in units of meters)

$$\epsilon_{\text{ref}} \backsim \mathcal{N}(\mathbf{0}, \sigma^2 \boldsymbol{I}), \sigma = 25 \text{ meters} \tag{41}$$

This parameter is created using the built-in `Matlab`® function `randn`. The normal distribution is justified based on the fact that the error may be from an imprecise GPS position, a "last known" position, or simply a guess of the position. Figure 16 shows the inserted position error. The dashed line to the position estimate block indicates that the coordinates of the reference receiver are not a direct input to the baseline estimation algorithm. However, the direct effect on the range estimate does impact the accuracy of the final position estimate.

3.2.2   Two-Unknown Receivers Estimator.   In the previous section, the case of an imprecise a priori position for the reference receiver was explored. It is also
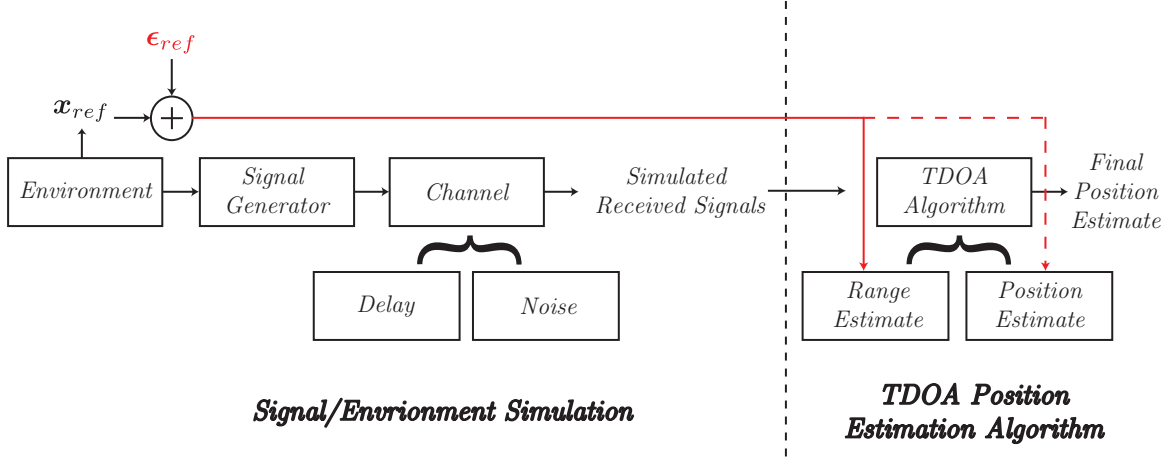
45

Figure 16:   Simulated Error in Reference Receiver Position

worth examining the related case where a reference receiver is known to be present but there is no a priori position information. Given this case, the estimator now has two or three additional unknowns to solve for (either a two or three dimensional position estimate). The immediate impact is that there must be enough transmitters present to estimate the coordinates for the mobile receiver, the clock bias, and the new unknown set of coordinates for the reference receiver.

The desire is to derive a ML estimator similar to (11) that computes corrections to an initial guess. To derive an estimator for this case, a two-dimensional position estimate is considered. The following derivation closely follows that from Section 2.2.2. Let the vector of unknown parameters be defined

$$\boldsymbol{x} = [x_m \ \ y_m \ \ x_r \ \ y_r \ \ b]^T \tag{42}$$

where

x_m is the unknown x coordinate of Rx_{mob},

y_m is the unknown y coordinate of Rx_{mob},

x_r is the unknown x coordinate of Rx_{ref},

y_r is the unknown y coordinate of Rx_{ref},

b is the unknown clock bias in meters.

46

As compared to the derivation in Chapter II, the unknown position of the reference receiver is the only addition to the vector of unknown parameters. Therefore, the model relating the true position and clock bias to the observations is still linear, similar to other derivations where only one receiver was unknown [15, 19, 39]. Specifically, the model for this case is

$$c\hat{\boldsymbol{d}} = \boldsymbol{Gx} + \boldsymbol{w} \tag{43}$$

where

c is the speed of light,

$\hat{\boldsymbol{d}}$ is the vector containing the TDOA values as described in Section 2.4.1.1,

$\boldsymbol{G}$ is the *observation matrix* (see (47)),

$\boldsymbol{w}$ is the AWGN noise vector as described in Section 3.1.3.4.

Since the desire is to generate the ML correction estimate, let the correction vector be

$$\Delta\boldsymbol{x} = [\Delta x_m \ \ \Delta y_m \ \ \Delta x_r \ \ \Delta y_r \ \ \Delta b]^T. \tag{44}$$

Given that the linearized model still holds true, the general expression for a ML estimator of $\Delta\boldsymbol{x}$ is

$$\Delta\hat{\boldsymbol{x}} = (\mathbf{G}^T\mathbf{G})^{-1}\mathbf{G}^T\boldsymbol{h} \tag{45}$$

where the terms for $\boldsymbol{G}$ and $\boldsymbol{h}$ must be derived for the new five-element $\Delta\boldsymbol{x}$. For the case derived in Section 2.2.2, $\boldsymbol{h}$ was the sum of the TDOA measurement and the known distance between the transmitters and the reference receiver. In this case, the latter distance is no longer a known quantity. Therefore, the only remaining element in the measurement vector $\boldsymbol{h}$ is the TDOA measurement. Let the elements

47

of the measurement vector be the difference between the observed TDOA $c\hat{d}^{(k)}$ and the distance between the receivers given the initial guess $c\hat{d}_0^{(k)}$:

$$\boldsymbol{h} = [(c\hat{d}^{(1)} - c\hat{d}_0^{(1)}) \ (c\hat{d}^{(2)} - c\hat{d}_0^{(2)}) \ \ldots \ (c\hat{d}^{(K)} - c\hat{d}_0^{(K)})]^T \tag{46}$$

The elements of the observation matrix $\boldsymbol{G}$ are defined as

$$\boldsymbol{G} = \begin{bmatrix} \frac{\partial c\hat{d}^{(1)}}{\partial x_m} & \frac{\partial c\hat{d}^{(1)}}{\partial y_m} & \frac{\partial c\hat{d}^{(1)}}{\partial x_r} & \frac{\partial c\hat{d}^{(1)}}{\partial y_r} & \frac{\partial c\hat{d}^{(1)}}{\partial b} \\ \frac{\partial c\hat{d}^{(2)}}{\partial x_m} & \frac{\partial c\hat{d}^{(2)}}{\partial y_m} & \frac{\partial c\hat{d}^{(2)}}{\partial x_r} & \frac{\partial c\hat{d}^{(2)}}{\partial y_r} & \frac{\partial c\hat{d}^{(2)}}{\partial b} \\ \vdots & \vdots & \vdots & \vdots & \vdots \\ \frac{\partial c\hat{d}^{(K)}}{\partial x_m} & \frac{\partial c\hat{d}^{(K)}}{\partial y_m} & \frac{\partial c\hat{d}^{(K)}}{\partial x_r} & \frac{\partial c\hat{d}^{(K)}}{\partial y_r} & \frac{\partial c\hat{d}^{(K)}}{\partial b} \end{bmatrix} \tag{47}$$

To explicitly solve for the elements of $\boldsymbol{G}$, the kth term of the first column of $\boldsymbol{G}$ is examined first. The partial derivative simplifies to

$$\begin{aligned} \frac{\partial c\hat{d}^{(k)}}{\partial x_m} &= \frac{\partial}{\partial x_m}(r_{\text{mob}}^{(k)} - r_{\text{ref}}^{(k)} + b) \\ &= \frac{1}{2\sqrt{(x_k - x_m)^2 + (y_k - y_m)^2}}\bigg(-2(x_k - x_m)\bigg) \\ &= -\frac{(x_k - x_m)}{r_{\text{mob}}^{(k)}} \end{aligned} \tag{48}$$

By analogy, this extends to the other derivatives with respect to y_m, x_r, and y_r. The bias term differentiates to 1 just as in (11). Therefore, $\boldsymbol{G}$ is rewritten

$$\boldsymbol{G} = \begin{bmatrix} -\frac{(x_1 - x_m)}{r_{\text{mob}}^{(1)}} & -\frac{(y_1 - y_m)}{r_{\text{mob}}^{(1)}} & \frac{(x_1 - x_r)}{r_{\text{ref}}^{(1)}} & \frac{(y_1 - y_r)}{r_{\text{ref}}^{(1)}} & 1 \\ -\frac{(x_2 - x_m)}{r_{\text{mob}}^{(2)}} & -\frac{(y_2 - y_m)}{r_{\text{mob}}^{(2)}} & \frac{(x_2 - x_r)}{r_{\text{ref}}^{(2)}} & \frac{(y_2 - y_r)}{r_{\text{ref}}^{(2)}} & 1 \\ \vdots & \vdots & \vdots & \vdots & \vdots \\ -\frac{(x_K - x_m)}{r_{\text{mob}}^{(K)}} & -\frac{(y_K - y_m)}{r_{\text{mob}}^{(K)}} & \frac{(x_K - x_r)}{r_{\text{ref}}^{(K)}} & \frac{(y_K - y_r)}{r_{\text{ref}}^{(K)}} & 1 \end{bmatrix} \tag{49}$$

Using these definitions for $\boldsymbol{h}$ and $\boldsymbol{G}$, the Newton-Raphson method is again implemented such that the final estimate is

$$\hat{\boldsymbol{x}} = \boldsymbol{x_0} + \Delta\hat{\boldsymbol{x}} \tag{50}$$

where $\hat{\boldsymbol{x}}$ is the vector containing the sum of the initial guess for all five unknown parameters and all corrections such that a predetermined threshold is met similar to the terms in (14) and (15).

3.2.3 Multiple Reference Receivers Estimator. As a mitigation technique to combat errors in the a priori knowledge, multiple reference receivers may be added to the system. In this research, the multiple reference receiver algorithm is developed around the baseline algorithm presented in Section 2.2.2. Specifically, the position of all of the reference receivers was known. The method of computing a position estimate remains the same iterative method described for the baseline case. The expression for $\boldsymbol{G}$ and $\boldsymbol{h}$ are modified to account for additional observations from the additional reference receivers. The additional observations are similar to multiple instances of the baseline case that are combined to form a single expression. Any number of reference receivers may be added to the system. For example if there are K transmitters and a two-dimensional estimate was desired, $\boldsymbol{G}$ would be $K \times 3$. Adding more reference receivers such that there is a total of three reference receivers, two additional clock bias estimates become required. In this example, the vector of unknown parameters is

$$\Delta\boldsymbol{x} = [\Delta x_m \ \ \Delta y_m \ \ \Delta b_1 \ \ \Delta b_2 \ \ \Delta b_3]^T. \tag{51}$$

In this case, $\boldsymbol{G}$ becomes a 24×5:

$$G = \begin{bmatrix} -\frac{(x_1-x_m)}{r_m^{(1)}} & -\frac{(y_1-y_m)}{r_m^{(1)}} & 1 & 0 & 0 \\ \vdots & \vdots & \vdots & \vdots & \vdots \\ -\frac{(x_k-x_m)}{r_m^{(K)}} & -\frac{(y_k-y_m)}{r_m^{(K)}} & 1 & 0 & 0 \\ \\ -\frac{(x_1-x_m)}{r_m^{(1)}} & -\frac{(y_1-y_m)}{r_m^{(1)}} & 0 & 1 & 0 \\ \vdots & \vdots & \vdots & \vdots & \vdots \\ -\frac{(x_k-x_m)}{r_m^{(K)}} & -\frac{(y_k-y_m)}{r_m^{(K)}} & 0 & 1 & 0 \\ \\ -\frac{(x_1-x_m)}{r_m^{(1)}} & -\frac{(y_1-y_m)}{r_m^{(1)}} & 0 & 0 & 1 \\ \vdots & \vdots & \vdots & \vdots & \vdots \\ -\frac{(x_k-x_m)}{r_m^{(K)}} & -\frac{(y_k-y_m)}{r_m^{(K)}} & 0 & 0 & 1 \end{bmatrix} \tag{52}$$

where the first two columns repeat every K rows with the possible exception of the addition of different clock bias estimates between the multiple reference receivers and the mobile receiver. Using the same example, there would be two additional sets of TDOA-based pseudorange measurements computed using the positions of the additional reference receivers:

$$\boldsymbol{h} = [\Delta\rho_{r1}^{(1)} \quad \ldots \quad \Delta\rho_{r1}^{(K)} \; \Delta\rho_{r2}^{(1)} \quad \ldots \quad \Delta\rho_{r2}^{(K)} \; \Delta\rho_{r3}^{(1)} \quad \ldots \quad \Delta\rho_{r3}^{(K)}]^T \tag{53}$$

where the subscript indicates the reference receiver position that the range estimate is based on and $\Delta\rho^{(k)}$ is generally defined in (7).

3.2.4 Transmitter Position Correction Estimator. The estimator proposed in this section is similar to the case described in Section 3.2.1.1 where the a priori transmitter positions are known to contain errors (within some bound), except the desire is to estimate the error in the transmitter positions and correct it to improve the accuracy of the estimate of the mobile receiver. The number of known param-

eters must still exceed the number of unknown parameters in order to be able to solve the system of equations. Therefore, in this case, there will be a certain number of precisely known transmitter positions, and instead of the baseline estimator (as described in Section 3.2.1.1), the multiple reference receiver scenario is implemented and the corresponding estimator altered. For the purposes of presenting the transmitter position correction estimator (herein referred to as the "transmitter correction estimator"), the case of two unknown transmitters is considered. In the simulations, the erroneous transmitters are the seventh and eighth transmitters. For the explanation of the concept, the two erroneous transmitters are generically labeled here as the first and second transmitters. The position of the three reference receivers are known and accurate, and the position of the mobile receiver, the clock biases, and the two erroneous transmitter positions are to be estimated. Therefore, the vector of unknown parameters is

$$\Delta \boldsymbol{x} = [\Delta x_m \ \Delta y_m \ \Delta x_{T1} \ \Delta y_{T1} \ \Delta x_{T2} \ \Delta y_{T2} \ \Delta b_1 \ \Delta b_2 \ \Delta b_3]^T \qquad (54)$$

where x_{Ti} and y_{Ti} indicate the erroneous x or y coordinate of the transmitters. There is no change to the linear model described in (43); therefore, given the number of reference receivers, $\boldsymbol{G}$ is the same matrix described in (52) except the partial derivative terms now reflect the elements of the vector shown in (54). The partial derivative terms for the first two columns are the same and repeat every K rows in the same way described in the Section 3.2.3:

$$\boldsymbol{G}_{mobile} = \begin{bmatrix} -\frac{(x_1 - x_m)}{r_m^{(1)}} & -\frac{(y_1 - y_m)}{r_m^{(1)}} \\ -\frac{(x_2 - x_m)}{r_m^{(2)}} & -\frac{(y_2 - y_m)}{r_m^{(2)}} \\ -\frac{(x_3 - x_m)}{r_m^{(3)}} & -\frac{(y_3 - y_m)}{r_m^{(3)}} \\ \vdots & \vdots \\ -\frac{(x_K - x_m)}{r_m^{(K)}} & -\frac{(y_K - y_m)}{r_m^{(K)}} \end{bmatrix} \qquad (55)$$

51

The clock bias columns also repeat and share the same pattern as in (52). The unique part of this estimator is in the terms expressing the partial derivative of the TDOA measurement with respect to the x and y coordinates of the erroneous transmitters. Using the model for the TDOA measurements described in (48), for this example, the columns containing these terms take the form

$$
\boldsymbol{G}_{Tx1}^{(ri)} = \begin{bmatrix} \left(\dfrac{(x_1 - x_m)}{r_m^{(1)}} - \dfrac{(x_1 - x_{ri})}{r_{ri}^{(1)}} \right) & \left(\dfrac{(y_1 - y_m)}{r_m^{(1)}} - \dfrac{(y_1 - y_{ri})}{r_{ri}^{(1)}} \right) \\ 0 & 0 \\ \vdots & \vdots \\ 0 & 0 \end{bmatrix}
\tag{56}
$$

$$
\boldsymbol{G}_{Tx2}^{(ri)} = \begin{bmatrix} 0 & 0 \\ \left(\dfrac{(x_2 - x_m)}{r_m^{(2)}} - \dfrac{(x_2 - x_{ri})}{r_{ri}^{(2)}} \right) & \left(\dfrac{(y_2 - y_m)}{r_m^{(2)}} - \dfrac{(y_2 - y_{ri})}{r_{ri}^{(2)}} \right) \\ 0 & 0 \\ \vdots & \vdots \\ 0 & 0 \end{bmatrix}
\tag{57}
$$

where the ri superscript indicates the reference receiver. This pattern repeats for as many reference receivers as are present. The final estimator for the three reference receiver case is written as

$$
\boldsymbol{G} = \begin{bmatrix} \boldsymbol{G}_{mobile} & \boldsymbol{G}_{Tx1}^{(r1)} & \boldsymbol{G}_{Tx2}^{(r1)} & \boldsymbol{1}_{K \times 1} & \boldsymbol{0}_{K \times 1} & \boldsymbol{0}_{K \times 1} \\ \boldsymbol{G}_{mobile} & \boldsymbol{G}_{Tx1}^{(r2)} & \boldsymbol{G}_{Tx2}^{(r2)} & \boldsymbol{0}_{K \times 1} & \boldsymbol{1}_{K \times 1} & \boldsymbol{0}_{K \times 1} \\ \boldsymbol{G}_{mobile} & \boldsymbol{G}_{Tx1}^{(r3)} & \boldsymbol{G}_{Tx2}^{(r3)} & \boldsymbol{0}_{K \times 1} & \boldsymbol{0}_{K \times 1} & \boldsymbol{1}_{K \times 1} \end{bmatrix}
\tag{58}
$$

The observation vector $\boldsymbol{h}$ contains the TDOA measurements as described in (46). The difference between the estimator described in Section 3.2.2 and this estimator is that the positions of the reference receivers are all known (so that the quantity of known parameters outnumbers the quantity of unknown parameters). Therefore, the

52

known positions of the reference receivers are combined with the measured TDOAs and the $\boldsymbol{h}$ for this case becomes the vector described in (53).

For the simulation of this estimator, the transmitter errors were inserted to the a priori data as described in Section 3.2.1.1, except that only two transmitter positions were altered. Once corrections to the transmitter positions were computed, they were added to the a priori data just as the corrections to the mobile receiver and clock bias were added to the initial guess. In this scenario, the error of the transmitter was known to be present and the magnitude of the error was bounded. Therefore, as the algorithm iterates, a check was put in place to ensure that all corrections to the initial data did not place the transmitter position estimate outside of the bound. If any correction caused the transmitter position estimate to exceed the bound, the correction from that iteration was omitted.

3.3   Simulation Test Environments

The previous sections discussed the baseline simulation and the subsequent variations that can be made to it. This section discusses the order in which these simulations were executed and explains the needed modifications to the baseline simulation (if any). Table 2 outlines the different variations of simulations performed.

The environment geometry is herein defined as the combination of the transmitter configuration and the receiver configuration detailed in Section 3.1.1.1 and Section 3.1.1.2, respectively. Each of the six transmitter configurations were paired with the four receiver configurations to create the total number of environment geometries. All of the environment geometry combinations were subjected to each of the simulation conditions and estimators listed in Table 2. Furthermore, within each environment geometry, a total of 100 observations were taken for each SNR value. A total of 26 SNR values were simulated where the range was from -10 dB to 10 dB in 1 dB steps and then from 20 dB to 60 dB in 10 dB steps, unless otherwise noted in Chapter IV.

Table 2:   Simulation Variations

	Simulation	A Priori		True b	Error		Estimated		
#	Description	Rx_{ref}	Tx	(sec)	Rx_{ref}	Tx	Rx_{mob}	b	Rx_{ref}
1	Baseline w/ Bias	✓	✓	0			✓	✓	
2	Baseline w/o Bias	✓	✓	10^{-7}			✓	✓	
3	Tx Uncertain	✓	✓	0		✓	✓	✓	
4	Rx_{ref} Uncertain	✓	✓	0	✓		✓	✓	
5	Tx/Rx_{ref} Uncertain	✓	✓	0	✓	✓	✓	✓	
6	Two-Unk w/ Bias		✓	0	N/A		✓	✓	✓
7	Two-Unk w/o Bias		✓	10^{-7}	N/A		✓	✓	✓
8	Multi-Ref w/ Bias	✓	✓	0			✓	✓	
9	Multi-Ref w/o Bias	✓	✓	Varies*			✓	✓	
10	Tx Correction	✓	✓	0		⌣	✓	✓	

*For three reference receivers the true biases are $10^{-7}, 5 \times 10^{-6}$, and 2×10^{-5}.
The "⌣" symbol indicates that error is added to two transmitters only.

For additional clarity of Table 2, the a priori data columns indicate the truth data available to the estimator to calculate the position estimate. The true bias b column shows the clock bias between the receivers that was inserted to the simulation. The error column indicates whether or not an error was inserted into the a priori data (as described in Section 3.2.1). The estimated column indicates which parameters the output of the estimator contained. Since Simulation #10 was the only estimator that output transmitter position estimates, it was not explicitly noted in Table 2. Also, the initial conditions described in Section 3.1.4.2 are true for all cases except Simulation #6 and #7. In order to ensure convergence, the initial guess was 2 km off in both coordinates for the reference receiver and 1 km off in both coordinates for the mobile receiver. The clock bias initial guess remained 0 sec.

3.4   Accuracy and Error Statistics

For each of the simulations detailed in Table 2, the MSE of the range estimate and position estimate were computed as described in Section 2.4.3. The simulation also allowed for the bias, variance/covariance, and generalized variance to be examined for a particular combination of simulation parameters or environment geometries.

The simulated statistics may be compared to each other or may be discussed (if not directly compared) to the theoretical bounds derived in the CRLB. The CRLB for the range estimate was derived in Section 2.4.1.1. The CRLB derivations presented here use the general forms discussed by Foy [11] and Torrieri [39], with specific assumptions and notation based on Chan and Ho [19] and Martin et al. [27]. A general CRLB for the baseline estimator was presented in Section 2.4.1.2. The following sections explicitly derive the CRLB for the two-unknown receiver estimator, the multiple reference receiver estimator, and the transmitter correction estimator.

3.4.1   CRLB for Baseline Estimator.   The CRLB for estimating the unknown position of Rx_{mob} is similar to the well-developed CRLB for the source localization problem. Since this CRLB is defined here specifically for the baseline case, let the baseline parameter vector be similar to the vector solved for in Section 2.2.2:

$$\boldsymbol{x}_b = [x_m \ \ y_m \ \ b]^T. \tag{59}$$

where the subscripted "b" indicates the vector contains the parameters for the baseline case. The estimator described in Section 2.2.2 is an implementation of a ML estimator of a vector of TDOA measurements which is known to be asymptotically Gaussian with a covariance matrix given by $\boldsymbol{Q}$ from (25) [15, 19]. Recall from (5) and (7) that the measurement vector consisted of the sum of the measured TDOAs and the known range between Rx_{ref} and the transmitters. Let the measurement vector or pseudoranges to the mobile receiver be explicitly defined here as

$$\boldsymbol{\rho}_m = [(r_m^{(1)} + b) \ \ (r_m^{(2)} + b) \ \ \dots \ \ (r_m^{(K)} + b)]^T \tag{60}$$

Therefore, the conditional probability density function (PDF) of the measurement vector $\boldsymbol{\rho}_m$ is

$$p(\boldsymbol{\rho}_m|\boldsymbol{x}_b) \;=\; \frac{1}{(2\pi)^{\frac{K}{2}}|\boldsymbol{Q}|^{\frac{1}{2}}}$$
$$\times \exp\left[-\frac{1}{2}\left(\boldsymbol{\rho}_m - \boldsymbol{r}_m\right)^T \boldsymbol{Q}^{-1}\left(\boldsymbol{\rho}_m - \boldsymbol{r}_m\right)\right] \tag{61}$$

where it is noted that $\boldsymbol{r}_m$ is a function of the position of the mobile receiver and the clock bias, as in (59).

A parallel is drawn between the source localization CRLB derivation by Chan and Ho [19] and the desired expression for the CRLB for the baseline estimator. For the source localization problem, the conditional PDF is computed based on the TDOA measurement vector and the estimated position. In this baseline navigation case, the TDOA measurement vector is replaced by the pseudorange vector which, as discussed, is the same as the TDOA measurement vector with the known constant of the range between Rx_{ref} and the transmitters added to it. Therefore, since only a scalar — independent of the TDOA measurement and the position of Rx_{mob} — is added to the TDOA measurement vector, the derivation presented by Chan and Ho is applied to this case.

Each position coordinate of Rx_{mob} can be expressed as a nonlinear function of the pseudorange measurement $\boldsymbol{\rho}_m$, namely the TDOA measurement. Using Taylor-series expansion around the pseudorange vector, the bias and variance of the position are found to be proportional to the pseudorange covariance matrix $\boldsymbol{Q}$. If the TDOA variations are sufficiently small such that the variance is the dominant error term compared to the bias, the estimator is considered unbiased and the CRLB on $\boldsymbol{x}_b$ is

$$\text{COV}(\boldsymbol{x}_b) \geq \left\{\text{E}\left[\left(\frac{\partial}{\partial \boldsymbol{x}_b}\ln p(\boldsymbol{\rho}_m|\boldsymbol{x}_b)\right)\left(\frac{\partial}{\partial \boldsymbol{x}_b}\ln p(\boldsymbol{\rho}_m|\boldsymbol{x}_b)\right)^T\right]\right\}^{-1} \tag{62}$$

The partial derivative of the log-likelihood term is

$$\frac{\partial}{\partial \boldsymbol{x}_b} \ln p(\boldsymbol{\rho}_m | \boldsymbol{x}_b) = \frac{\partial \boldsymbol{r}_m}{\partial \boldsymbol{x}_b} \boldsymbol{Q}^{-1} (\boldsymbol{\rho}_m - \boldsymbol{r}_m) \tag{63}$$

This simplifies the CRLB expression to

$$\mathrm{COV}(\boldsymbol{x}_b) \geq \left(\frac{\partial \boldsymbol{r}_m}{\partial \boldsymbol{x}_b}^T \boldsymbol{Q}^{-1} \frac{\partial \boldsymbol{r}_m}{\partial \boldsymbol{x}_b} \right)^{-1} \tag{64}$$

The partial derivative terms are equivalent to the derivation shown in (48). Given that the partial derivative of the vector $\boldsymbol{x}_b$ contains three elements, the CRLB simplifies to

$$\mathrm{COV}(\boldsymbol{x}_b) \geq \left(\boldsymbol{G}_b^T \boldsymbol{Q}^{-1} \boldsymbol{G}_b \right)^{-1} \tag{65}$$

where $\boldsymbol{G}_b$ is the matrix $\boldsymbol{G}$ defined in (12).

3.4.2 CRLB for Two-Unknown Receivers Estimator. This section derives the CRLB for the estimation technique detailed in Section 3.2.2. The parameter vector $\boldsymbol{x}$ is defined in (42). In Section 3.4.1, the conditional PDF was derived for the pseudorange measurement $\boldsymbol{\rho}_m$ based on the known range between Rx_{ref} and the transmitters. In the case considered here, the range is no longer known and the position of Rx_{ref} must be estimated. Therefore, the conditional PDF of the vector containing the TDOA measurements (multiplied by the speed of light for unit consistency) $c\hat{\boldsymbol{d}}$ is

$$
\begin{aligned}
p(c\hat{\boldsymbol{d}} | \boldsymbol{x}) &= \frac{1}{(2\pi)^{\frac{K}{2}} |\boldsymbol{Q}|^{\frac{1}{2}}} \\
&\quad \times \exp\left[-\frac{1}{2} \left(\boldsymbol{d} - \left(\frac{\boldsymbol{r}_{\mathrm{TDOA}}}{c} \right) \right)^T \boldsymbol{Q}^{-1} \left(\boldsymbol{d} - \left(\frac{\boldsymbol{r}_{\mathrm{TDOA}}}{c} \right) \right) \right]
\end{aligned} \tag{66}
$$

$$\boldsymbol{r}_{\mathrm{TDOA}} = \boldsymbol{r}_{\mathrm{mob}} - \boldsymbol{r}_{\mathrm{ref}} + b \tag{67}$$

57

where $\boldsymbol{r}_{\text{TDOA}}$ is the vector containing the range between the receivers (in units of meters) and is a function of the position of the receivers and the clock bias $\boldsymbol{x}$.

Assuming that the TDOA variations are sufficiently small such that the estimator may be considered unbiased, the expression for the CRLB from (62) is modified:

$$\text{COV}(\boldsymbol{x}) \geq \left\{ \text{E}\left[\left(\frac{\partial}{\partial \boldsymbol{x}} \ln p(c\hat{\boldsymbol{d}}|\boldsymbol{x}) \right) \left(\frac{\partial}{\partial \boldsymbol{x}} \ln p(c\hat{\boldsymbol{d}}|\boldsymbol{x}) \right)^{T} \right] \right\}^{-1} \tag{68}$$

Similar to the simplification shown in Section 3.4.1 the partial derivatives are shown to simplify the CRLB to

$$\text{COV}(\boldsymbol{x}) \geq \left(\boldsymbol{G}^{T}\boldsymbol{Q}^{-1}\boldsymbol{G} \right)^{-1} \tag{69}$$

where $\boldsymbol{G}$ is the matrix defined in (49).

3.4.3   CRLB for Multiple Receivers and Transmitter Correction Estimators.
The distribution of the observations given the position of the mobile receiver for the multiple reference receiver and the transmitter correction estimator is the same as that shown in (66). Therefore, for both estimators the CRLB is of the form shown in (69). For the multiple reference receiver estimator $\boldsymbol{G}$ is the matrix in (52) and for the transmitter correction estimator, $\boldsymbol{G}$ is the matrix in (58).

3.5   Summary

This chapter outlined the methodology for synthesizing the concepts presented in Chapter II into an executable simulation. First, a description of the system model was provided. Second, the baseline simulation was altered to examine the effects of errors in the a priori data and additional estimators were derived. Third, the order of simulation execution was discussed. Fourth, additional derivations were presented for the CRLB for all of the position estimators.

IV. Results and Analysis

This chapter presents the simulated results using the simulation environment and estimation techniques detailed in Chapter III. The chapter begins with the presentation of the theoretical bounds of the estimators as computed using the CRLB. The results from the simulations are then presented. The chapter concludes with a summary and overall findings from the simulations. Portions of the following results and the related findings were presented in [34].

4.1 Theoretical Simulations

The CRLB for the range estimator was derived in Section 2.4.1.1, and for the position estimators in Sections 3.4.1 and 3.4.2. This section presents the simulated results of the these theoretical bounds. The range estimate CRLB is presented, followed by the the CRLB for the baseline, two-unknown receiver, and multiple-reference receiver estimators. To allow greater intuition as to the meaning of the CRLB surface plots for the position estimates, the values have been plotted in meters by taking the fourth root of the generalized variance, which produced a standard deviation. However, since the CRLB is typically discussed in terms of variance, the values presented are discussed in terms of "root of the variance" to relate it to the output of the CRLB expression. Also note that the transmitter correction estimator has been omitted for reasons to be discussed in Section 4.2.5.3.

4.1.1 Range Estimate CRLB. The simplifying assumptions about the noise characteristics mentioned in Section 2.4.1.1 were used to simplify the CRLB expression to the form shown in (25) and (26). To compute an exact solution, the remaining parameters were identified using the quantities from the simulation environment. The number of transmitters K was known given the transmitter configuration, therefore $K = 8$. The observation time was a function of the sampling period and the total number of samples, "N." In this case,

$$T = T_s \times N \tag{70}$$

In the simulation environment, $T_s = 0.1$ μsec as discussed in Section 3.1.3.1 and $N = 10,000$ samples as discussed in Section 3.1.2. Therefore, $T = 1$ $m$sec. The frequency band parameter was the bandwidth of the message signal that was broadcast. Section 2.1 discussed how the approximate bandwidth of AM signals is 50 Hz to 16 kHz. Therefore, the quantity presented as $(0, \Omega)$ becomes $(50, 16 \times 10^3)$ Hz.

As presented in Section 2.4.1.1, both the signal and noise were assumed to be uniform over the entire frequency range. As a result, the signal and noise terms appear as a ratio in the CRLB expression. The simulation environment examined a maximum of 26 SNR values, so the CRLB for each SNR was computed and is shown in Figure 17.
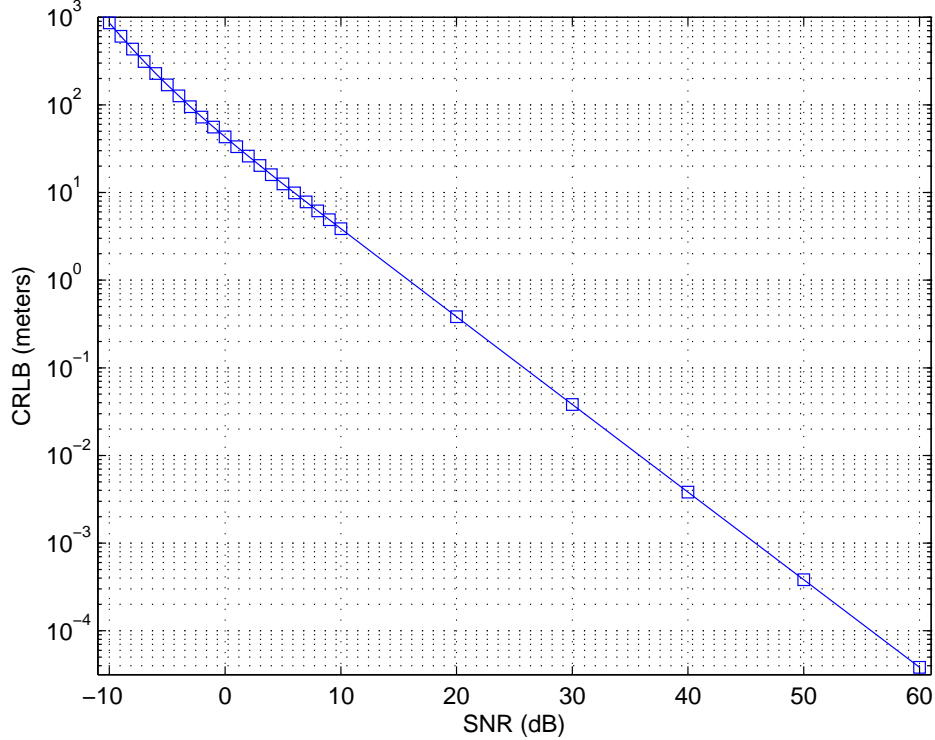
Figure 17:   Range Estimate CRLB

4.1.2 Baseline Estimator CRLB. The CRLB for the baseline estimator was derived in Seciton 3.4.1. To compute the CRLB surface, the true positions of the transmitters were input to $\boldsymbol{G}$. For the x and y coordinates spaced every 75 meters the fourth root of the determinant of the upper 2×2 of the covariance matrix was computed, similar to the generalized variance discussed in Section 2.4.2. For the purposes of computing $\boldsymbol{Q}$, SNR = 20 dB. The results are shown in Figure 18. Note that the color scale spans 3.0 meters to 15.0 meters. The six transmitter configurations show that if the receivers were able to be within the the range of the transmitters, the root of the variance was minimized.

4.1.3 Two-Unknown Receivers Estimator CRLB. The process for computing the CRLB surface described in Section 4.1.2 was repeated for the two-unknown receiver estimator using the corresponding $\boldsymbol{G}$. Since two receiver positions were estimated, the correct position for the reference receiver was input to the matrix, given that the position of the mobile receiver was the position of interest. The results are shown in Figure 19. The range of the color scale increased relative to the baseline CRLB, and regions of high variance are observed around the location of the reference receiver at (-2500, 1200). This indicates that the estimator would degrade in accuracy if the two receivers were close to each other, even with an accurate estimate of the reference receiver position. Plots showing the ratio of difference between this estimator and the baseline estimator CRLB are provided in Appendix A.1.

4.1.4 Multiple Reference Receivers Estimator CRLB. The process for computing the CRLB surface described in Section 4.1.2 was repeated again for the multiple receiver estimator using the corresponding $\boldsymbol{G}$. When two additional reference receivers were added to the baseline estimator, the overall variance was decreased. Note that the color scale is the same as in Figure 18 to illustrate the decrease in variance. The dependency on the transmitter configuration was still present.
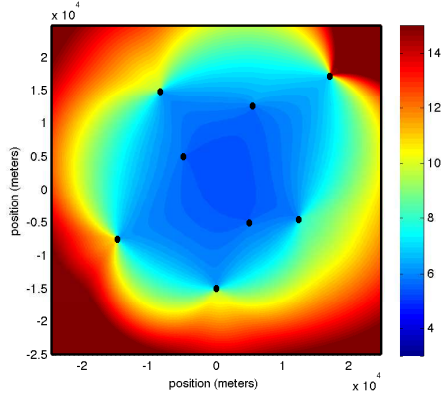
(a) Arbitrary
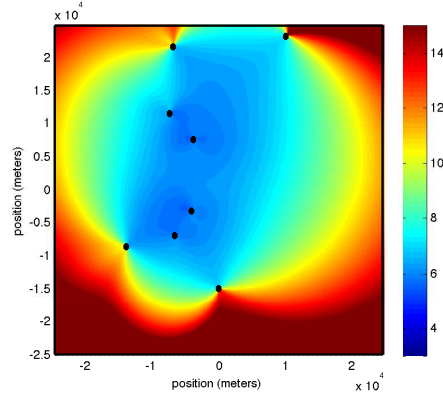
(b) Cincinnati
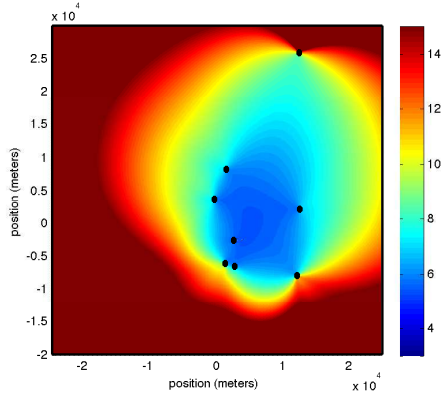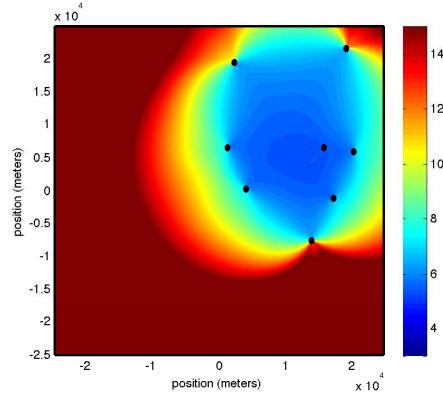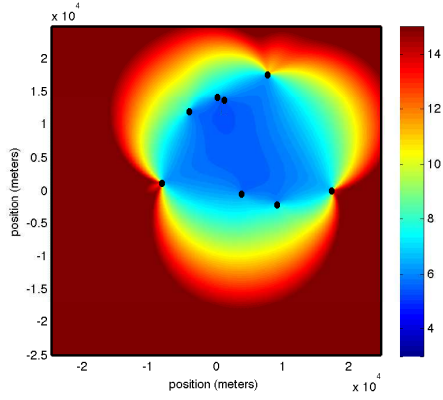
(c) Phoenix
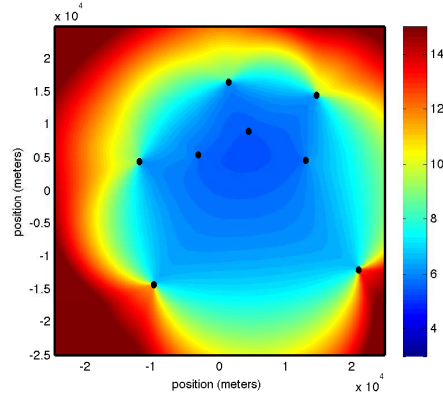
(d) Seattle

(e) Boston

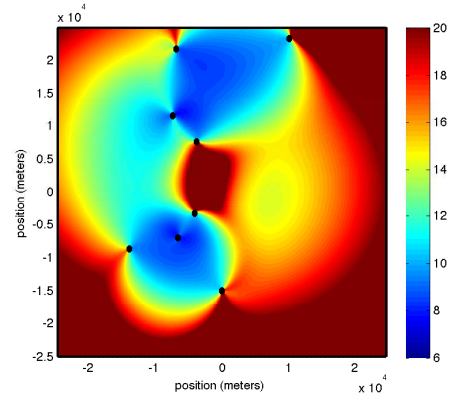(f) Los Angeles

Figure 18:   Baseline CRLB Surface, SNR = 20 dB, Rx_{ref} at $(-2500, 1200)$
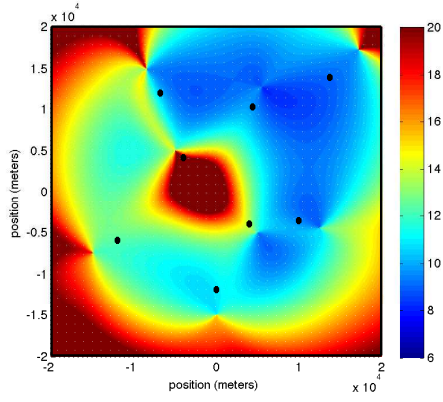
(a) Arbitrary

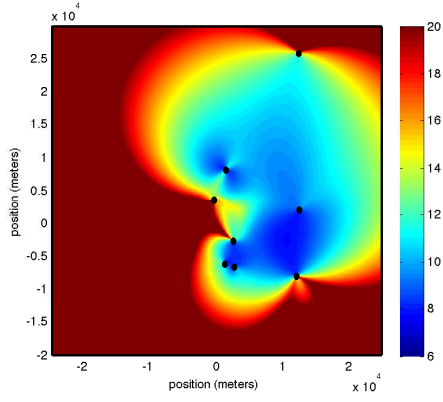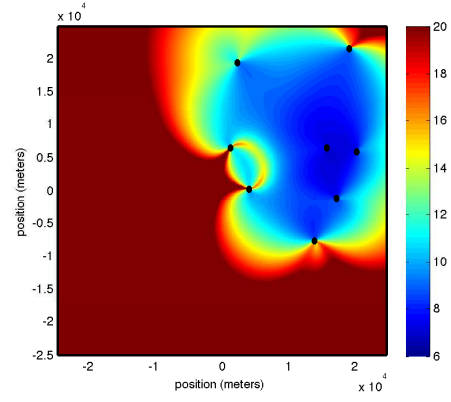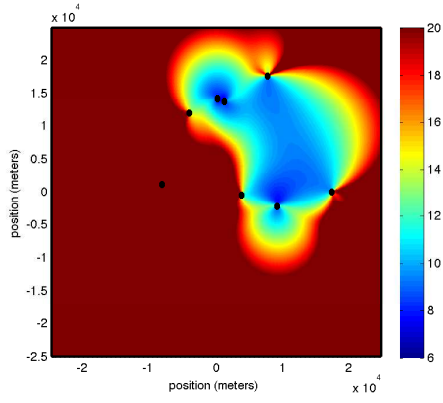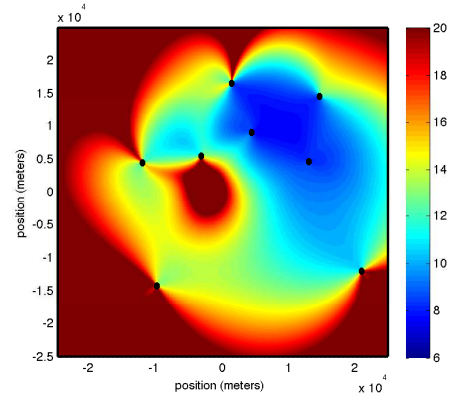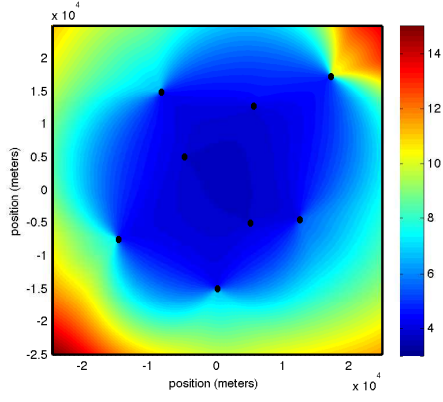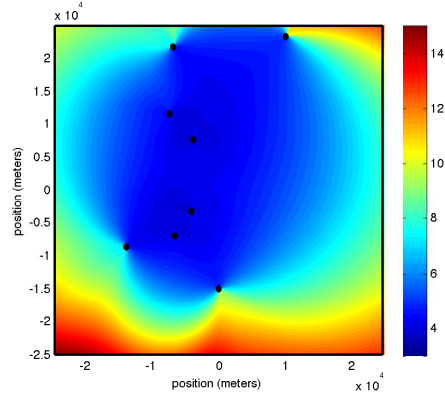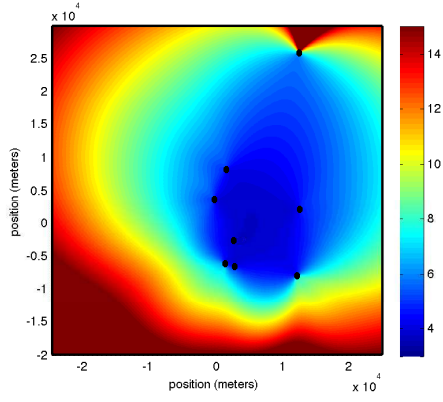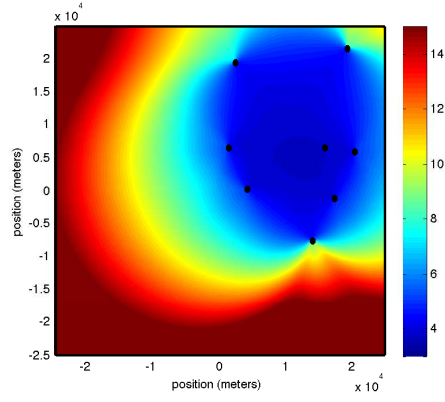(b) Cincinnati

(c) Phoenix

(d) Seattle

(e) Boston

(f) Los Angeles

Figure 19: Two-Unknown Receiver CRLB Surface, SNR = 20 dB, Rx_{ref} at $(-2500, 1200)$

63

(a) Arbitrary

(b) Cincinnati
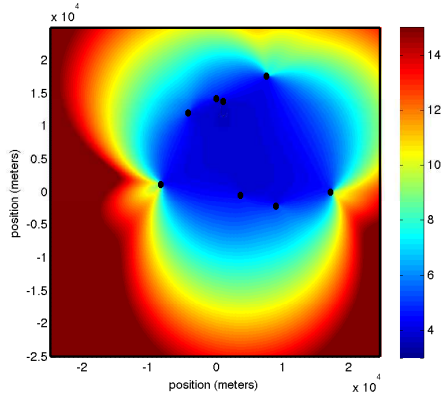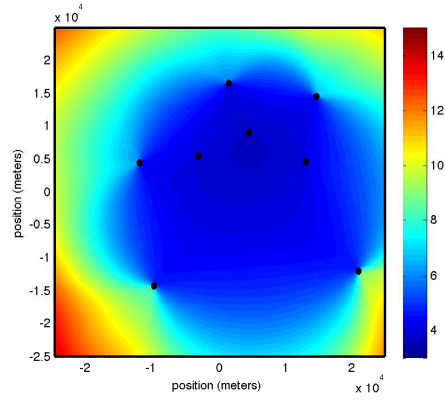
(c) Phoenix

(d) Seattle

(e) Boston

(f) Los Angeles

Figure 20: Multiple Reference Receiver CRLB Surface, SNR = 20 dB, Rx_{ref1} at $(-2500, 1200)$, Rx_{ref2} at $(-14000, -13500)$, Rx_{ref3} at $(17500, -5000)$

4.2   System Simulations

Table 3 repeats Table 2 which described all of the simulation types executed for this research. From the data collected, there are three metrics that are discussed in this section to compare and contrast all of the estimators. The metrics discussed in this section are

- Range Estimate RMSE

- Position Estimate Generalized Variance

- Position Estimate RMSE

Each metric is presented in the order listed above, followed by a general discussion of the strengths and weaknesses of each transmitter/receiver configuration, and a summary of the findings from the simulations. The results for the transmitter position correction estimator are discussed separately in Section 4.2.5.3 and are not included in the following discussion.

A total of 100 observations were executed for each transmitter/receiver configuration pair resulting in 400 observations for each SNR value for a given transmitter configuration. Each metric was averaged across all receiver configurations to compute

Table 3:   Simulation Variations

	Simulation	A Priori		True b	Error		Estimated		
#	Description	Rx_{ref}	Tx	(sec)	Rx_{ref}	Tx	Rx_{mob}	b	Rx_{ref}
1	Baseline w/ Bias	✓	✓	0			✓	✓	
2	Baseline w/o Bias	✓	✓	10^{-7}			✓	✓	
3	Tx Uncertain	✓	✓	0		✓	✓	✓	
4	Rx_{ref} Uncertain	✓	✓	0	✓		✓	✓	
5	Tx/Rx_{ref} Uncertain	✓	✓	0	✓	✓	✓	✓	
6	Two-Unk w/ Bias		✓	0	N/A		✓	✓	✓
7	Two-Unk w/o Bias		✓	10^{-7}	N/A		✓	✓	✓
8	Multi-Ref w/ Bias	✓	✓	0			✓	✓	
9	Multi-Ref w/o Bias	✓	✓	Varies*			✓	✓	
10	Tx Correction	✓	✓	0		∿	✓	✓	

*For three reference receivers the true biases are $10^{-7}, 5 \times 10^{-6}$, and 2×10^{-5}.
The "∿" symbol indicates that error is added to two transmitters only.

a single statistic for each SNR value as described in Section 3.3. The only exceptions to this statement were Simulations #6 and #7, which only executed simulations at -10 dB and -5 dB when SNR < 0.

4.2.1   Range Estimate RMSE.   The range estimate RMSE showed distinction between the simulations, namely because the RMSE combined bias and variance to compute the final value. Therefore, the dominance of the bias was observed in this statistic at higher SNRs where the variance approached zero in the simulation environment (see Appendix A.2). The basic trend in the plots is similar to that of the CRLB in Figure 17 until the bias begins to dominate as the source of error. The plots of the average RMSE for all environment geometries are shown in Figures 21 - 26.

For all geometries, for SNR $\leq$ 10 dB, the RMSE showed no significant distinction between the ideal baseline scenario in Simulation #1, the addition of clock bias in Simulation #2 or any of the errors added to the a priori data in the remaining simulations. This indicates that the channel noise was the dominant source of errors in the range estimates. This was further confirmed by the increased RMSE as SNR decreased. As the channel conditions improved, and hence approached ideal conditions (SNR $\geq$ 20 dB), the aforementioned distinction of the error sources became apparent. The ideal baseline scenario of Simulation #1 approached 10 meters for all geometries. Simulation #3 showed a trend similar to Simulation #1 and in the Cincinnati geometry, performed at a lower average RMSE than the ideal baseline scenario. Uncertainty in the receiver demonstrated a more direct impact on the range estimate RMSE. This may result from the fact that the potential magnitude of the error added to the reference receiver was 25 meters compared to 15 meters for the transmitter errors, thus, resulting in a higher overall error. The clock bias also demonstrated a direct impact on the final RMSE. Since the pseudorange measurement was computed based on the a priori positions, as well as the measured TDOA, any error in the TDOA measurement would necessarily degrade the final position estimate accuracy. This trend was observed across all of the environment geometries.
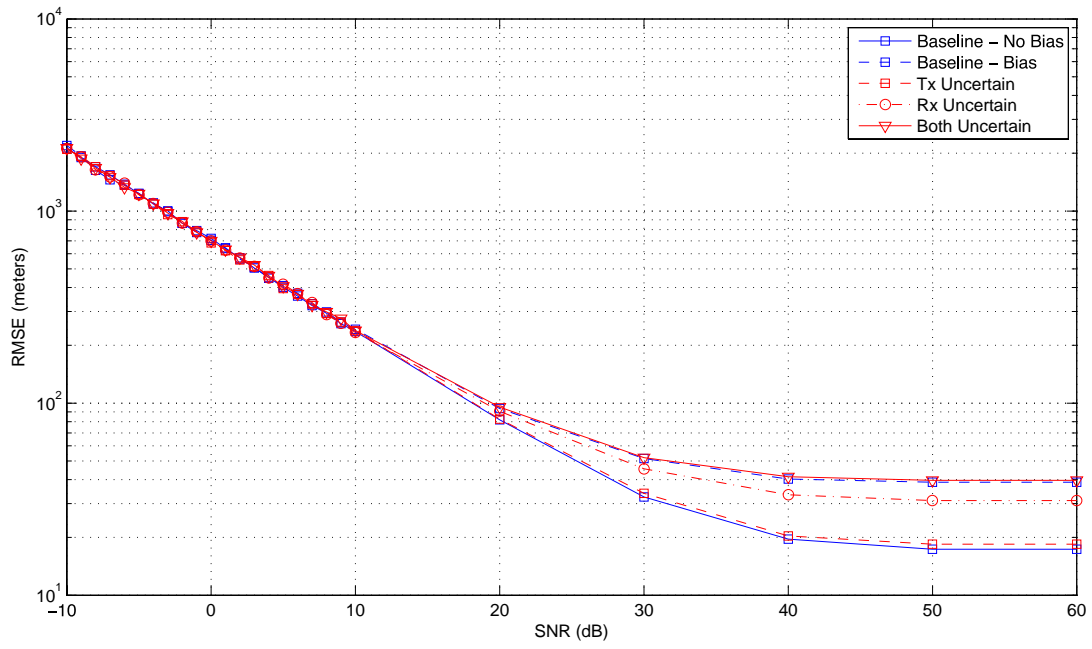
Figure 21:   Range Estimate RMSE: Arbitrary
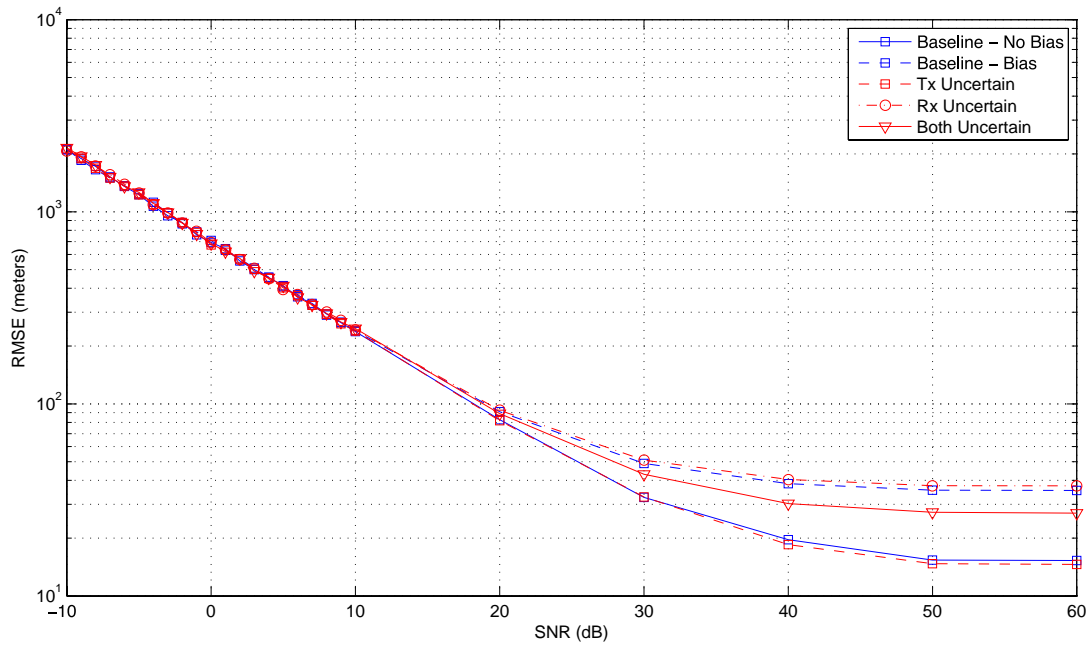

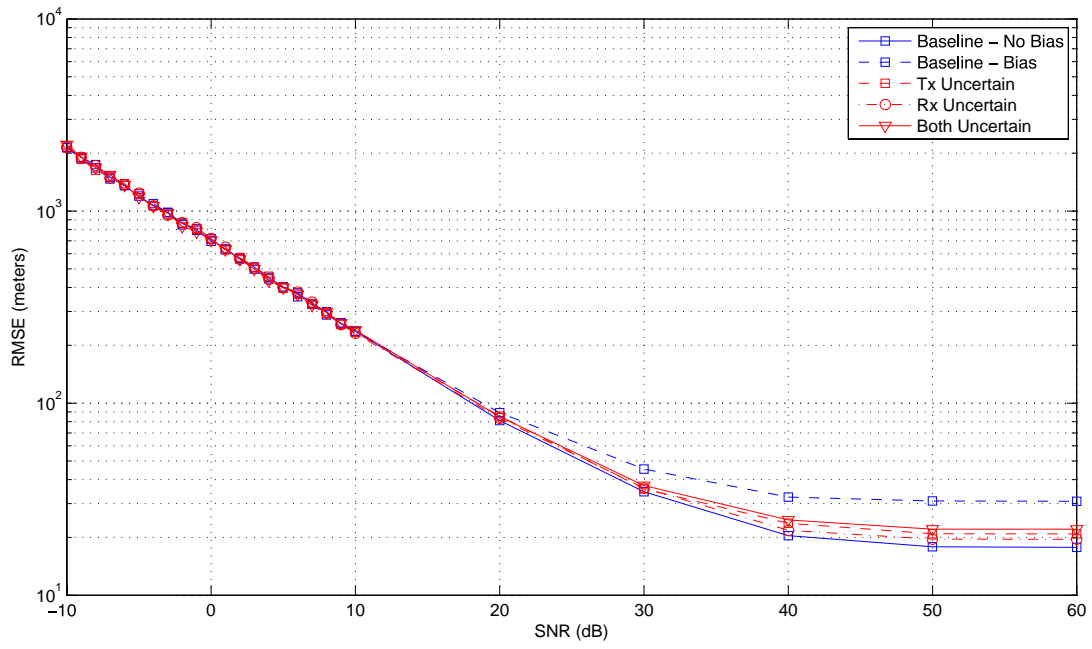Figure 22:   Range Estimate RMSE: Cincinnati

Figure 23:   Range Estimate RMSE: Phoenix
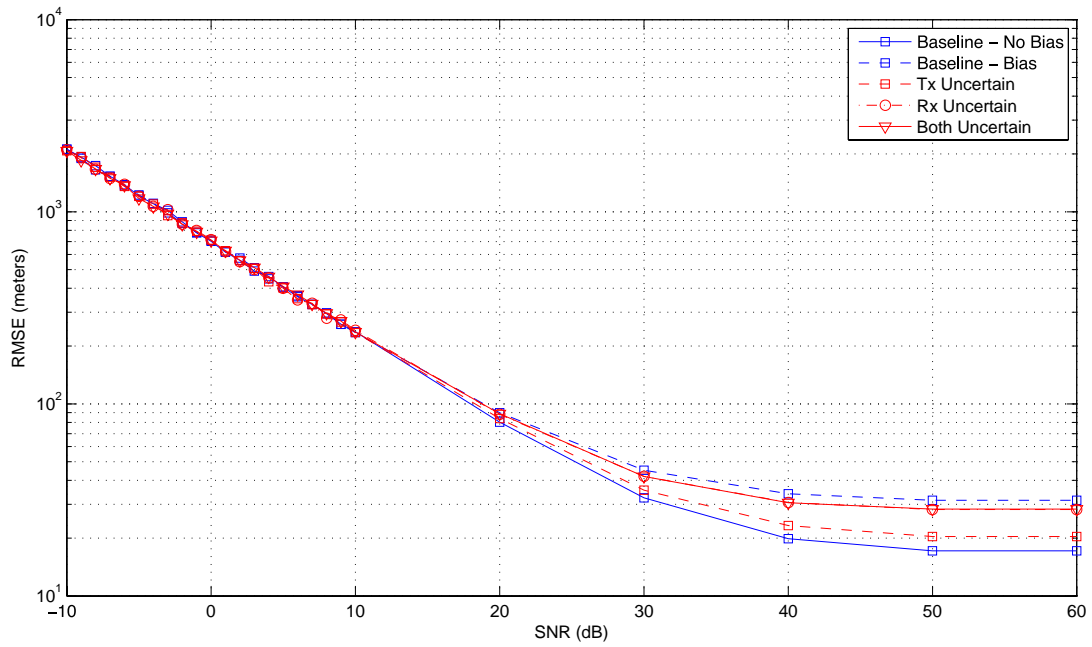

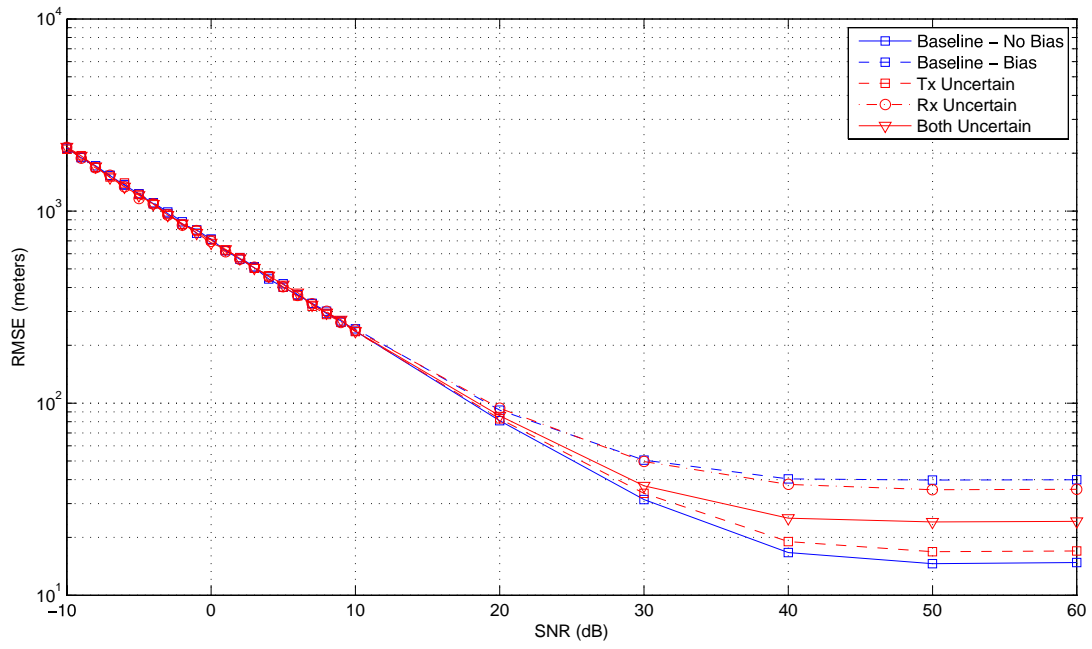Figure 24:   Range Estimate RMSE: Seattle
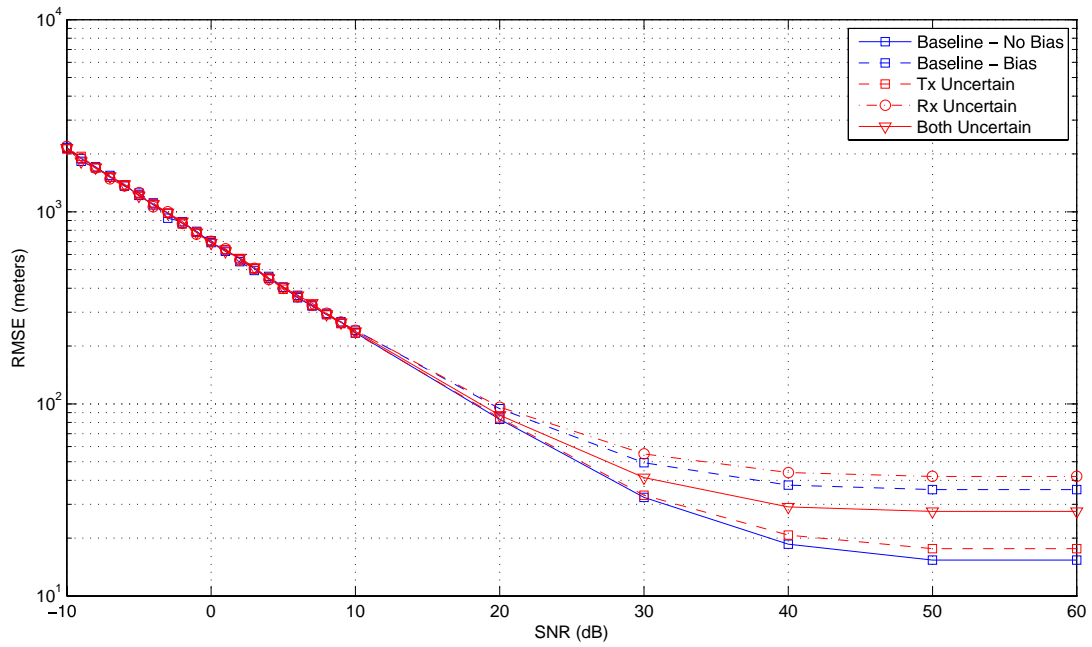
Figure 25:   Range Estimate RMSE: Boston

Figure 26:   Range Estimate RMSE: Los Angeles

4.2.2 Position Estimate Generalized Variance. The position estimate generalized variance was expected to show a dependancy on the environment geometry based on the expressions for the position estimate CRLBs, and the simulated CRLB surfaces presented in Section 4.1. The average generalized variances for the final position estimates are shown in Figures 27 - 32. These data serve as further validation of the simulations compared to the theoretical expressions as they demonstrated dependancy on the environment geometry. Additionally, the trends for the estimators are all similar in that they improve or degrade based on SNR. Therefore, any deviations may be attributed to some characteristic of the environment geometry that would improve or degrade the final position estimate.

For all environment geometries, except Seattle, for 0 dB $\leq$ SNR ≤ 30 dB, the multiple-reference receiver estimator with no clock bias achieved the lowest RMSE, followed by the baseline estimator cases, and the two-unknown receiver estimator. The clock bias between the multiple reference receivers has the significantly degraded the generalized variance in the Arbitrary transmitter configuration and to a lesser extent in the Los Angeles configuration. In general, at 50 dB or 60 dB, the variance went to zero, similar to the range estimate generalized variance (see Appendix A.2 for further proof). Since this was a result of the ideal noiseless conditions of the simulation environment, those values are not explicitly plotted and the emphasis is placed on the SNR values below 50 dB.

The Seattle transmitter configuration proved to have the most variance in the position estimate errors. Compared to the other estimators, the mobile receiver was more often located in the highest variance regions on the CRLB surfaces seen in Figure 18(d), Figure 19(d), and Figure 20(d). In this simulation, the multiple reference receiver values remained above the upper bound of the vertical axis until 50 dB at which point the value was on the order of 10^{-4} meters. As such, the curve is not visible in Figure 30. Except in the case of the two-unknown receiver estimator, no estimator produced results under 100 meters until SNR ≥ 20 dB. The two-unknown receiver scenarios, however, began with a closer initial guess for the position of both

receivers. This case illustrates the tradeoff between the maximum allowable error in the initial guess, and the effect the environment geometry had on the estimator. Therefore, even general knowledge about the CRLB or theoretical performance of the transmitter configuration can greatly improve the effectiveness of the estimator, and also determine initial requirements.

The multiple reference receiver estimator demonstrated a smoother trend in the error variance for SNR ≤ 0 dB, as well as provided a consistent improvement compared to the baseline estimator (except in the Seattle environment geometry as previously discussed). The two-unknown receiver estimator showed that the error variance increased above 10^3 meters for SNR ≤ 0 dB. Given the requirement to have a closer initial guess than the baseline or multiple reference receiver estimator to ensure convergence on a solution, another limitation could have been added stating that the estimator should only operate when SNR > 0 dB.
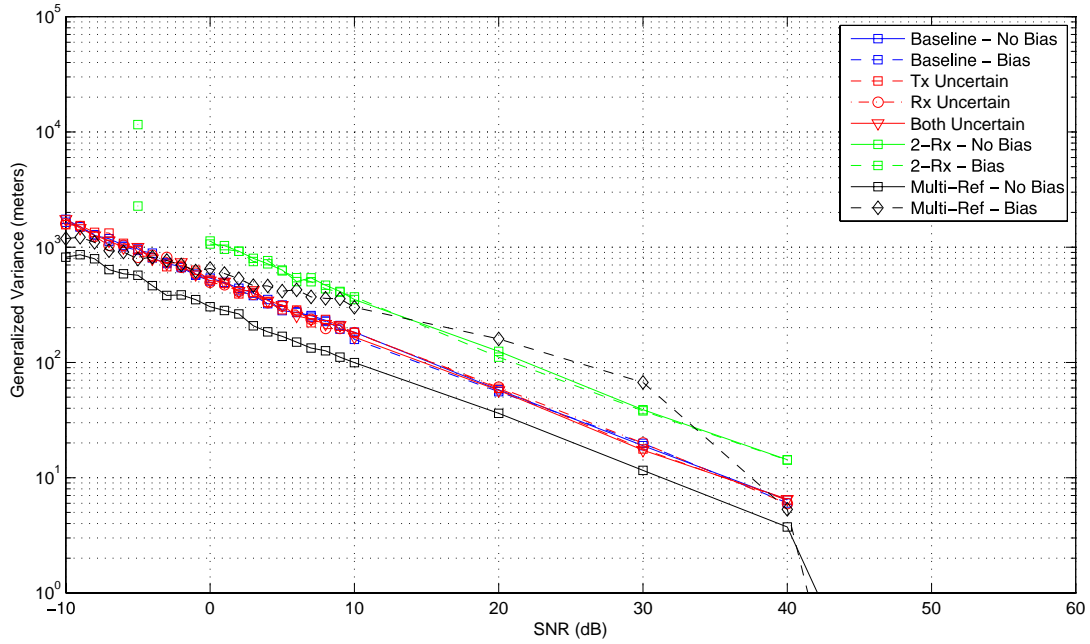

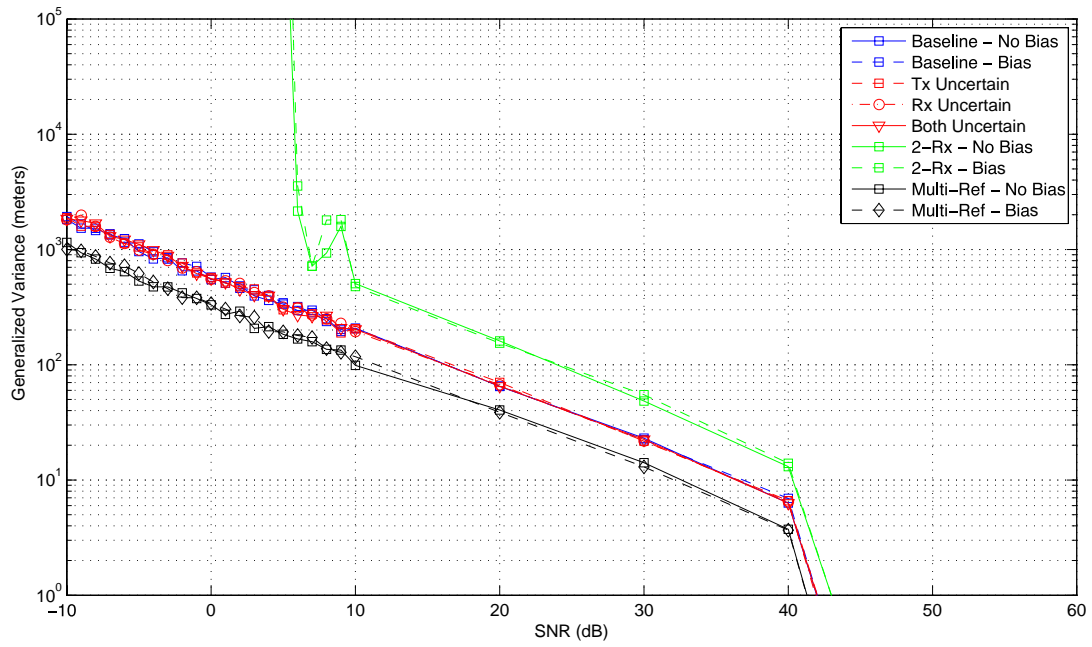Figure 27: Position Estimate Generalized Variance: Arbitrary

71

Figure 28:   Position Estimate Generalized Variance: Cincinnati
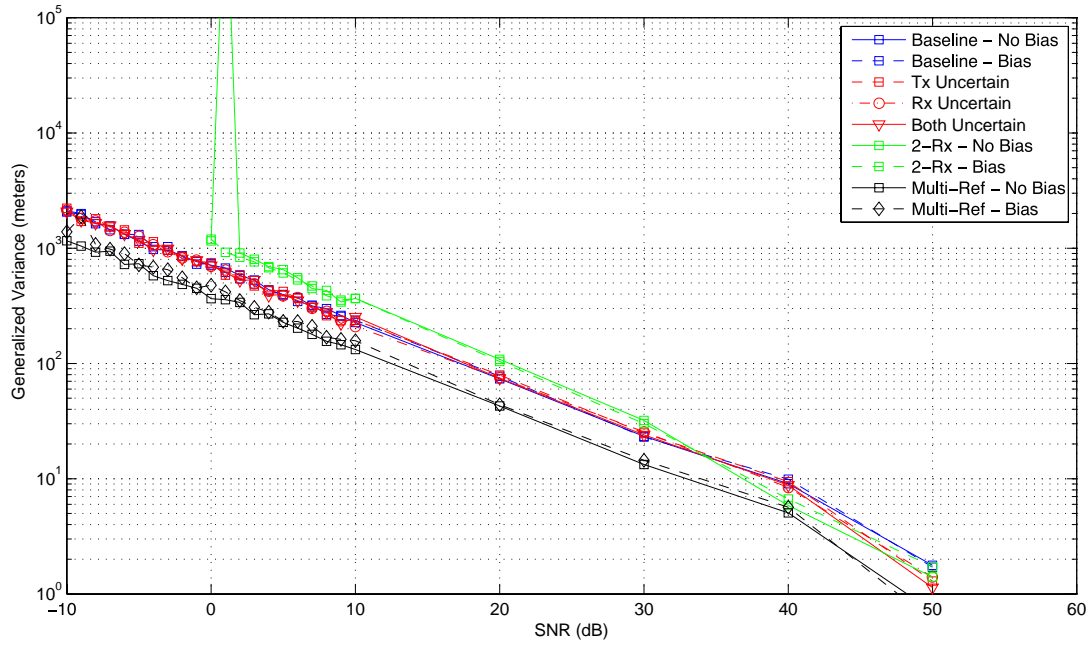

Figure 29:   Position Estimate Generalized Variance: Phoenix
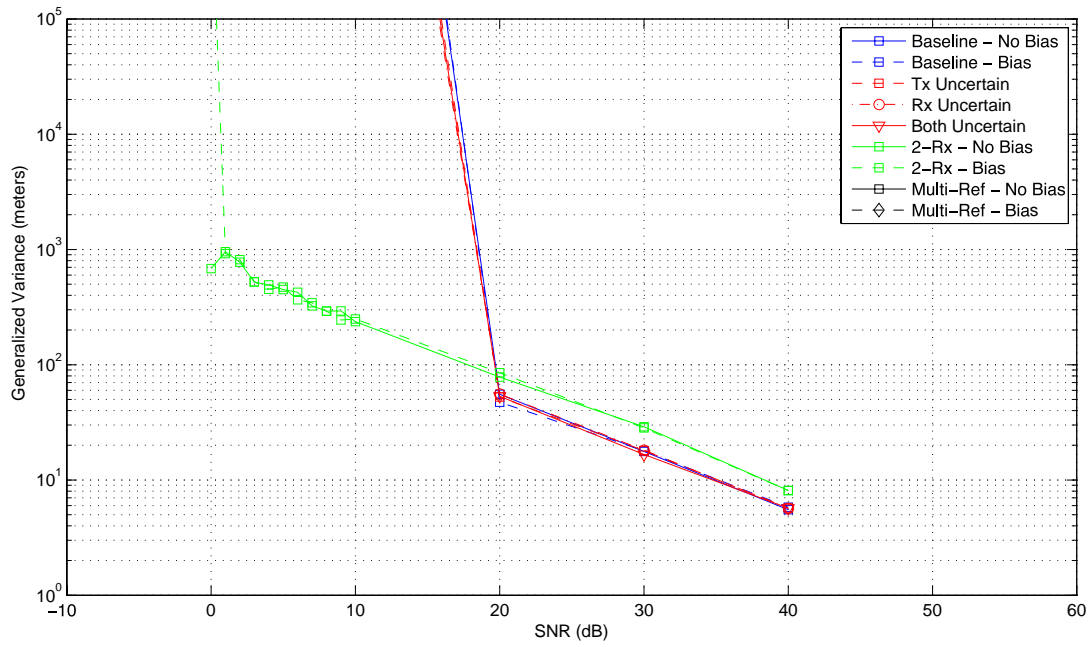
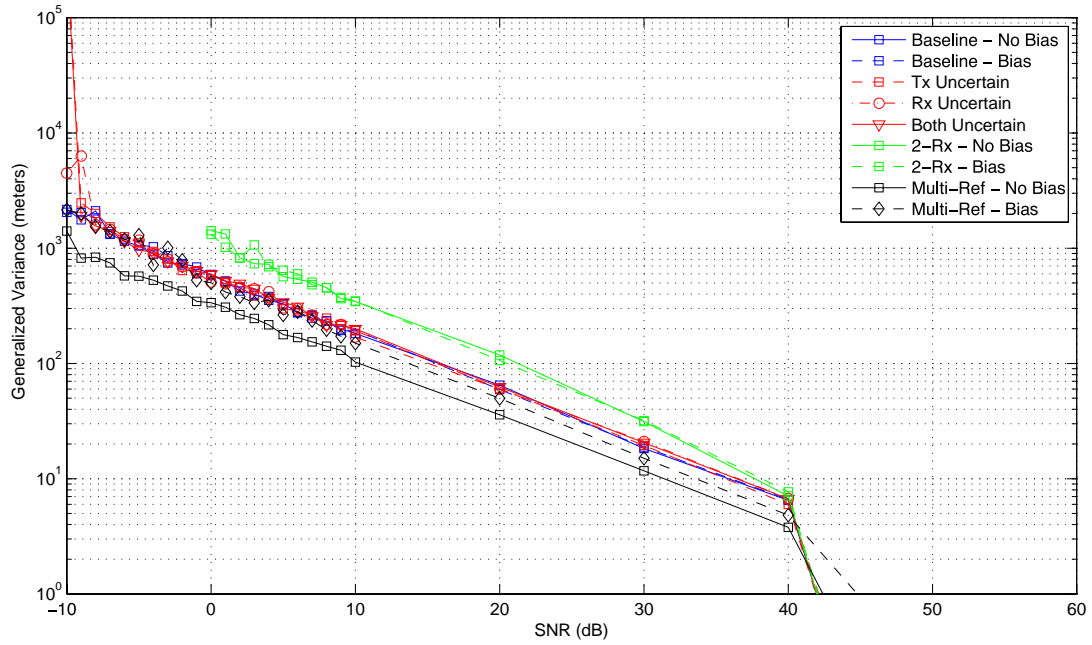Figure 30:   Position Estimate Generalized Variance: Seattle

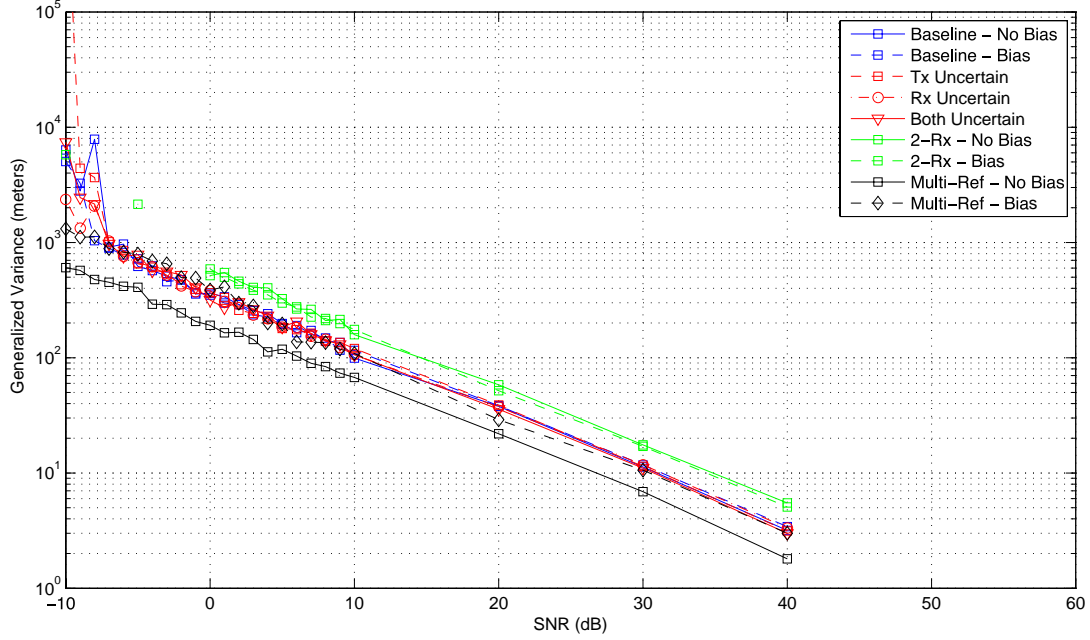Figure 31:   Position Estimate Generalized Variance: Boston

73

Figure 32:   Position Estimate Generalized Variance: Los Angeles

4.2.3   Position Estimate RMSE.   Just as the range estimate RMSE values showed the distinction between the conditions simulated with the baseline estimator, the position estimate RMSE showed additional distinction between all of the estimator performances. The plots of the average RMSE for all environment geometries are shown in Figures 33 - 38.

Generally, the clock bias did not demonstrate a significant difference compared to the respective estimator without a clock bias except in the case of the multiple reference receiver estimator. This was due to the fact that there were larger clock bias values simulated. The RMSE for this simulation in Los Angeles compared to the other simulations illustrates the dependency between the environment geometry and the impact the clock bias has on the estimator accuracy. The uncertainty added to the reference receiver position proved to be the dominant impact to the accuracy of the baseline estimator, just as it did in the case of the range estimation.

The results for the Seattle geometry using the multiple reference receiver case, again remained above the upper bound of the vertical axis, as discussed in Section 4.2.2. This further supports the conclusion that the transmitter geometry paired with the four different receiver configurations was not conducive to ensuring consistent convergence on a position solution. For the other five geometries the multiple reference receiver estimator with no clock bias and the multiple conditions of the baseline estimator were varied, but relatively similar for SNR $\leq$ 10 dB. Except in the environment geometries of Cincinnati and Phoenix, above 10 dB the multiple reference receiver estimator with no clock bias performed better in terms of RMSE than the baseline estimator.

The Cincinnati and Phoenix transmitter configurations placed the transmitters in a vertical line pattern as opposed to spread out across the simulation environment. The reference receivers were placed in a configuration that resembled a triangle which, from the view of the estimators, began to resemble a horizontal line of receivers. The multiple reference receiver estimator without clock bias performed better than the baseline in the Boston environment geometries as it does in the Arbitrary and Los Angeles environment geometries, which both had a relatively wide spread of transmitter locations. This observation indicates the importance of not only the transmitter configuration, but also emphasizes the importance of the location of the reference receiver(s) relative to the transmitters. This is an important consideration when deciding on the trade-offs between the additional computation time and bandwidth introduced by adding reference receivers or relying on a single reference receiver as in the baseline estimator. To add to this observation, the clock bias degraded the solution in the Boston environment geometry, which would negate any improvement offered by using additional reference receivers. The clock bias simulations emphasize that all aspects of the estimator and receiver system must be considered when selecting an estimator.

The two-uknown receiver produced the same general trend as the other estimators once a certain SNR threshold was reached. The dependancy on the environment

geometry was still apparent for this estimator. In the Arbitrary, Cincinnati, and Phoenix environment geometries this SNR threshold was between 0 dB and 10 dB. In the Boston environment geometry, the threshold was at approximately 30 dB and at SNRs higher than that, the two-unknown receiver RMSE exceeded the performance of the baseline estimator. A similar situation occurred in the Phoenix environment geometries at 50 dB and 60 dB. This was due to the fact that this estimator began with an initial guess closer to the actual location of both receivers to ensure convergence. In these cases, the initial guess was close enough that it exceeded the baseline estimator results.
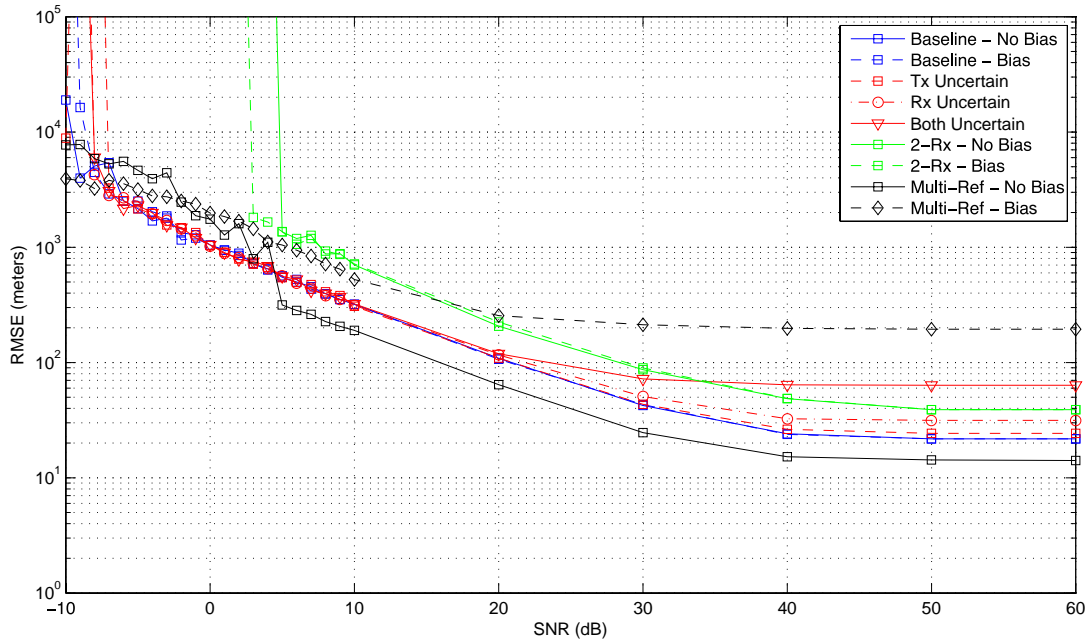

Figure 33:   Position Estimate RMSE: Arbitrary

4.2.4   Transmitter/Receiver Configuration Findings.   The transmitter configurations proved to be an important factor in the accuracy of the estimators. The Seattle transmitter configuration demonstrated the most sensitivity for all estimators. If the receivers were moved closer to the transmitters, the results would likely be more similar to those of the Boston transmitter configuration given that the two
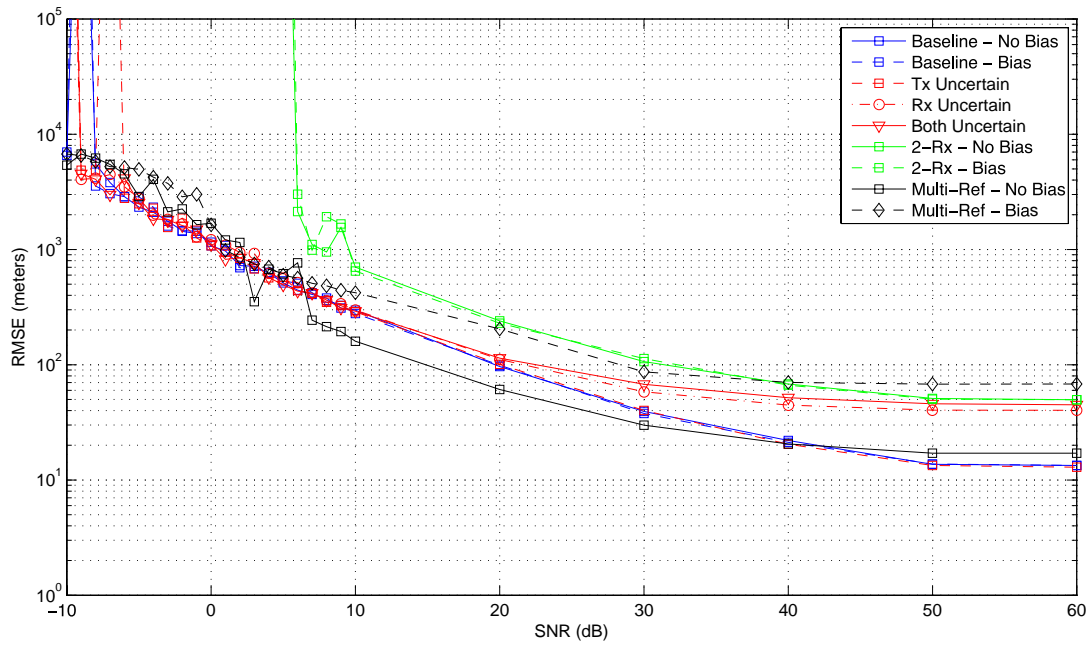
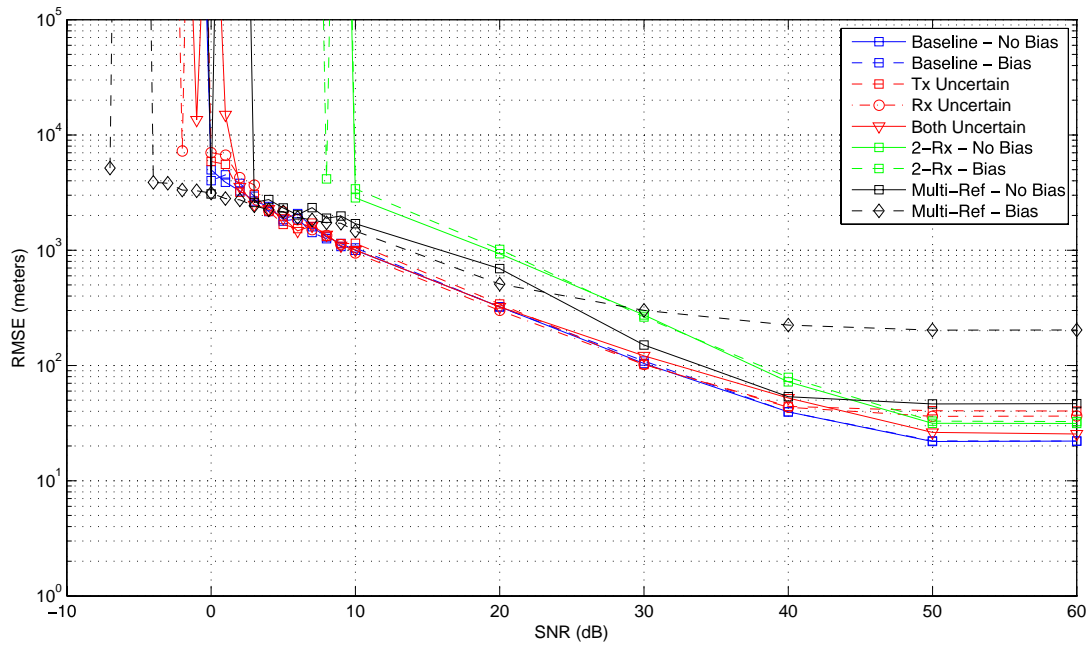Figure 34:   Position Estimate RMSE: Cincinnati

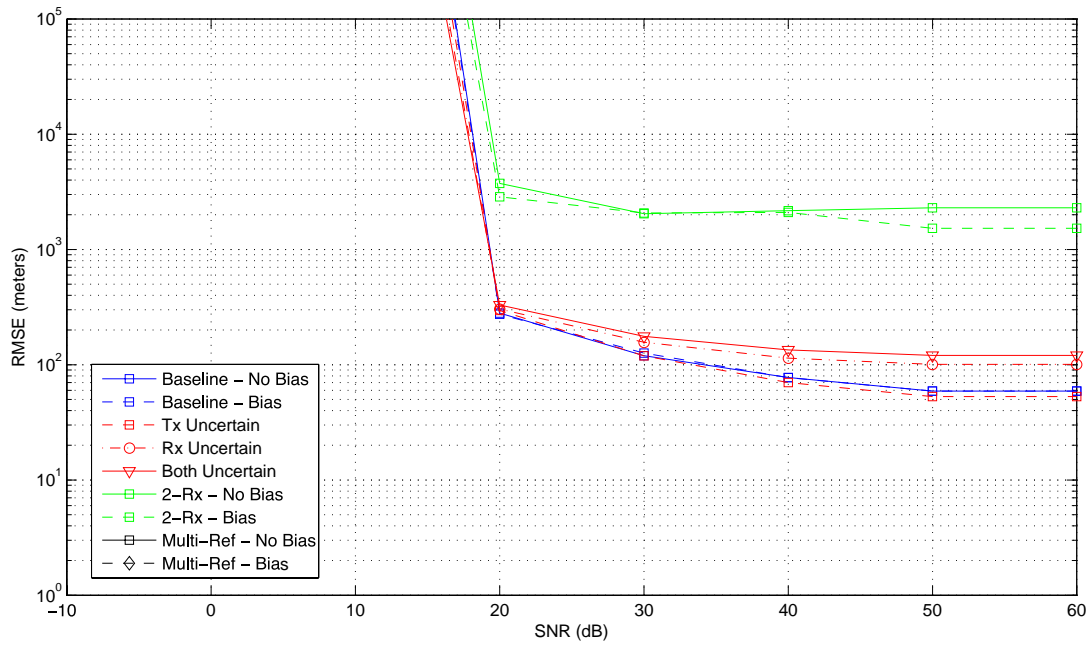Figure 35:   Position Estimate RMSE: Phoenix

Figure 36:   Position Estimate RMSE: Seattle
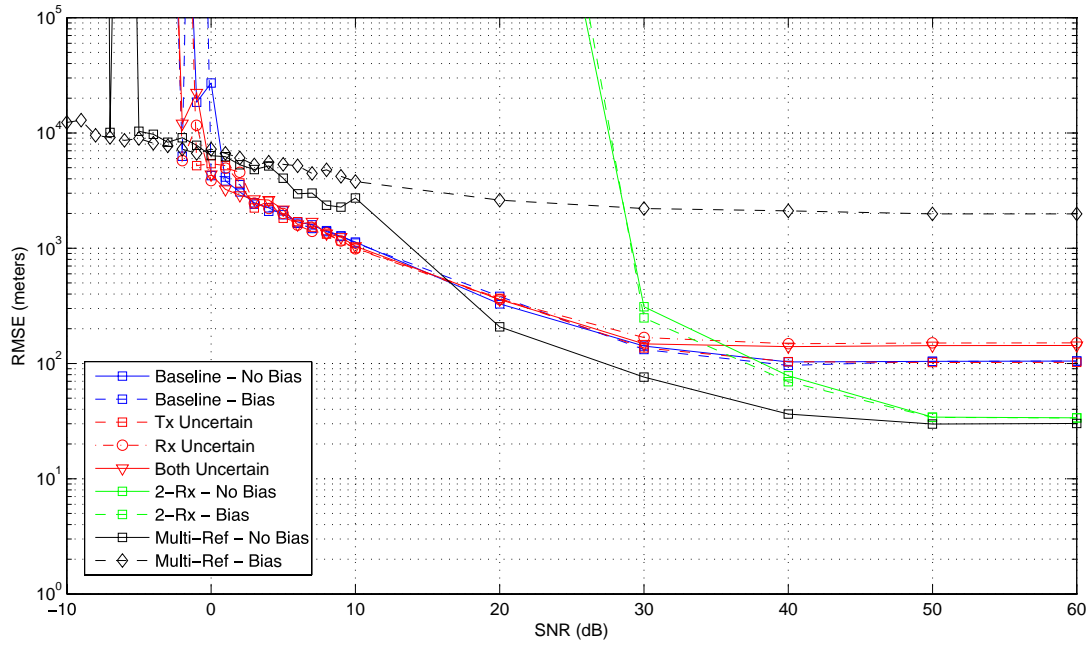

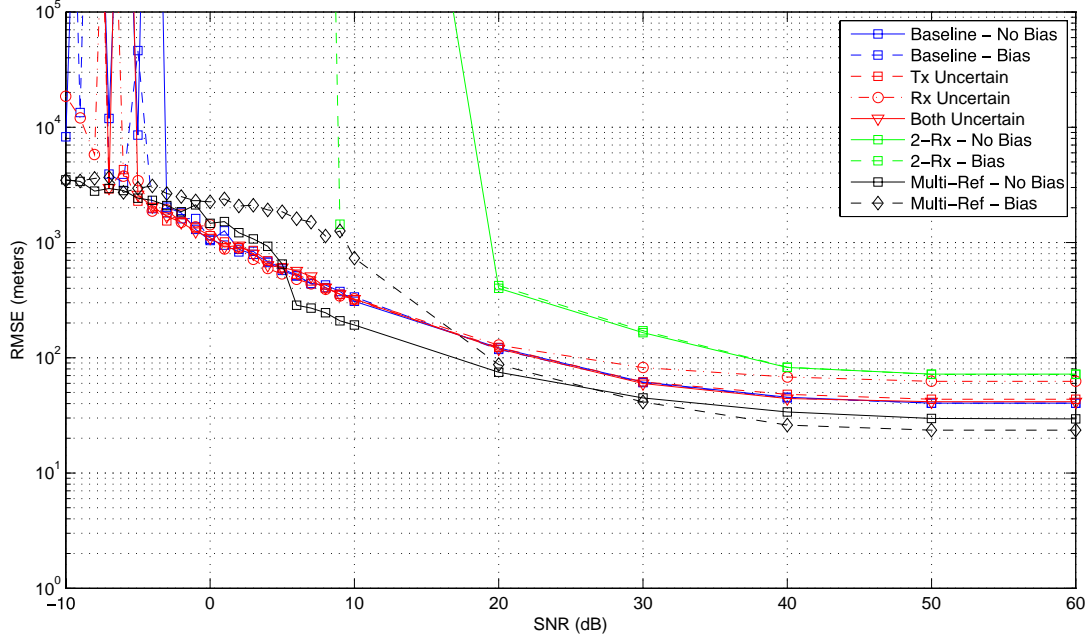Figure 37:   Position Estimate RMSE: Boston

Figure 38:   Position Estimate RMSE: Los Angeles

configurations are similar. The spread of transmitters, particularly in the Arbitrary and Los Angeles transmitter configurations, proved to offer the most consistent trends for all estimators. In the Phoenix and Cincinnati configurations, the vertical transmitter pattern exposed a weakness of the multiple reference receiver placement. The Boston transmitter configuration, which had a similar cluster to the Phoenix configuration except the transmitters were more horizontally spread, showed that placing the receivers closer to the transmitters mitigated the effect.

4.2.5   Estimator Findings.   In all of the statistics presented here, the trend between all of the estimators plotted was consistent with the baseline case (with any exceptions noted and explained in the preceding sections). Furthermore, the trend of the range estimate RMSE was similar to the range estimate CRLB at SNR levels where the variance dominated as the source of error. This general trend carried over to the position estimate RMSE and added the demonstrated dependancy on the transmitter configuration as the theoretical expressions and CRLB surface plots indicated.

Therefore, the simulated results of the multiple reference receiver and two-uknown receiver estimators are considered valid. Given this observation, it indicates that with additional mitigation techniques, the two-unknown receiver estimator may produce position estimates results that approach the baseline estimator, and the multiple reference receiver estimator may offer further improvement compared to the baseline estimator.

4.2.5.1   Two-Unknown Receiver Estimator.   The two-unknown receiver estimator required the initial guess to be closer to the true position than the baseline or multiple reference receiver estimators. This limitation of the estimator, along with a higher sensitivity to SNR $\leq$ 0 dB than the other estimators, would certainly define the scenarios in which it could be implemented. However, the strength of this estimator is that while the initial guess must be close, the estimator does not require *precise* a priori knowledge of the position of the reference receiver, hence, it would best be utilized in a tracking situation.

4.2.5.2   Multiple Reference Receiver Estimator.   The multiple reference receiver estimator showed that given most of the simulated conditions, it would perform better than the baseline estimator. A specific limitation was noted in the receiver configuration relative to the transmitters, discussed in Section 4.2.4. However, given the consistency of the results, aside from the Cincinnati, Phoenix and Seattle configurations (the latter of those proved sensitive for all estimators), the multiple reference receiver estimator simulated here demonstrated an improved performance compared to the baseline estimator. With additional reference receivers placed such that they would not be vulnerable to the situations encountered in the Cincinnati or Phoenix transmitter configurations, further improvement relative to the baseline case could potentially be achieved. However, when clock bias is present, the estimator output may show degraded accuracy compared to the baseline estimator depending on the transmitter configuration.

4.2.5.3   Transmitter Correction Estimator.   The transmitter correction estimator was unique from the other estimators in that it proved to be the most sensitive to the simulation conditions. Originally the simulation environment included the transmitter uncertainty scenario described in Section 3.2.1.1 except with three reference receivers instead of only one, and the error was only applied to two transmitters. However, even at high SNR levels the accuracy of the final estimate for the mobile receiver was degraded. The initial guess was moved from (0,0) to (12400,12400) which placed it 100 meters off from the true position of the mobile receiver in both directions. Since the magnitude of the errors inserted were only up to 15 meters, the ability of the estimator to correctly detect and correct it was limited given the fidelity of the simulation environment and the nature of the AM signals (referring to the relatively low bandwidth compared to other SoOP). Therefore, the error was increased such that the error magnitude could be as high as 50 meters. As an additional step in the simulations, before implementing the transmitter correction estimator, the columns inserted to estimate the transmitter positions were removed such that the estimator computed an estimate for the mobile receiver and the clock bias only. The initial data was then reset and the full transmitter correction estimator was used to compute solution. This allowed for the comparison (under the exact same error conditions) of attempting to correct for the error, and simply allowing the errors to exists in the data and compute a solution.

Table 4:   Transmitter Correction Simulation RMSE (meters)

SNR (dB)	Arbitrary	Cincinnati	Phoenix	Seattle	Boston	LA
0	834.08	479.78	481.81	2306.46	471.36	4778.74
10	280.03	149.56	172.27	248.78	173.68	187.98
20	62.23	58.69	56.43	76.14	50.17	57.81

The simulations were executed for 25 observations for only the environment geometry where the mobile receiver was placed at (12500,12500) at three SNR levels. The results of the average RMSE of the estimate for the mobile receiver per transmitter configuration are shown for the transmitter correction estimator in Table 4 and for

Table 5:   Transmitter Error/No Correction Simulation RMSE (meters)

SNR (dB)	Arbitrary	Cincinnati	Phoenix	Seattle	Boston	LA
0	328.05	409.82	403.71	321.23	430.71	277.80
10	110.73	142.88	148.01	108.84	159.59	112.98
20	43.94	63.55	50.80	49.28	55.62	35.68

the multiple reference receiver estimator (i.e., without estimating the transmitter position error) in Table 5. Ultimately (with only two exceptions at 20 dB) the addition of the transmitter correction technique degraded the overall RMSE for the position estimate of the mobile receiver. Tables 6 and 7 show the RMSE of the estimates for the transmitter positions.

Table 6:   Transmitter Estimate RMSE for x-Coordinates (meters)

SNR (dB)	Arbitrary	Cincinnati	Phoenix	Seattle	Boston	LA
0	84.83	47.68	89.60	76.39	59.80	87.74
10	70.36	51.87	96.55	64.62	68.87	116.52
20	22.37	47.03	48.08	61.41	54.99	93.16

Table 7:   Transmitter Estimate RMSE for y-Coordinates (meters)

SNR (dB)	Arbitrary	Cincinnati	Phoenix	Seattle	Boston	LA
0	46.19	63.81	44.88	84.39	72.99	87.89
10	67.94	59.86	91.69	30.92	89.26	46.09
20	55.66	34.92	62.77	48.35	39.31	80.94

These data show that the error of the transmitter position estimates are approximately on the same order of magnitude for both the x and y coordinates for all transmitter configurations. This indicates the possibility that a limit on the accuracy and consistency of the estimator to compute corrections of the transmitter positions was imposed by the fidelity of the simulation environment and/or the AM signals. As previously discussed, the initial attempt to mitigate this limit was to increase the error in the transmitter positions such that the ability to correct the error in the transmitter could be more adequately demonstrated. However, the overall accuracy would not likely have exceeded the values presented here.

4.3 Summary

This chapter presented simulated results for the baseline estimator from previous works and the three estimators derived from this research. The simulations presented both the theoretical bounds and the overall performance of the estimators in the simulation environment. The simulations were validated by comparing the results to the theoretical performance. The behavior and trends of the estimators, various conditions, and the transmitter and receiver locations were discussed, and the resulting observations were presented.

V. Conclusions and Recommendations

This chapter summarizes the findings from the simulation results of algorithms developed for navigation from TDOA measurements using AM SoOP. Recommendations for future research using TDOA measurements from AM and any SoOP are also provided.

5.1 Conclusion

The two goals of this research were to prove the concept that a revised TDOA algorithm using SoOP is sufficient for navigation with limited or no a priori position data for the reference receiver or transmitters, and to examine the effect of erroneous a priori position data in the baseline estimator.

To address the primary goal of this research, Chapter II and Chapter III derived the baseline estimator and three additional estimators: the two-unknown receiver estimator, the multiple receiver estimator, and the transmitter correction estimator. The simulations were validated against theoretical bounds, and similar trends were observed as presented in Chapter IV. Thus, the primary goal of the research was accomplished in demonstrating that accuracy consistent with the baseline estimator is possible under certain conditions when the estimator is altered to allow for the removal of a priori data. The two-unknown receiver estimator specifically addressed the primary goal. The multiple reference receiver contributed to the primary goal in the sense that it could improve the accuracy of the baseline estimator in certain conditions. The limited demonstration of the transmitter correction estimator did not significantly contribute to this goal, however, the derivation allows for this to be explored in future work.

The secondary goal was detailed in Chapter IV in the simulation of the baseline estimator with uncertainty added to the reference receiver position and the transmitter positions. The former proved to be the more significant source of degraded accuracy given the magnitude of the errors simulated in this research. It was noted that the magnitude was different for the two errors. The transmitter position error

was bounded at 15 meters, whereas the reference receiver could contain errors of approximately as much as 25 meters. Also, the errors were generated according to two different distributions as discussed in Chapter III. This research demonstrated that given the error magnitudes considered, the error added to the reference receiver was more significant than errors in the a priori transmitter positions. This provides further justification for the derivation and implementation of the two-unknown receiver estimator, and demonstrates how the derivation and simulation of this estimator also addressed the secondary goal of this research.

The two-unknown receiver estimator described in Section 3.2.2 and the CRLB expression discussed throughout Section 3.4.2 contributed to [27]. The results for the baseline, two-unknown receiver, and multiple reference receiver estimators for the Cincinnati, Phoenix, and Los Angeles transmitter configurations were presented to the Institute of Navigation [34].

5.2   Future Work

This research focused exclusively on the derivation and proof-of-concept simulations for variations on the existing navigation via TDOA algorithm. There were many assumptions made to limit the scope of this research, time constraints for simulations, and other areas that allow for many opportunities to expand on this research. Some of those areas are recommended here.

- **Transmitter Correction Estimator**

  Time constraints prevented further exploration of this estimator. The derivation is complete, however, sufficient initial conditions were not found in order to simulate it to the same extent as the two other estimators derived during the course of this research. As such, this estimator could potentially offer further robustness to the navigation environment where a priori SoOP transmitter positions are known to contain errors. Furthermore, the same concept allows for other derivations of the estimator. For example, a Gaussian prior distribution

of the transmitter position could be added (with σ corresponding to the known error distribution) to aid in the convergence on a transmitter position estimate.

- **Multipath**

  To limit the scope and constrain errors in the simulation to those allowed by the algorithm, multipath was assumed to not be present. However, in order to explore the reality of implementation of this system, multipath should be incorporated in the simulation along with a mitigation technique.

- **TDOA Environment**

  Many of the conditions used to simulate the received SoOPs can be altered to explore the effect on the system output. The conditions that could be changed include adding or removing transmitters, increasing or decreasing the distances between transmitters, changing the signal power and station availability to simulate day/night conditions, or using different message signals from the stations. Furthermore, in addressing the secondary goal of this research, the error added to the position of the reference receiver proved to be the dominant source of error compared to the error added to the transmitter positions. It would be beneficial to further explore the effect of different magnitudes of errors added to both cases.

- **Different SoOP**

  For proof-of-concept demonstration, AM was the only SoOP used in the simulations. Since real-world conditions may allow for higher bandwidth signals, or even a mixture of SoOP depending on the requirement, it would be useful to explore use of SoOP other than AM.

- **Cross-Correlation Technique**

  The simplest and most basic cross-correlation technique was intentionally used in this research. If AM signals are to be used in a hardware implementation, it may be desirable to test more robust techniques which could possibly enhance

TDOA estimation and mitigate potential deficiencies of the position estimation algorithm.

- **Mobile Receiver In Motion**

  These simulations tested discrete instances of the location of the mobile receiver. For implementation in to any system, the effectiveness of the algorithm while the mobile receiver is in motion must be explored. This may also necessitate different methods of computation in order to provide a real-time continuous navigation solution, such as a Kalman filter, which may be an area of yet further research based on the algorithms presented here.

- **Altitude/z-coordinate Estimation**

  To reduce computation time, the estimators only output two-dimensional estimates for this research. If a system were intended to replace or supplement GPS, three-dimensional outputs would be desired, or perhaps even required. Therefore, examining the effects of transmitter height and position on the third dimension would add to the overall determination of the effectiveness of the algorithms.

- **Hardware**

  As many of these recommendations have indicated, testing the algorithms in the simulation environments allows for a certain level of confidence in the underlying theory to produce a useable navigation solution. However, for these algorithms' true effectiveness to be examined, they must be implemented into a physical system that can be tested under real-world conditions.

This research used the simulation environment to demonstrate a successful proof-of-concept for the two-unknown receiver estimator and the multiple reference receiver estimator algorithms. It further provided an examination of the effect of the errors added to the baseline algorithm. This research provides exciting new baseline data and results to motivate further research and experimentation in the study of using SoOP for navigation.

Appendix A. Additional Plots

This appendix provides additional plots from the simulations that are not included in Chapter 4.

A.1   CRLB Comparisons

Figure A.1 shows the magnitude of the baseline divided by the magnitude of the two-unknown receiver CRLB surface for each point simulated. The plots indicate the magnitude of additional variance in the two-receiver estimator. Compared to the CRLB surface plots shown in Figure 18 and Figure 19, the most variance in the two-unknown receiver estimator occured in this region around the reference receiver at (-2500, 1200).

A.2   Bias vs. Variance Comparisons

Figures A.2 - A.10 present the bias and variance as a percentage of the total error. Some plots have gaps from when `Matlab`® computed `NaN` (not a number) for some observations.
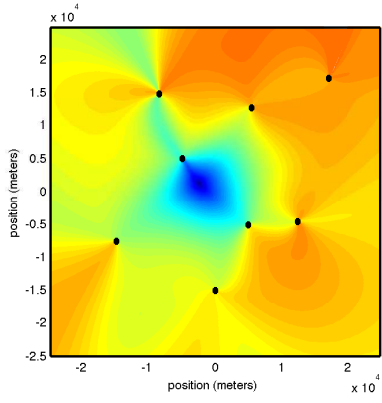
(a) Arbitrary
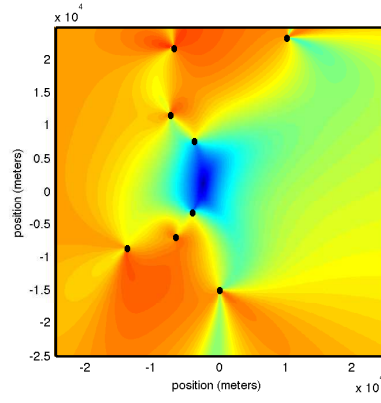
(b) Cincinnati
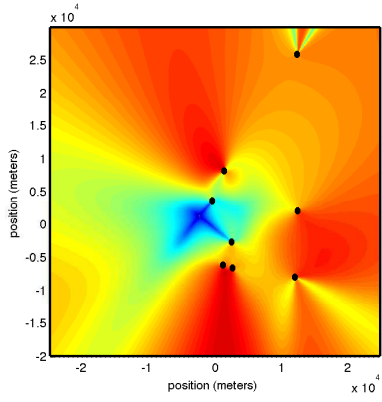
(c) Phoenix
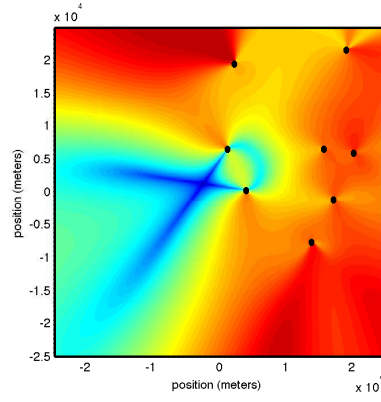
(d) Seattle
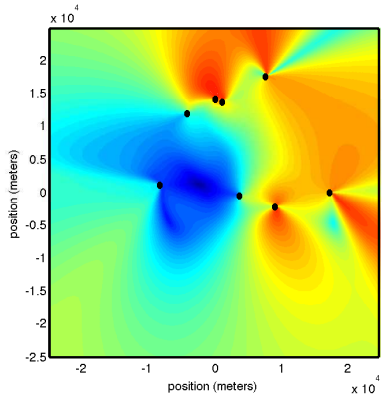
(e) Boston
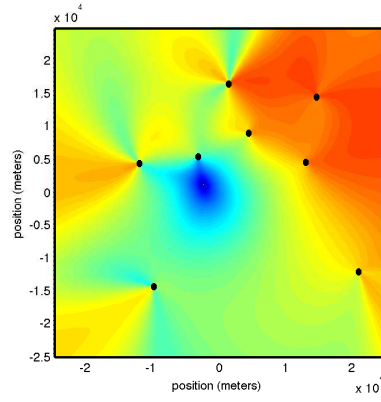
(f) Los Angeles

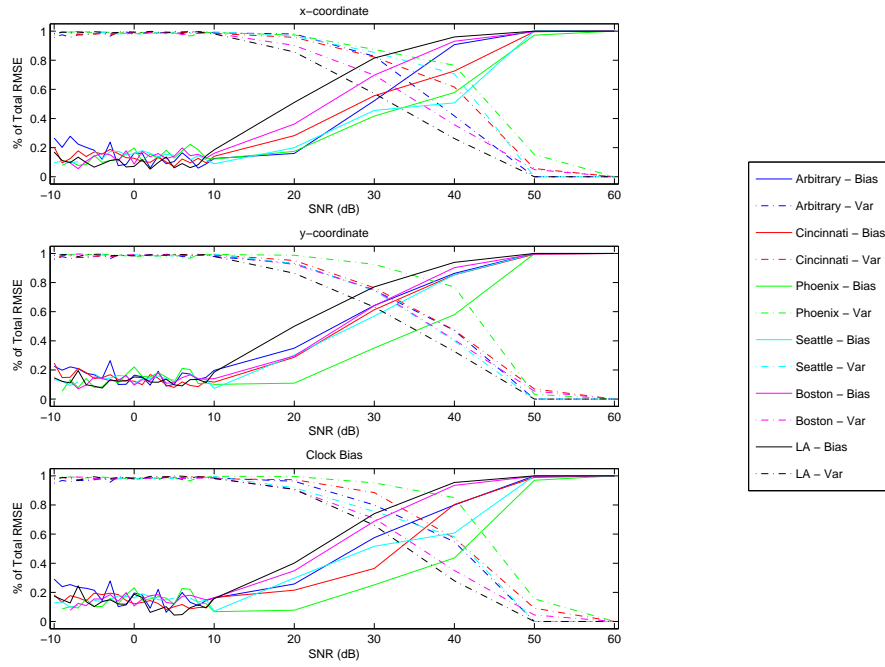Figure A.1:   Baseline divided by 2-Unknown Receivers CRLB, SNR = 20 dB

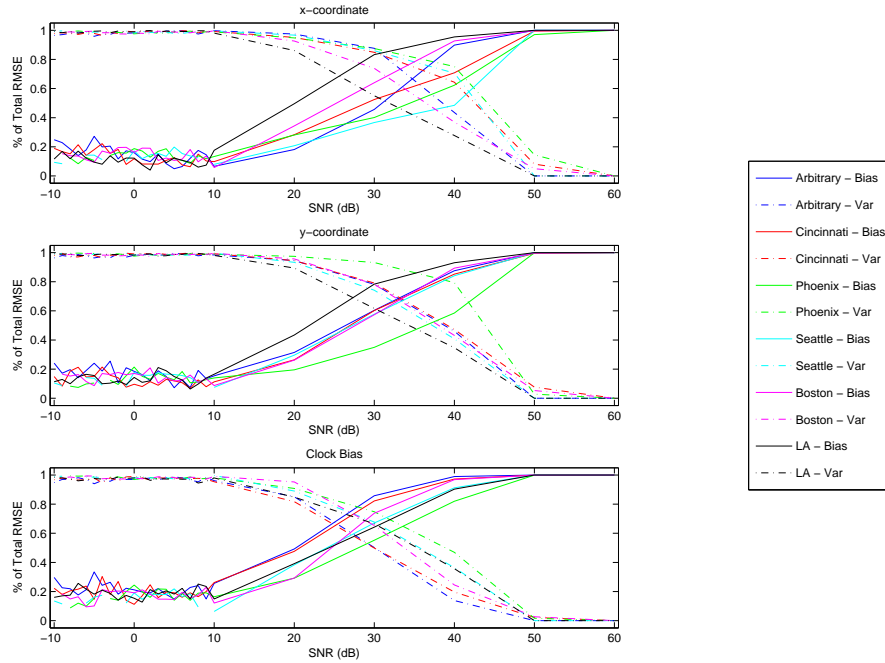Figure A.2:   Bias vs. Variance as % of Total Error for Simulation #1

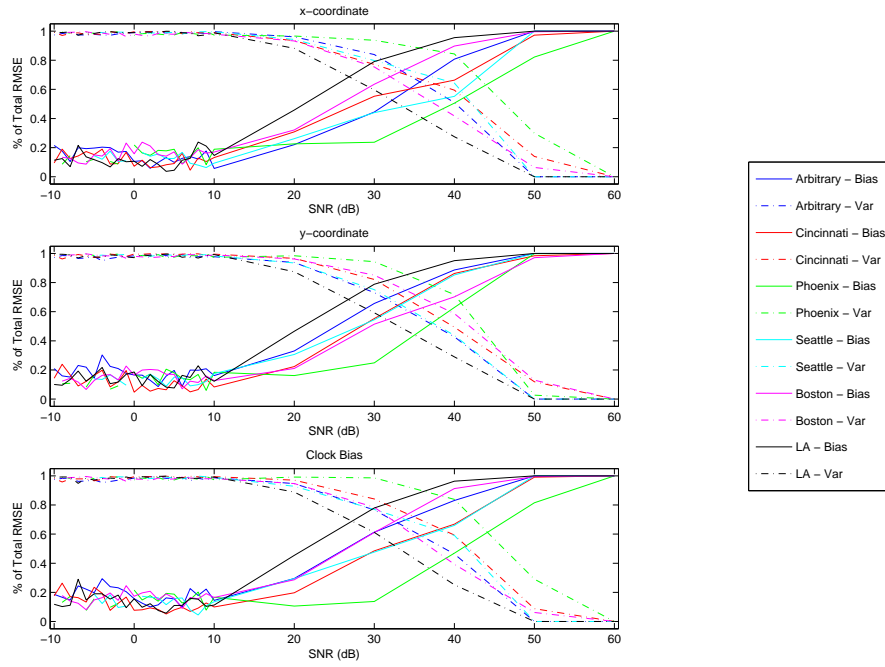Figure A.3:   Bias vs. Variance as % of Total Error for Simulation #2

90

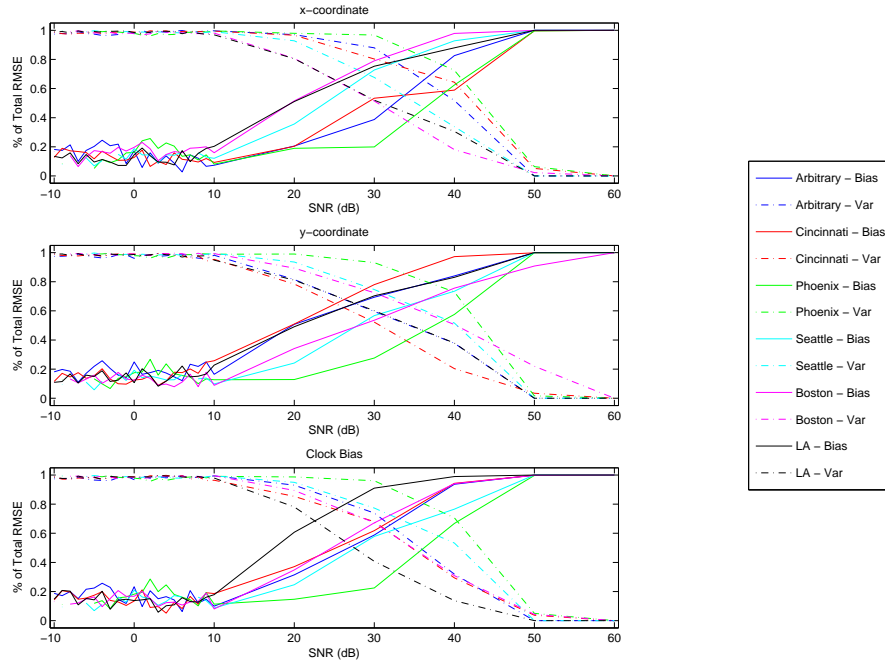Figure A.4:   Bias vs. Variance as % of Total Error for Simulation #3

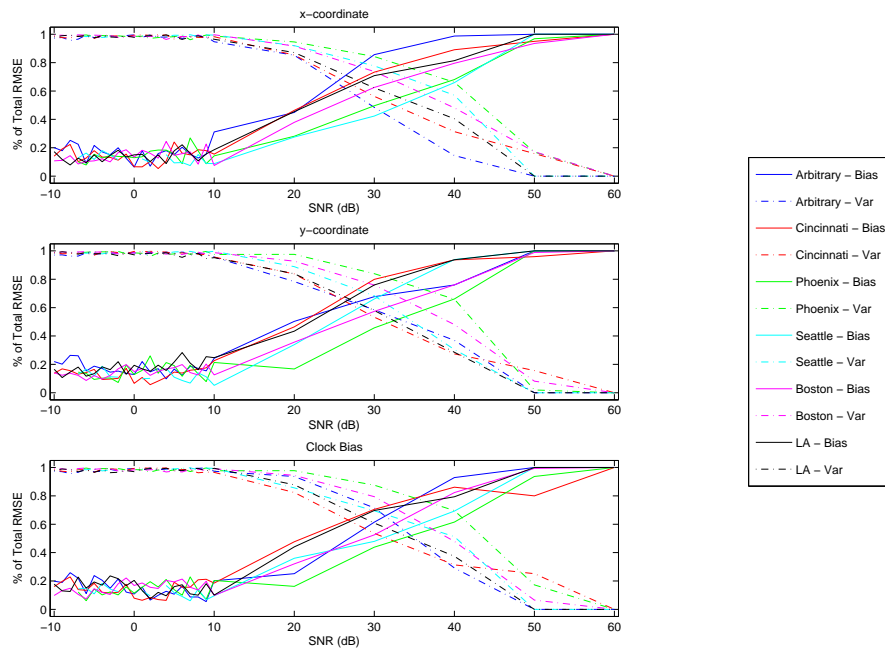Figure A.5:   Bias vs. Variance as % of Total Error for Simulation #4

91

Figure A.6:   Bias vs. Variance as % of Total Error for Simulation #5
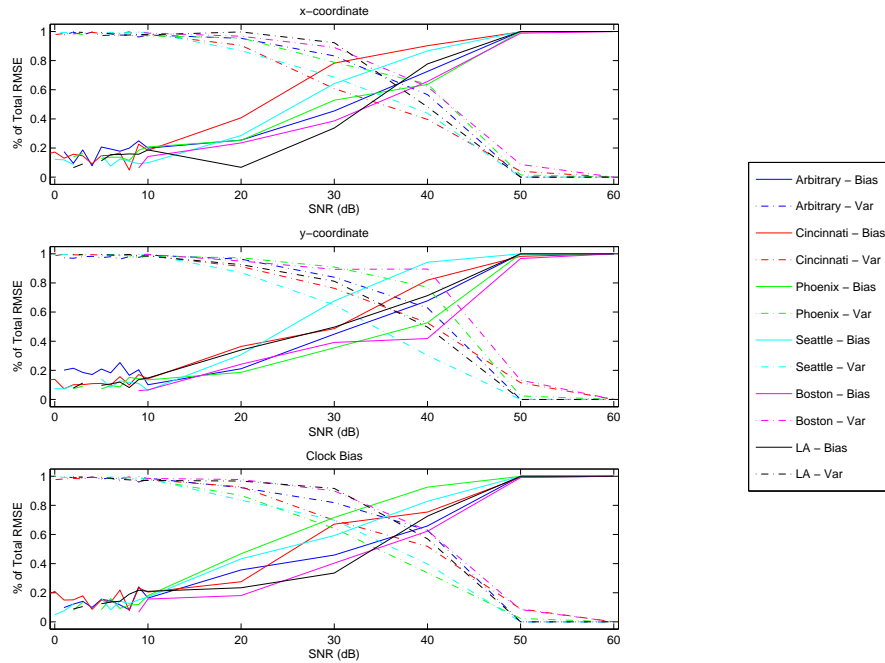

Figure A.7:   Bias vs. Variance as % of Total Error for Simulation #6
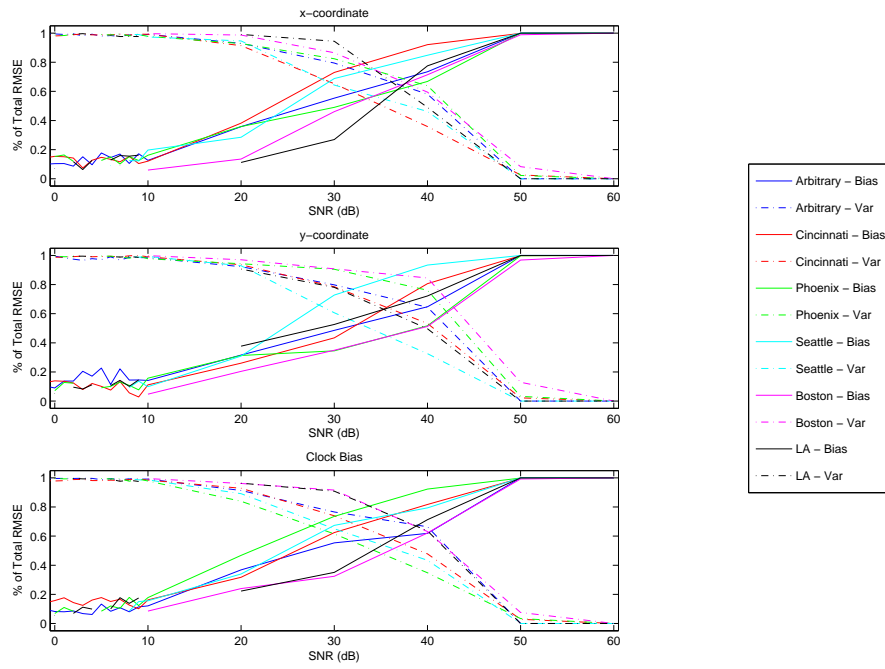
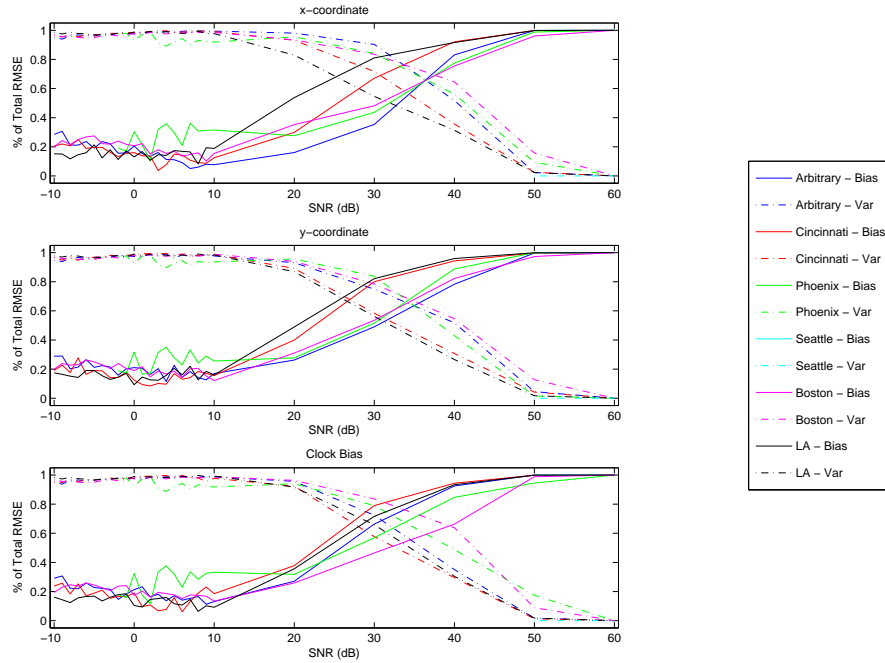Figure A.8:   Bias vs. Variance as % of Total Error for Simulation #7

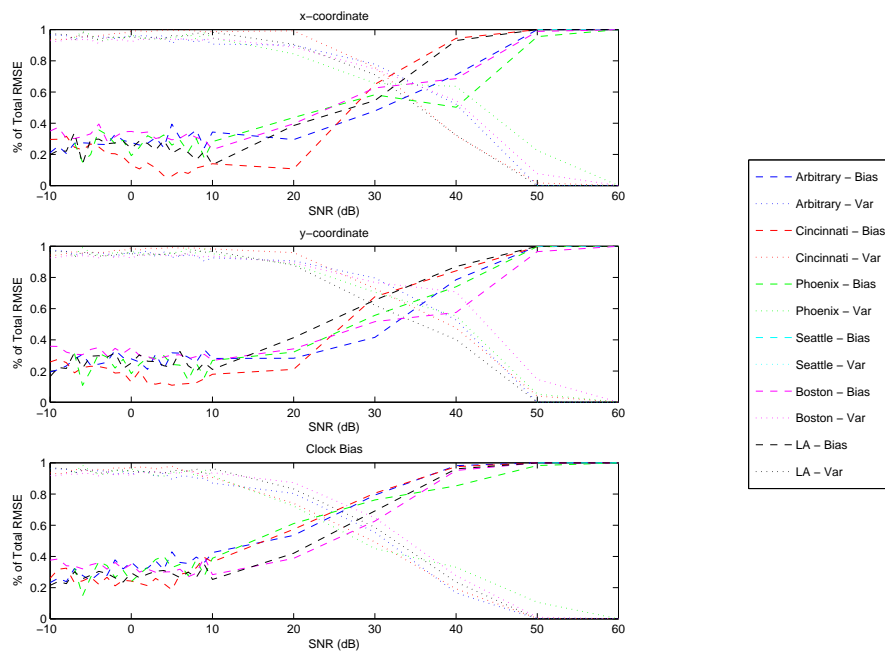Figure A.9:   Bias vs. Variance as % of Total Error for Simulation #8

Figure A.10:   Bias vs. Variance as % of Total Error for Simulation #9

Bibliography

1. Abel, Jonathan S. "A Divide and Conquer Approach to Least Squares Estimation". *IEEE Transactions on Aerospace and Electronic Systems*, 26(2):423–427, March 1990.

2. Ahlers, Mike M. "World War II-era navigation system shut down", February 8 2010. [Online]. Available at http://www.cnn.com/2010/TECH/02/08/loran.navigation.shutdown. [Accessed: 16 February, 2010].

3. Bellows, Charlie. "GPS Operations Center - A User Focused Center of Excellence". *Civil Global Positioning System Service Interface Committee (CGSIC) - 47th Meeting*. September 2007.

4. Caffery, James J. and Gordon L. Stüber. "Overview of radiolocation in CDMA cellular systems". *IEEE Communications Magazine*, 36(4):38–45, April 1998.

5. Code of Federal Regulations. "AM Broadcast Stations". Title 47, Part 73, Subpart A, 2009 edition.

6. Department of the Air Force. "Air Force Doctrine Document 1", November 2003. AFDD-1.

7. Eggert, Ryan J. *Evaluating the Navigation Potential of the National Television System Committee Broadcast Signal*. Master's thesis, Graduate School of Engineering, Air Force Institute of Technology (AETC), Wight-Patterson AFB OH, March 2004. AFIT/GE/ENG/04-08. [Online]. Available at http://handle.dtic.mil/100.2/ADA423977.

8. Fang, Bertrand T. "Simple Solutions for Hyperbolic and Related Position Fixes". *IEEE Transactions on Aerospace and Electronic Systems*, 26(5):748–753, September 1990.

9. Federal Communications Commission. "AMQ AM Radio Database Query". [Online]. Available at http://www.fcc.gov/mb/audio/amq.html. [Accessed: 10 July, 2010].

10. Fisher, Kenneth A. *The Navigation Potential of Signals of Opportunity-Based Time Difference of Arrival Measurements*. Ph.D. dissertation, Graduate School of Engineering, Air Force Institute of Technology (AETC), Wight-Patterson AFB OH, March 2005. AFIT/DS/ENG/05-02. [Online]. Available at http://handle.dtic.mil/100.2/ADA442340.

11. Foy, Wade H. "Position-Location Solutions by Taylor-Series Estimation". *IEEE Transactions on Aerospace and Electronic Systems*, 12(2):187–194, March 1976.

12. Frevert, Ronny, Joachim Haase, and Roland Jancke. *Modeling and simulation for RF System Design*. Springer, Dordrecht, The Netherlands, 2005.

13. Friedlander, Benjamin. "A Passive Localization Algorithm and Its Accuracy Analysis". *IEEE Journal of Oceanic Engineering*, 12(1):234–245, January 1987.

14. Grant, Alan, Paul Williams, Nick Ward, and Sally Basker. "GPS Jamming and the Impact on Maritime Navigation". *The Journal of Navigation*, 62(02):173, April 2009.

15. Hahn, William R. and Steven A. Tretter. "Optimum processing for delay-vector estimation in passive signal arrays". *IEEE Transactions on Information Theory*, 19(5):608–614, September 1973.

16. Hall, Timothy D. *Radiolocation Using AM Broadcast Signals*. Ph.D. dissertation, Massachusetts Institute of Technology, Cambridge MA, September 2002.

17. Hall, Timothy D. "Radiolocation using AM broadcast signals: The role of signal propagation irregularities". *IEEE Position Location and Navigation Symposium (PLANS) 2004*, 752–761. Monterey, CA, April 2004.

18. Ho, K. C. and Y. T. Chan. "Solution and performance analysis of geolocation by TDOA". *IEEE Transactions on Aerospace and Electronic Systems*, 29(4):1311–1322, October 1993.

19. Ho, K. C. and Y. T. Chan. "A Simple and Efficient Estimator for Hyperbolic Location". *IEEE Transactions on Signal Processing*, 42(8):1905–1915, August 1994.

20. Hu, Hui and Na Wei. "A study of GPS jamming and anti-jamming". *2nd International Conference on Power Electronics and Intelligent Transportation System (PEITS)*, volume 1, 388–391. Shenzhen, China, December 2009.

21. Kay, Steven M. *Fundamentals of Statistical Signal Processing*, volume 1. Prentice Hall PTR, Upper Saddle River NJ, 1993.

22. Kerr, Richard A. "Are We Ready for the Next Solar Maximum? No Way, Say Scientists". *Science*, 324(5935):1640–1641, June 26 2009.

23. Kim, Bryan S. *Evaluating the Correlation Characteristics of Arbitrary AM and FM Radio Signals for the Purpose of Navigation*. Master's thesis, Graduate School of Engineering, Air Force Institute of Technology (AETC), Wight-Patterson AFB OH, March 2006. AFIT/GE/ENG/06-08. [Online]. Available at http://handle.dtic.mil/100.2/ADA446837.

24. Knapp, Charles H. and G. Clifford Carter. "The generalized correlation method for estimation of time delay". *IEEE Transactions on Acoustics, Speech and Signal Processing*, 24; 24(4):320–327, August 1976.

25. Krizman, K. J., T. E. Biedka, and T. S. Rappaport. "Wireless Position Location: Fundamentals, Implementation Strategies, and Sources of Error". *IEEE 47th Vehicular Technology Conference*, 2, 1997.

26. Lathi, Bhagawandas P. *Signal Processing and Linear Systems*. Berkeley Cambridge Press, Carmichael, CA, 1998.

27. Martin, Richard, Chunpeng Yan, H. Howard Fan, and Christopher Rondeau. "Algorithms and Bounds for Distributed TDOA-Based Positioning Using OFDM Signals". *IEEE Transactions on Signal Processing*, to appear in 2011. Approx. 10 pages.

28. McEllroy, Jonathan A. *Navigation Using Signals of Opportunity in the AM Transmission Band*. Master's thesis, Graduate School of Engineering, Air Force Institute of Technology (AETC), Wight-Patterson AFB OH, September 2006. AFIT/GE/ENG/06-04. [Online]. Available at http://handle.dtic.mil/100.2/ADA456511.

29. Misra, Pratap and Enge Per. *Global Positioning System: Signals, Measurements, and Performance*. Ganga-Jamuna Press, Lincoln, MA, second edition, 2006.

30. Montminy, Myrna B. *Passive Geolocation of Low-Power Emitters in Urban Environments Using TDOA*. Master's thesis, Graduate School of Engineering, Air Force Institute of Technology (AETC), Wight-Patterson AFB OH, March 2007. AFIT/GE/ENG/07-16. [Online]. Available at http://handle.dtic.mil/100.2/ADA471571.

31. National Communications System Technology and Standards Division. "Telecommunications: Glossary of Telecommunications Terms", August 1996. FED_STD-1037C.

32. Pace, Scott, Gerald P. Frost, Irving Lachow, David R. Frelinger, Donna Fossum, Don Wassem, and Monica M. Pinto. *The Global Positioning System - Assessing National Policies*. Technical Report MR-614-OSTP, RAND Corporation, Santa Monica, CA, 1995.

33. Pair, Laura. "GPS Applications Exchange". [Online]. Available at http://gpshome.ssc.nasa.gov. [Accessed: 25 April, 2010].

34. Rondeau, Christopher M. "Navigation Using TDOA Measurements From Signals of Opportunity". *Institute of Navigation, Autonomous Weapon Summit*. October 2010.

35. Sklar, Bernard. *Digital Communications*. Prentice Hall PTR, Upper Saddle River, NJ, second edition, 2001.

36. Smith, Julius O. and Jonathan S. Abel. "Closed-Form Least-Squares Source Location Estimation From Range-Difference Measurements". *IEEE Transactions on Acoustics, Speech and Signal Processing*, 35(12):1664–1669, December 1987.

37. Smith, Julius O. and Jonathan S. Abel. "The Spherical Interpolation Method For Closed-Form Passive Passive Source Localization Using Range Difference Measurements". *IEEE Journal of Oceanic Engineering*, 12:246–252, January 1987.

38. Streight, D. A. *Application of Cyuclostationary Signal Selectivity to the Carry-On Multi-Platform GPS Assisted TDOA System.* Master's thesis, Naval Postgraduate School, Monterey CA, March 1997.

39. Torrieri, D. J. "Statistical Theory of Passive Location Systems". *IEEE Transactions on Aerospace and Electronic Systems*, 20(2):183–198, March 1984.

40. Trunzo, Angelo. "JAMFEST - A Cost Effective Solution to GPS Vulnerability Testing". *Joint Navigation Conference.* March 2008.

41. Tsimenidis, Charalampos. "Simulation of Wireless Communications", May 2010. [Online]. Available at http://www.staff.ncl.ac.uk/charalampos.tsimenidis/EEE8041/EEE8041Slidespdf.html [Accessed: 20 July, 2010].

42. Velotta, Jamie S. *Navigation Using Orthogonal Frequency Division Multiplexed Signals of Opportunity.* Master's thesis, Graduate School of Engineering, Air Force Institute of Technology (AETC), Wight-Patterson AFB OH, September 2007. AFIT/GE/ENG/07-31. [Online]. Available at http://handle.dtic.mil/100.2/ADA485142.

43. White, Thomas H. "United States Early Radio History", July 2 2010. [Online]. Available at http://earlyradiohistory.us/sec005.htm. [Accessed: 2 July, 2010].

44. Yang, Chun, Thao Nguyen, D. Venable, M. White, and R. Siegel. "Cooperative position location with signals of opportunity". *Proceedings of the IEEE 2009 National Aerospace & Electronics Conference (NAECON)*, 18–25. July 2009.

REPORT DOCUMENTATION PAGE

1. REPORT DATE *(DD–MM–YYYY)*
22–12–2010

2. REPORT TYPE
Master's Thesis

3. DATES COVERED *(From — To)*
August 2009 - December 2010

4. TITLE AND SUBTITLE

Navigation With Limited Prior Information
Using Time Difference of Arrival Measurements
From Signals of Opportunity

5a. CONTRACT NUMBER

5b. GRANT NUMBER

5c. PROGRAM ELEMENT NUMBER

6. AUTHOR(S)

Rondeau, Christopher. M., Captain, USAF

5d. PROJECT NUMBER
N/A

5e. TASK NUMBER

5f. WORK UNIT NUMBER

7. PERFORMING ORGANIZATION NAME(S) AND ADDRESS(ES)

Air Force Institute of Technology
Graduate School of Engineering and Management (AFIT/EN)
2950 Hobson Way
WPAFB OH 45433-7765 DSN: 785-3636

8. PERFORMING ORGANIZATION REPORT NUMBER

AFIT/GE/ENG/10-32

9. SPONSORING / MONITORING AGENCY NAME(S) AND ADDRESS(ES)

Air Force Research Laboratory
Attn: AFRL/RYRN (Dr. Thao Nguyen)
2241 Avionics Circle
WPAFB OH 45433
DSN: 785-6127 x4132
thao.nguyen@wpafb.af.mil

10. SPONSOR/MONITOR'S ACRONYM(S)

11. SPONSOR/MONITOR'S REPORT NUMBER(S)

12. DISTRIBUTION / AVAILABILITY STATEMENT

APPROVED FOR PUBLIC RELEASE; DISTRIBUTION UNLIMITED

13. SUPPLEMENTARY NOTES

14. ABSTRACT

The Global Positioning System (GPS) provides world-wide availability to high-accuracy navigation and positioning information. However, the threats to GPS are increasing, and many limitations of GPS are being encountered. Simultaneously, systems previously considered as viable backups or supplements to GPS are being shut down. This creates the need for system alternatives. Navigation using signals of opportunity (SoOP) exploits any signal that is available in a given area, regardless of whether or not the original intent of the signal was for navigation. Common techniques to compute a position estimate using SoOP include received signal strength, angle of arrival, time of arrival, and time difference of arrival (TDOA). To estimate the position of a SoOP receiver, existing TDOA algorithms require one reference receiver and multiple transmitters, all with precisely known positions. This thesis considers modifications to an existing algorithm to produce a comparable position estimate without requiring precise a priori knowledge of the transmitters or reference receiver(s). Using Amplitude Modulation (AM) SoOP, the effect of erroneous a priori data on the existing algorithm are investigated. A proof-of-concept for three new estimation algorithms is presented in this research. Two of the estimators successfully demonstrate comparable performance to the existing algorithm. This is demonstrated in six different transmitter environments using four different receiver configurations.

15. SUBJECT TERMS

Signals of Opportunity, Time Difference of Arrival, Amplitude Modulation, Navigation

16. SECURITY CLASSIFICATION OF:

a. REPORT	b. ABSTRACT	c. THIS PAGE
U	U	U

17. LIMITATION OF ABSTRACT
UU

18. NUMBER OF PAGES
112

19a. NAME OF RESPONSIBLE PERSON
Dr. Richard K. Martin (ENG)

19b. TELEPHONE NUMBER *(include area code)*
(937)255-3636x4625; email:richard.martin@afit.edu